2017

INVESTIGATION OF AN AXIAL FLOW ROTARY VALVE SEAL

Joseph K. Stieha
University of Kentucky, joseph.stieha@uky.edu
Digital Object Identifier: https://doi.org/10.13023/ETD.2017.451

STUDENT AGREEMENT:

I represent that my thesis or dissertation and abstract are my original work. Proper attribution has been given to all outside sources. I understand that I am solely responsible for obtaining any needed copyright permissions. I have obtained needed written permission statement(s) from the owner(s) of each third-party copyrighted matter to be included in my work, allowing electronic distribution (if such use is not permitted by the fair use doctrine) which will be submitted to UKnowledge as Additional File.

I hereby grant to The University of Kentucky and its agents the irrevocable, non-exclusive, and royalty-free license to archive and make accessible my work in whole or in part in all forms of media, now or hereafter known. I agree that the document mentioned above may be made available immediately for worldwide access unless an embargo applies.

I retain all other ownership rights to the copyright of my work. I also retain the right to use in future works (such as articles or books) all or part of my work. I understand that I am free to register the copyright to my work.

REVIEW, APPROVAL AND ACCEPTANCE

The document mentioned above has been reviewed and accepted by the student's advisor, on behalf of the advisory committee, and by the Director of Graduate Studies (DGS), on behalf of the program; we verify that this is the final, approved version of the student's thesis including all changes required by the advisory committee. The undersigned agree to abide by the statements above.

Joseph K. Stieha, Student

Dr. Lyndon Scott Stephens, Major Professor

Dr. Haluk E. Karaca, Director of Graduate Studies

INVESTIGATION OF AN AXIAL FLOW ROTARY VALVE SEAL

THESIS

A thesis submitted in partial fulfillment of the
requirements for the degree of Master of Science in Mechanical Engineering in the
College of Engineering
at the University of Kentucky

By

Joseph Kelly Stieha

Lexington, Kentucky

Director: Dr. Lyndon Scott Stephens, Professor of Mechanical Engineering

Lexington, Kentucky

2017

ABSTRACT OF THESIS

INVESTIGATION OF AN AXIAL FLOW ROTARY VALVE SEAL

This thesis investigates potential materials to be used in the rotary sealing industry that provide low power loss and minimize cost. The studied rotary valve utilizes slots that act as timing valves to allow for flow axially, through the seal face, at particular times within a heat pump cycle. This investigation examines various combinations of multiple PTFE materials, plastics, and soft metals that have been proven to provide low friction coefficients. Leakage and wear requirements are stated for the future use of the rotary valve and are used to determine the effectiveness of sealing the fluid while examining the power loss. In conclusion, the study finds the combination of a modified PTFE stationary ring and Aluminum Bronze rotating face to provide the lowest power loss. Numerical analysis was completed to verify the lubrication regime to be partial lubrication and was also used to investigate geometry changes and impact on the power loss.

KEYWORDS: Rotary Seal, Sealing, Heat Pump Seal, End Face Mechanical Seal, Valve Seal

Joseph Stieha

November 14th, 2017

INVESTIGATION OF AN AXIAL FLOW ROTARY VALVE SEAL

By

Joseph Kelly Stieha

Dr. Lyndon S. Stephens
Director of Thesis

Dr. Haluk E. Karaca
Director of Graduate Studies

November 14th, 2017

Acknowledgements

This thesis benefited from the assistance and support of a number of individuals and organizations. I first want to thank my Thesis Chair and Advisor, Dr. Lyndon Scott Stephens, for sharing his knowledge as well as his guidance and advice, both personally and professionally. This work would not have been possible without his insights and inspiration. Thanks to Dr. Mike Benedict for the professional guidance as he oversaw the project from GE Appliances. I want to thank my wife, Shannon Stieha, for the love and support in pursuing this degree as there were many nights that required me to go into the lab to continue the advancement of this research. I would also like to thank the members of my Thesis Committee, Dr. Johné Parker and Dr. Keith Rouch, for their recommendations and support.

The following organizations are recognized for their support of the project and of the author: GE Appliances, a Haier Company, and the University of Kentucky Department of Mechanical Engineering. Other organizations that participated in the research by providing material suggestions and professional knowledge are Ticona-Celanese Corporation and Trelleborg Sealing Solutions America.

I would also like to thank a number of current and former members of the University of Kentucky Bearings and Seals Laboratory: Daniel Impellizzeri for his outstanding contributions to the data acquisition system utilized and modified for this experimental design; Daryl Schneider and Matt Hayden for their prior work on the experimental setup; A special thanks to Bo Tan for his technical support and friendship.

Finally, thank you to my family and friends for your encouragement, support, and patience throughout my graduate studies.

Table of Contents

List of Tables

List of Figures

1. Introduction

1.1 Rotary Seal

Rotary seals are very common components within the rotating equipment industry where a shaft is rotating relative to the casing. Basic mechanical equipment that utilize these seals include pumps, compressors, and others within the process, transportation, household appliances and many other industries. The rotary seal, also known as an end face mechanical seal, is used to control leakage for the necessary application and must have an acceptable life. Typically, an end face mechanical seal is composed of five main components: a primary ring (rotating), a mating ring (stationary), a secondary seal, a spring, and a drive mechanism. Common materials used for these seals are tungsten carbide, ceramic, silicon carbide, and carbon. A cross-sectional view of a common end face mechanical seal is shown in (Lebeck A. O., 1991).

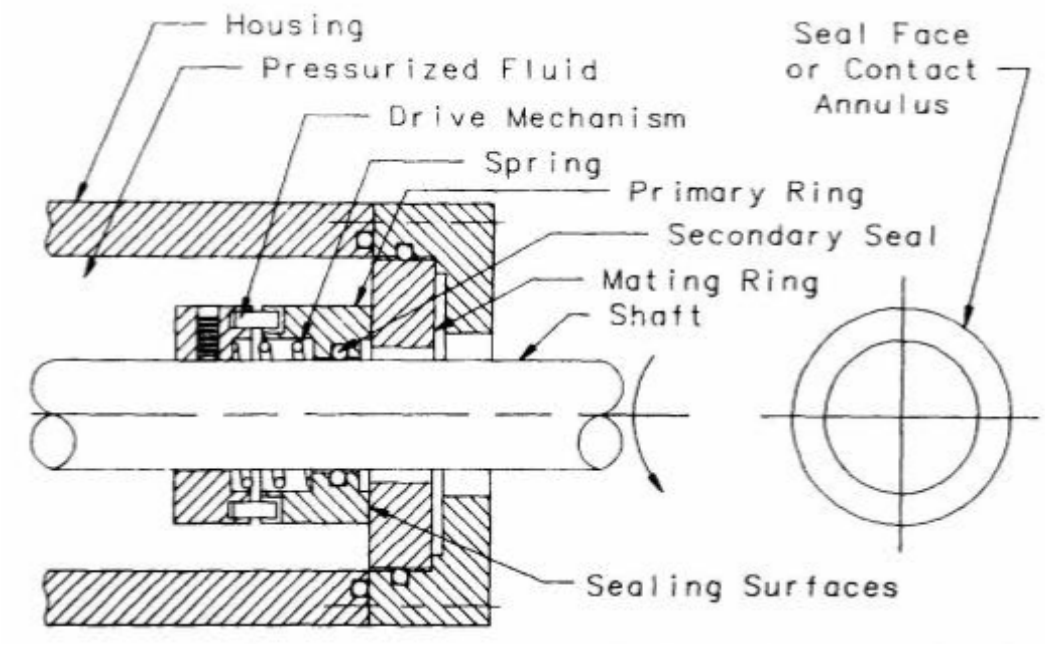

Figure 1.1: Mechanical face seal- outside pressurized, rotating primary ring, fixed mating ring (Lebeck A. O., 1991)

1.2 Magneto Caloric Effect

One application where a rotary seal is being considered is within the developing heat pump technology related to compressor-based appliances where this application is based on the magnetocaloric effect (Benedict M. A., 2016). Magnetocaloric materials (MCM) contain two energy reservoirs that are well coupled to the spin lattice which allows for loss-free energy transfer within millisecond time scales (Brück, 2005). These two energy channels come from the phonon excitations related to the lattice structure and the magnetic excitations. Some benefits related to using this type of material within compressor-based refrigeration are seen by reducing the environmental impact through replacing currently used hazardous chemicals, the reduction in space required to facilitate the MCM, and the energy consumption related to the process (Benedict M. A., 2016) (Zimm, 1998).

To generate the magnetic refrigeration cycle, the MCM is transitioned into a magnetic field where the MCM experiences an increase in temperature, heat is then expelled from the material, the MCM is transitioned out of the magnetic field where the material experiences a decrease in temperature, heat is then transferred to the material, and the cycle repeats. This process is depicted in Figure 1.2 (Brück, 2005). During this process, the MCM is required to rotate in and out of the magnetic field while fluid passes over the MCM preferably at the highest and lowest magnetic field points (Benedict M. A., 2016). Since a stationary fluid pump is necessary to help propel the fluid through the rotating heat pump (United States of America Patent No. 20140165594, 2012), a rotary seal that allows for bi-directional flow on each side of the heat pump is optimal. This allows the magnets to be held internally and seals the fluid from the environment while the heat pump rotates.

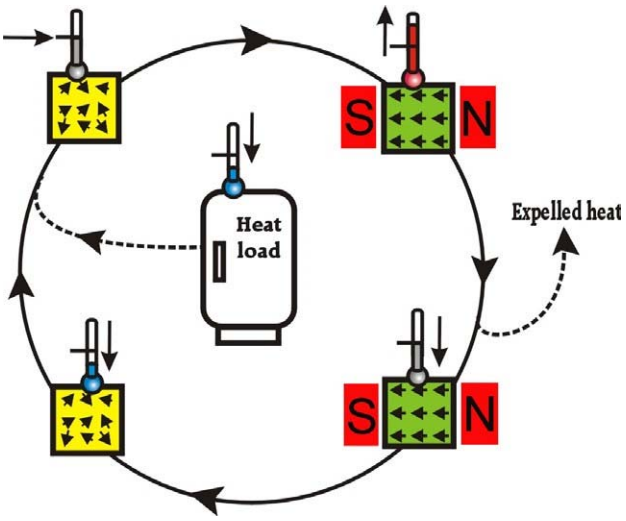

Figure 1.2: A magnetic-refrigeration cycle schematic transporting excess heat to ambient through a change in magnetic field (Brück, 2005)

1.3 Literature Review

The mechanical seal industry is over 100 years old, although papers, reports, books, and manuals on rotary seals began to be published in the 1960s to disseminate information to the community. Lebeck wrote Principles and Design of Mechanical Face Seals to provide a unified and in-depth treatment of the principles of operation along with design of mechanical face seals (Lebeck A. O., 1991) while Müller and Nau wrote Fluid Sealing Technology: Principles and Applications to provide background for the application of the many rotating seals that exist (Müller, 1998). A discussion of materials in sealing was added by Warring's Seals and Sealing Handbook (Warring, 1981). As for material investigations, there are multiple ASTM standards for testing wear and the coefficient of friction. The results have been cataloged within Booser's Tribology Data Handbook (Booser, 1997) which was sponsored by the Society of Tribologists and Lubrication Engineers. Each of these books discusses how any change in a particular parameter can cause a large change to the running of a seal including the geometry of the seal, the surface preparation, load, etc which all require consideration through the testing process.

A considerable amount of analysis has been conducted on the common rotary seal, as shown in Figure 1.1. However, except for that found in patents, there is little or no analysis or information regarding rotary seals with slots and holes in the primary and secondary faces. Nichols et al utilizes a sealing face with inner diameter of zero that rotates from one position to another and back utilizing a fluorocarbon-containing polymer and Tungsten Carbide/Carbon surfaces (United States of America Patent No. 6,453,946, 2001). Nichols continued developing different configurations in the early 2000s (United States of America Patent No. 6,672,336, 2001) (United States of America Patent No. 6,012,488, 1998). In the early 2010s, Moeller et al and Wan developed seal faces that allow rotation to select a particular fluid to flow, but is utilized as a static seal that can be rotated to a different setting (United States of America Patent No. 20140007660, 2012) (United States of America Patent No. 8,813,785, 2012). In the early 1990s, Stich utilized a seal surface that is located on the surface of a shaft where fluid flows through the shaft and then is directed circumferentially to the outer diameter of the shaft and expelled into the static sealing area (United States of America Patent No. 5,080,401, 1991). In the 1960s there was the development of a rotary distributing valve claimed by Carson et al that utilized valves to transfer the fluid stream from one conduit to any other conduit by using circular grooves and horizontal channels. This rotary distributing valve can be used simultaneously with other fluid transfers seen using the other circular grooves within the sealing face (United States of America Patent No. 3,040,777, 1959). While these patents each deal with rotary seals, the research used for this thesis differs in that the seal to be discussed requires continuous rotation in one direction to reduce start-stop power inefficiencies and a flow path that has the liquid flow into the seal, flow out of the seal, and at certain times become a static fluid as required by the magneto caloric effect.

This thesis contributes to the current body of knowledge regarding axial flow rotary valve seals by providing experimental results for power, leakage, and wear that do not exist in the literature today. It examines unconventional rotary seal materials (e.g. PTFE, acetals, etc.) to keep cost down for industries where product margins are very small. It also provides a simple, first order hydrodynamic model to analyze the lubrication regime and to provide results showing the impact of changing different design parameters.

1.4 Thesis Overview

Chapter 1 provides an introduction to the rotary seal and magneto caloric materials and how this type of seal can be utilized to progress the application. It also provides a literature review of the types of seals that have been developed to allow for switching to occur using a rotary seal. Chapter 2 presents the seal design and the derivation of a first order model to predict film thickness based on leakage rate. In Chapter 3, the experimental design is discussed along with the procedures. Chapter 4 contains the experimental results, surface analysis relative to the wear of the seal, and the results from the model. Chapter 5 provides the discussion of the results while Chapter 6 presents the recommendations for future testing and modeling along with the conclusions of this paper as a starting point for future experimentation in low power loss applications utilizing a rotary seal that allows for bi-directional fluid flow through the seal faces.

The objectives accomplished in this work are as follows:

a. Provide a seal design that can be utilized for the application
b. Design of a rotary seal testing apparatus
c. Collection of experimental data from the testing apparatus
d. Develop a first order model representation

e. Analysis of experimental data

f. Recommend future experimentation and modeling to guide the rotary seal research.

2. Seal Design and Initial Model

2.1 Introduction

This chapter discusses the seal design that was utilized for the future application and experimentally tested in this work. It also provides the derivation of a first order model based on the seal geometry and the numerical analysis necessary to provide the leakage and load generated by the fluid.

2.2 Seal Design

Due to the seal timing related to when fluid is passed from the stationary seal through the rotating section and back, the following seal design was developed and shown as Figure 2.1 (Stieha, 2016). This figure shows the schematic of a 4 slot, 8 port timing valve that simultaneously functions as the seal for the fluid flowing from the 4 slots into or out of the 8 ports as the end faces of the two rings are mated together. This seal layout allows for independent testing and analysis of different material pairs without building and testing a completely new rotating section. The design allows for testing to occur on a Falex Tribometer and for the sealing parts to be easily exchanged between tests.

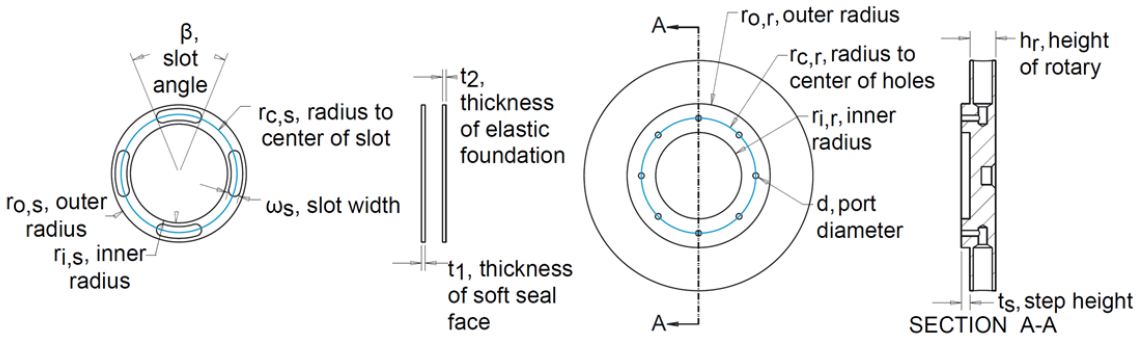

Figure 2.1: nomenclature for dimensions of the axial flow rotary valve seal

There are two major sealing requirements because of the bi-directional flow that occurs within the seal as demonstrated in Figure 2.2. The most important requirement is the sealing between each of the slots and the environment on the inside and outside radius of the seal. Within the experimental testing, there were two different pressure values (50 psi and atmospheric pressure were utilized in the experimentation) due to the drop in pressure created throughout the system which leads to the second major requirement in sealing which is the sealing of the high pressure slots to the low pressure slots located on the stationary seal face.

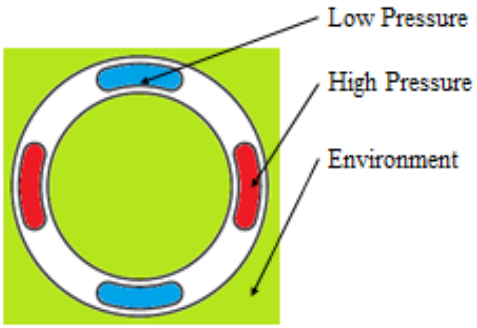

Figure 2.2: Schematic of the different pressure zones within the seal

Figure 2.3 shows a cross-section of the mating surfaces with the lower mount that holds the stationary seal in place. This figure illustrates the flow through the seal face axially from the supplied high pressure, represented by the teal arrows, into the upper rotating seal; blue represents the stationary seal; purple represents an elastomer backing; and the red arrows indicate potential leakage into the environment. The low pressure slots would portray a very similar figure as Figure 2.3, but with the teal arrows in the opposite direction where the flow would travel from the upper rotating seal axially into the stationary seal slot.

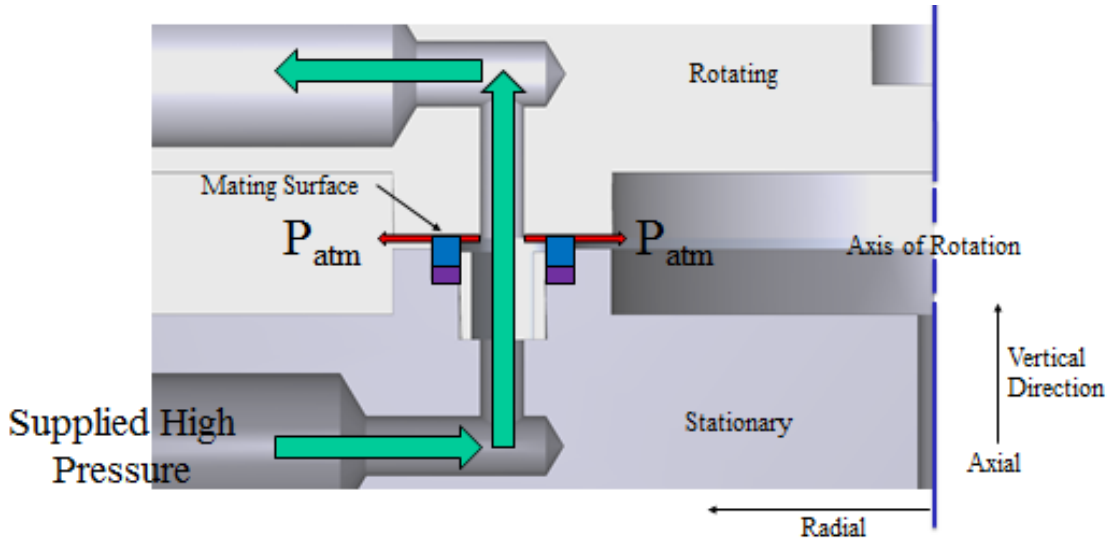

Figure 2.3: Cross section of the sealing faces demonstrating flow through the seal face from the supplied high pressure

This seal works by the port rotating over the high pressure slot. During that time, fluid is transferred into the rotating seal body. As the port continues to rotate, the port is then covered and sealed with fluid. At the same time this is occurring, this section of the rotating seal body transitions into a magnetic field. At the peak of the magnetic field, the rotating port becomes unsealed by transitioning to the low pressure slot. During this time of exposure, fluid transfers out of the rotating seal and into the stationary seal. As the port continues to rotate, the port is then covered and sealed again. During this time, this section of the rotating pump then transitions out of the magnetic field and the process would repeat again once the rotating port was over the next high pressure slot. Since there are eight ports, as shown, each port would be going through one of the four sections described.

2.3 First-Order Seal Model

From the geometry of the seal presented in the previous section, a first-order model was developed to predict the pressure profile of the sealing surface based on the boundary conditions of the inner seal radius, outer seal radius, inlet valve, and outlet valve pressures. The

pressure profile was then used to evaluate an approximation of the film height for a given leakage to predict the operating lubrication regime of the running seal and its generated load. The assumptions used to create the model are listed below.

1. Thin film: $\mathrm{h} \ll \mathrm{L}$
2. No pressure variation across the film, $\frac{dP}{dz} = 0$
3. No-slip at the surfaces
4. No body forces and no inertial forces
5. Newtonian fluid
6. Incompressible fluid: $\rho = constant$
7. Constant viscosity
8. Laminar flow: $Re \ll 2000$
9. Two parallel-flat plates: $\frac{dh}{dr} = 0,\ \frac{dh}{d\theta} = 0$
10. No velocity in radial direction
11. No contact of surfaces
12. Steady-state run conditions

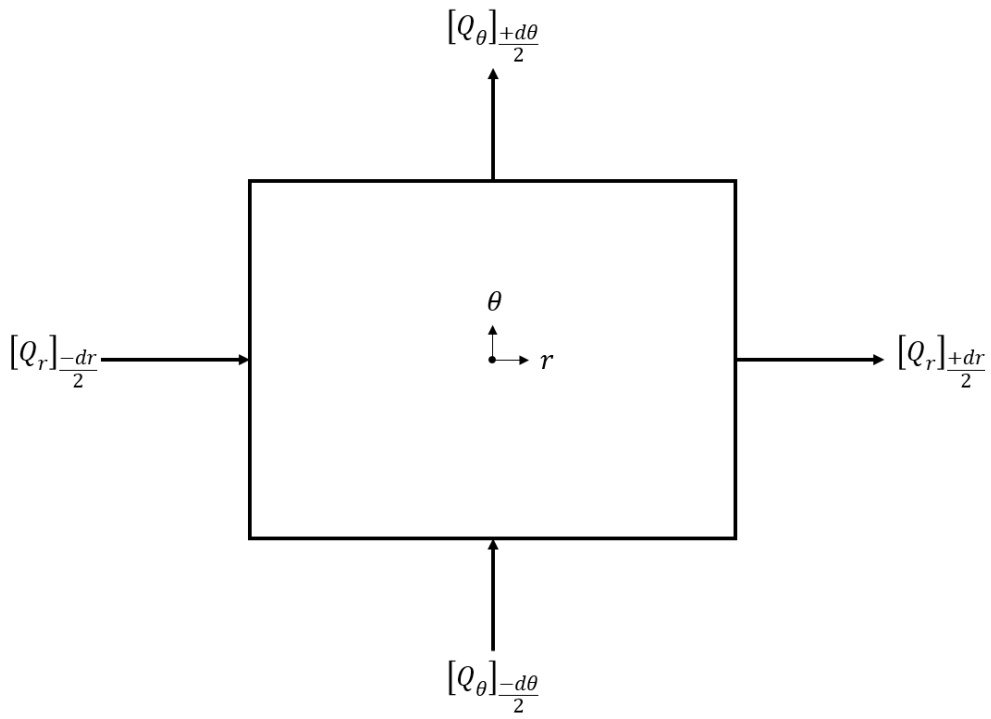

Figure 2.4: Diagram of the volume flowrate thru an element

The model was derived starting with the first principle, Conservation of Mass (Equation 2.1), in cylindrical coordinates demonstrated in Figure 2.4, where $[Q_r]$ and $[Q_\theta]$ are the total volume flowrate thru the faces located at $r = \pm\frac{dr}{2}$ or $\theta = \pm\frac{d\theta}{2}$, where dr and $d\theta$ are steps in the radial and circumferential direction, respectively.

$$[Q_r]_{\frac{-dr}{2}} + [Q_r]_{\frac{+dr}{2}} + [Q_\theta]_{\frac{-d\theta}{2}} + [Q_\theta]_{\frac{+d\theta}{2}} + [\dot{Q}] = 0 \tag{2.1}$$

$[\dot{Q}]$ is defined as the volume rate of change of the column in the z-direction. By setting $Q_r, Q_\theta,$ and $\dot{Q}$ to be the volumetric flowrates in each direction about the center of the infinitesimally small element of fluid shown in Figure 2.4, the mass conservation term for Q_r can be rewritten as Equation 2.2a and 2.2b and the mass conservation terms for Q_θ will be of similar form.

$$[Q_r]_{\frac{-dr}{2}} = -\left(Q_r - \frac{dQ}{dr}\frac{dr}{2}\right) \tag{2.2a}$$

$$[Q_r]_{\frac{+dr}{2}} = \ + \left(Q_r + \frac{dQ}{dr}\frac{dr}{2}\right) \tag{2.2b}$$

When these terms are substituted back into the conservation of mass equation (Eq. 2.1), the equation becomes,

$$\frac{dQ_r}{dr}dr + \frac{dQ_\theta}{d\theta}d\theta + \dot{Q} = 0 \tag{2.3}$$

To further define the volumetric flowrate, Q_r and Q_θ, the term q_r will be defined as the radial direction volumetric flowrate per unit length in the circumferential direction and the term q_θ will be defined as the circumferential direction volumetric flowrate per unit length in the radial direction. This relationship is shown as Equation 2.4a and 2.4b.

$$Q_r = q_r r d\theta \tag{2.4a}$$

$$Q_\theta = q_\theta dr \tag{2.4b}$$

Because $d\theta$ is in radians, $rd\theta$ must be used to denote the arc length of the step in the circumferential direction, where r is the radial distance from the rotational axis. To continue, the volumetric column defined by $\dot{Q}$ can be rewritten in terms of the z-direction velocity of one surface related to the other surface multiplied by the surface area. For this instance, it is assumed that the bottom surface will move toward the upper surface and close the distance between the two plates with a velocity, w_1.

$$\dot{Q} = -w_1 r dr d\theta \tag{2.5}$$

When Equations 2.4a, 2.4b, and 2.5 are substituted back into Equation 2.3 and factored, Equation 2.3 becomes Equation 2.6.

$$\frac{1}{r}\frac{dq_r r}{dr} + \frac{1}{r}\frac{dq_\theta}{d\theta} - w_1 = 0 \tag{2.6}$$

To further advance the derivation, the forces on the element must be examined. The free-body diagram is demonstrated in Figure 2.5. On the element, there exists compressive

stress due to pressure from the surrounding elements and shear forces caused by the surfaces of the two parallel plates being transferred from the elements above and below the element being examined at a height of $\frac{+dz}{2}$ and $\frac{-dz}{2}$. The forces are then summed in the radial and circumferential direction and set to zero based on assumption #4.

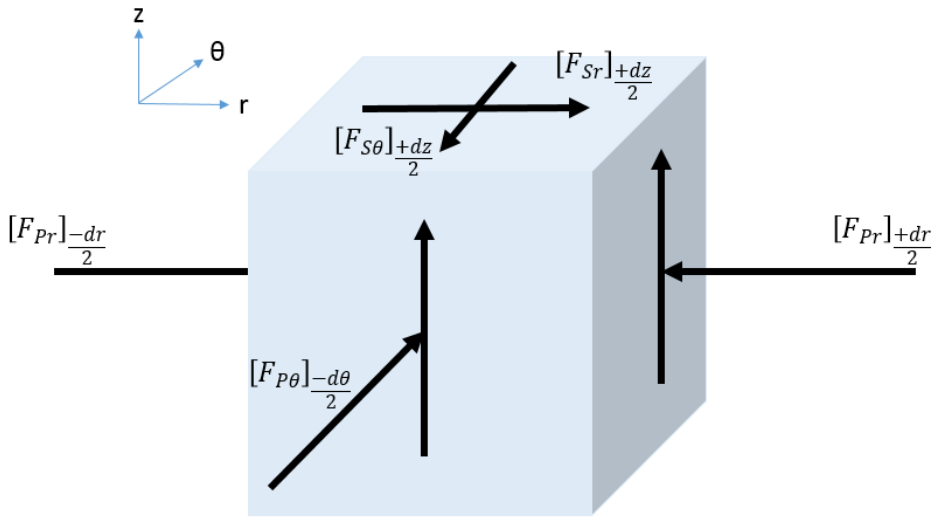

Figure 2.5: Free-Body Diagram of an element of fluid

$$\sum F_r = [F_{Pr}]_{\frac{-dr}{2}} + [F_{Pr}]_{\frac{+dr}{2}} + [F_{Sr}]_{\frac{-dz}{2}} + [F_{Sr}]_{\frac{+dz}{2}} = 0 \tag{2.7a}$$

$$\sum F_\theta = [F_{P\theta}]_{\frac{-d\theta}{2}} + [F_{P\theta}]_{\frac{+d\theta}{2}} + [F_{S\theta}]_{\frac{-dz}{2}} + [F_{S\theta}]_{\frac{+dz}{2}} = 0 \tag{2.7b}$$

If P is defined as the pressure at the center of the fluid element, the forces due to pressure can be written as Equations 2.8a and 2.8b with the circumferential pressure variables being of a similar form.

$$[F_{Pr}]_{\frac{-dr}{2}} = + \left(P - \frac{dP}{dr}\frac{dr}{2}\right) r d\theta dz \tag{2.8a}$$

$$[F_{Pr}]_{\frac{+dr}{2}} = -\left(P + \frac{dP}{dr}\frac{dr}{2}\right) r d\theta dz \tag{2.8b}$$

If τ_{zr} and $\tau_{z\theta}$ are defined as the shear stress at the center of the elements, the shear forces in Equations 2.7a and 2.7b can be expressed as Equations 2.9a and 2.9b with the circumferential shear force variables being again of a similar form.

$$[F_{Sr}]_{\frac{-dz}{2}} = -\left(\tau_{zr} - \frac{d\tau_{zr}}{dz}\frac{dz}{2}\right) r d\theta dr \tag{2.9a}$$

$$[F_{Sr}]_{\frac{+dz}{2}} = +\left(\tau_{z\theta} + \frac{d\tau_{z\theta}}{dz}\frac{dz}{2}\right) r d\theta dr \tag{2.9b}$$

Substituting the equations due to shear and pressure into Equations 2.7a and 2.7b and factoring, the following equations are derived.

$$-\frac{dP}{dr} + \frac{d\tau_{zr}}{dz} = 0 \tag{2.10a}$$

$$-\frac{1}{r}\frac{dP}{d\theta} + \frac{d\tau_{z\theta}}{dz} = 0 \tag{2.10b}$$

Since the previous equations contain shear stress, using Assumption #5 (a Newtonian fluid) the Newton Postulate (Stress-Velocity Gradient-Law) Equations, listed as Equations 2.11a, 2.11b, and 2.11c, will be used to further derive the model. The v, u, and w are the velocity terms that correspond with r-direction, θ-direction, and z-direction, respectively, and μ is the viscosity of the fluid.

$$\tau_{rz} = \tau_{zr} = \mu\left[\frac{du}{dz} + \frac{dw}{dr}\right] \tag{2.11a}$$

$$\tau_{\theta z} = \tau_{z\theta} = \mu\left[\frac{dv}{dz} + \frac{1}{r}\frac{dw}{d\theta}\right] \tag{2.11b}$$

$$\tau_{r\theta} = \tau_{\theta r} = \mu\left[r\frac{d}{dr}\left(\frac{v}{r}\right) + \frac{1}{r}\frac{du}{d\theta}\right] \tag{2.11c}$$

By using Newton's Postulate listed as Equation 2.11a and 2.11b and Assumption #9 (flat-parallel plates), the velocity w does not change with respect to the r-direction nor the θ-direction since

the assumption assumes a rigid body with no rotation about the r- or θ-axis with respect to the other plate/surface.

$$\tau_{rz} = \tau_{zr} = \mu\left[\frac{du}{dz}\right] \tag{2.12a}$$

$$\tau_{\theta z} = \tau_{z\theta} = \mu\left[\frac{dv}{dz}\right] \tag{2.12b}$$

When Equations 2.12a and 2.12b are substituted back into Equations 2.10a and 2.10b, the Momentum Equations are derived and shown below as Equations 2.13a and 2.13b.

$$-\frac{dP}{dr} + \frac{d}{dz}\left(\mu\frac{du}{dz}\right) = 0 \tag{2.13a}$$

$$-\frac{1}{r}\frac{dP}{d\theta} + \frac{d}{dz}\left(\mu\frac{dv}{dz}\right) = 0 \tag{2.13b}$$

From this point, the velocity components can be solved by integrating the Momentum Equations with respect to z. The boundary conditions are then considered for each velocity equation. Due to Assumption #10 (no velocity in the radial direction) and Assumption #3 (no-slip at the surface), the radial velocity at the surface of both plates is zero, $u(z = h) = u(z = 0) = 0$. Let h be the fluid film thickness between the two plates. Since the seal contains a stationary and rotating surface, the circumferential velocity is zero at the stationary plate and the velocity of the fluid adjacent to the rotary surface is equal to the rotary plate velocity, where ω is the rotational speed in radians per second, $v(z = h) = r\omega$ and $v(z = h) = 0$. Using the boundary conditions and momentum equations from above, the velocity vector equations are as follows.

$$u(z) = \frac{1}{2\mu}\frac{dP}{dr}(z^2 - hz) \tag{2.14a}$$

$$v(z) = \frac{1}{2\mu r}\frac{dP}{d\theta}(z^2 - hz) + r\omega\frac{z}{h} \tag{2.14b}$$

Since the velocity equations are known, the volumetric flowrate per unit length for both the radial, q_r, and circumferential, q_θ, directions can be derived by taking the integral of the velocity component with respect to z from the stationary surface to the rotary surface.

$$q_r = \int_0^h u(z)dz \tag{2.15a}$$

$$q_\theta = \int_0^h v(z)dz \tag{2.15b}$$

Using Equations 2.14a, 2.14b, 2.15a and 2.15b, the derived volumetric flowrate per unit length equations are shown below.

$$q_r = \frac{-h^3}{12\mu}\frac{dP}{dr} \tag{2.16a}$$

$$q_\theta = \frac{-h^3}{12\mu r}\frac{dP}{d\theta} + \frac{h}{2}r\omega \tag{2.16b}$$

When Equations 2.16a and 2.16b are substituted back into Equation 2.6, the Reynold's Equation in cylindrical coordinates for this seal geometry is generated.

$$\frac{1}{r}\frac{d}{dr}\left(r\frac{h^3}{\mu}\frac{dP}{dr}\right) + \frac{1}{r^2}\frac{d}{d\theta}\left(\frac{h^3}{\mu}\frac{dP}{d\theta}\right) = 6r\omega\frac{1}{r}\frac{dh}{d\theta} - 12w_1 \tag{2.17}$$

Due to Assumption #12 (steady-state run conditions), it is assumed the z-direction velocity, w_1, would be zero. With the implementation of Assumption #9 (two parallel-flat plates, $\frac{dh}{d\theta} = 0$), both terms on the right-hand side would be zero and would simplify Equation 2.17 to,

$$\frac{1}{r}\frac{d}{dr}\left(r\frac{h^3}{\mu}\frac{dP}{dr}\right) + \frac{1}{r^2}\frac{d}{d\theta}\left(\frac{h^3}{\mu}\frac{dP}{d\theta}\right) = 0 \tag{2.18}$$

which the Reynold's Equation becomes the Laplacian of the pressure in cylindrical coordinates when the height and viscosity are factored out since neither variable is dependent on position r nor θ.

$$\frac{1}{r}\frac{d}{dr}\left(r\frac{dP}{dr}\right)+\frac{1}{r^2}\frac{d}{d\theta}\left(\frac{dP}{d\theta}\right)=\nabla^2 P=0 \tag{2.19}$$

From this, numerical analysis can be applied with geometric boundary conditions that will then predict the fluid pressure profile between the seal faces which will then allow for a calculated leakage rate based on fluid viscosity and fluid height.

When it is considered that r will never be zero due to the geometry of this seal, the Reynold's Equation can be further factored to Equation 2.20 which will simplify the numerical analysis of the equation.

$$\frac{d}{dr}\left(r\frac{dP}{dr}\right)+\frac{1}{r}\frac{d}{d\theta}\left(\frac{dP}{d\theta}\right)=0 \tag{2.20}$$

2.4 Numerical Solution

To further solve the pressure profile, different techniques will be implemented and discussed. When the first term is considered, a first derivative will be approximated using the central difference technique shown as Equation 2.21 where Δr is the step length in the radial direction and P_{i-1} and P_{i+1} correspond to the pressure value at location $i-1$ and $i+1$ in the radial direction.

$$\frac{dP}{dr}\approx\frac{P_{i+1}-P_{i-1}}{2\Delta r} \tag{2.21}$$

When evaluating a second derivative, both forward and backward differencing can be implemented.

$$\frac{d^2P}{dr^2}\approx\frac{\left(\frac{dP}{dr}\right)_2-\left(\frac{dP}{dr}\right)_1}{\Delta r},where\left(\frac{dP}{dr}\right)_1=\frac{P_i-P_{i-1}}{\Delta r},\ \left(\frac{dP}{dr}\right)_2=\frac{P_{i+1}-P_i}{\Delta r} \tag{2.22}$$

Using the mentioned techniques, the first term can then be approximated as Equation 2.23.

$$\frac{d}{dr}\left(r\frac{dP}{dr}\right) \approx \frac{\left(r\frac{dP}{dr}\right)_2 - \left(r\frac{dP}{dr}\right)_1}{\Delta r}$$

$$\left(r\frac{dP}{dr}\right)_1 = r_{i-\frac{1}{2}}\left(\frac{P_i - P_{i-1}}{\Delta r}\right), \qquad \left(r\frac{dP}{dr}\right)_2 = r_{i+\frac{1}{2}}\frac{P_{i+1} - P_i}{\Delta r}$$

$$\frac{d}{dr}\left(r\frac{dP}{dr}\right) \approx \frac{1}{\Delta r^2}\left[r_{i+\frac{1}{2}}P_{i+1} - \left(r_{i+\frac{1}{2}} + r_{i-\frac{1}{2}}\right)P_i + r_{i-\frac{1}{2}}P_{i-1}\right] \tag{2.23}$$

When the same techniques are used for the second term in Equation 2.20, the circumferential component can be expressed as Equation 2.24 where j is used to designate a location in the circumferential direction.

$$\frac{1}{r}\frac{d}{d\theta}\left(\frac{dP}{d\theta}\right) \approx \frac{1}{r_i\Delta\theta^2}\left[P_{j+1} - 2P_j + P_{j-1}\right] \tag{2.24}$$

Since the pressure profile uses a 2-D map of points, the pressures expressed in Equation 2.23 are all at circumferential location j and the pressures expressed in Equation 2.24 are all at radial location i. Therefore, Equation 2.20 can be rewritten and approximated as Equation 2.25.

$$\frac{1}{\Delta r^2}\left[r_{i+\frac{1}{2}}P_{i+1,j} - \left(r_{i+\frac{1}{2}} + r_{i-\frac{1}{2}}\right)P_{i,j} + r_{i-\frac{1}{2}}P_{i-1,j}\right] + \frac{1}{r_i\Delta\theta^2}\left[P_{i,j+1} - 2P_{i,j} + P_{i,j-1}\right] \approx 0 \tag{2.25}$$

Since this process will require an iterative method, Equation 2.25 is solved for $P_{i,j}$.

$$P_{i,j} = \left(\frac{a_{i+1,j}}{a_{i,j}}\right)P_{i+1,j} + \left(\frac{a_{i-1,j}}{a_{i,j}}\right)P_{i-1,j} + \left(\frac{a_{i,j\pm1}}{a_{i,j}}\right)\left(P_{i,j+1} + P_{i,j-1}\right) \tag{2.26}$$

The coefficients of Equation 2.26 are listed below as Equations 2.27.

$$a_{i,j} = \frac{2r_i}{\Delta r^2} + \frac{2}{r_i\Delta\theta^2} \qquad\qquad a_{i,j\pm1} = \frac{1}{r_i\Delta\theta^2} \tag{2.27}$$

$$a_{i+1,j} = \frac{r_{i+\frac{1}{2}}}{\Delta r^2} \qquad\qquad a_{i-1,j} = \frac{r_{i-\frac{1}{2}}}{\Delta r^2}$$

To solve for the pressure profile, an iterative method was used since the pressure was unknown for all points not in one of the four slots or on the inner or outer boundary. The iterative method selected was the successive over-relaxation method with the mathematical expression shown as Equation 2.28. This method is a variant of Gauss-Seidel method which uses the data recently calculated to help speed up the convergence compared to the Jacobi method that uses only data from the previous iterative step, m. In the case of the successive over-relaxation method, there is an added relaxation factor, Ω, term that can vary the rate of convergence. If the relaxation factor is selected to be 1, the corresponding method mimics that of the Gauss-Seidel method. Normally, for this type of work, the relaxation factor is selected to be less than 1 as to not create a value that would cause the solution to diverge. Since the difference, ε, from one iteration to the next is much smaller compared to using one of the other methods, the maximum absolute discrepancy is usually set to $\varepsilon < 10^{-12}$ compared to $\varepsilon < 10^{-4}$ for the Jacobi method.

$$P_{i,j}^{(m+1)} = \Omega P_{i,j}^{(m+1)} + (1-\Omega) P_{i,j}^{(m)} \tag{2.28}$$

From the produced pressure profile, the generated fluid load and fluid leakage rate can be calculated based on a given film height and fluid viscosity. The pressure profile is a matrix of $(n \times l)$ where n is the number of data points in the radial direction and l is the number of data points in the circumferential direction. The load, W is calculated by integrating the pressure with respect to the surface area of the sealing zone. The equation to calculate the load for the given geometry is given as Equation 2.29.

$$W = \int_{R_{in}}^{R_{out}} \int_{0}^{2\pi} P(r,\theta)\, r d\theta dr \tag{2.29}$$

R_{in} and R_{out} correspond to the radius of the inner and outer boundary of the seal, respectively. A numerical analysis approximation is then applied to the load equation. To help reduce the error of the approximation, Simpson's 2-D Rule is used which requires n and l to be odd numbers and leads to Equation 2.30.

$$W \approx \Delta r \Delta\theta \sum_{i=1}^{n} \sum_{j=1}^{l} \left[S_{ij} P\left(r_i, \theta_j\right) r_i \right] \tag{2.30}$$

Where S_{ij} is the Simpson's 2-D Rule weight matrix where the value is either $1/9$, $2/9$, $4/9$, $8/9$, or $16/9$.

As for the leakage calculation, Equations 2.4a and 2.4b are utilized since the leakage rate per unit length are known as Equations 2.16a and 2.16b. When substituting the Equations 2.16a and 2.16b into Equations 2.4a and 2.4b, the following equations are derived where Q_r is calculated at a constant radius, R, and Q_θ is calculated at a constant θ value since a simplified version of the geometry was designed to exclude the rounded contours of the inlet and outlet slot corners to simplify the calculations.

$$Q_r(R) = -\frac{h^3 R}{12\mu} \int_{0}^{2\pi} \frac{d}{dr}\big(P(R,\theta)\big) d\theta \tag{2.31a}$$

$$Q_\theta(\theta) = -\frac{h^3}{12\mu} \int_{r_{in}}^{r_{out}} \frac{1}{r} \frac{d}{d\theta}\big(P(r,\theta)\big) dr + \frac{h\omega}{2}\left(r_{out}^2 - r_{in}^2\right) \tag{2.31b}$$

Again, using numerical analysis techniques since an iteration of the pressure profile was generated, Equations 2.31a and 2.31b can be approximated as the following equations using

Simpson's Rule or trapezoidal rule depending on the number of data points in the domain $j \in [a, b]$ or $i \in [c, d]$.

$$Q_r(R) \approx -\left(\frac{h^3 R}{12\mu}\right)\left(\frac{\Delta\theta}{\Delta r}\right)\left[\sum_{j=a}^{b} S_j P_{i+1,j} - \sum_{j=a}^{b} S_j P_{i,j}\right] \tag{2.32a}$$

$$Q_\theta(\theta) \approx \frac{h\omega}{2}\left(r_d^2 - r_c^2\right) - \left(\frac{h^3}{12\mu}\right)\left(\frac{\Delta\theta}{\Delta r}\right)\left[\sum_{i=c}^{d} \frac{S_j P_{i,j+1}}{r_i} - \sum_{i=c}^{d} \frac{S_j P_{i,j}}{r_i}\right] \tag{2.32b}$$

For Simpson's Rule, S_j would be either $1/3$, $2/3$, or $4/3$, while trapezoidal rule would be composed of $1/2$ or $2/2$.

In particular, the critical leakage value is the fluid that leaks at the inner and outer radius of the sealing zone which would leak into the environment. To calculate the leakage, $Q_r(r)$ would be evaluated at r_{inner} and r_{outer}. Since the direction of flow is in the positive radial direction, the inner radius would provide a negative value indicating flow towards $r = 0$, the axis of rotation.

The experimental design and procedures will be discussed in the next Chapter.

3. Experimental Design, Setup, and Procedures

3.1 Introduction

This chapter discusses the experimental apparatus and the design of experiment that is implemented to examine the leakage and power loss of different material pairs. This discussion includes improvements in the experimental apparatus and data acquisition systems compared to previous testing programs.

3.2 Tribotesting

3.2.1 Thrust Washer Rotary Tribometer

In this study, a series of experiments are performed using different material pairings through the use of a thrust washer rotary tribometer. To accommodate the rotary valve seal, modifications were made to the tribometer which include the previous modification for implementing fluid flow (Schneider, 2006). The modifications to a Falex Multi-Specimen Friction and Wear Test Machine are shown in Figure 3.1: Modified Falex Multi-specimen Friction and Wear Test MachineFigure 3.1. This tribometer utilizes a 2 HP motor with belt drive and multiple gear combinations to produce spindle speeds ranging from 10-7200 RPM. A redesigned stage was integrated to allow for the use of fluid flow through the seal faces. To monitor the temperature measurements for the rotating test specimen, slip rings on the tribometer spindle were used. A description of the data acquisition and instrumentation capabilities will be provided in section 3.2.3.

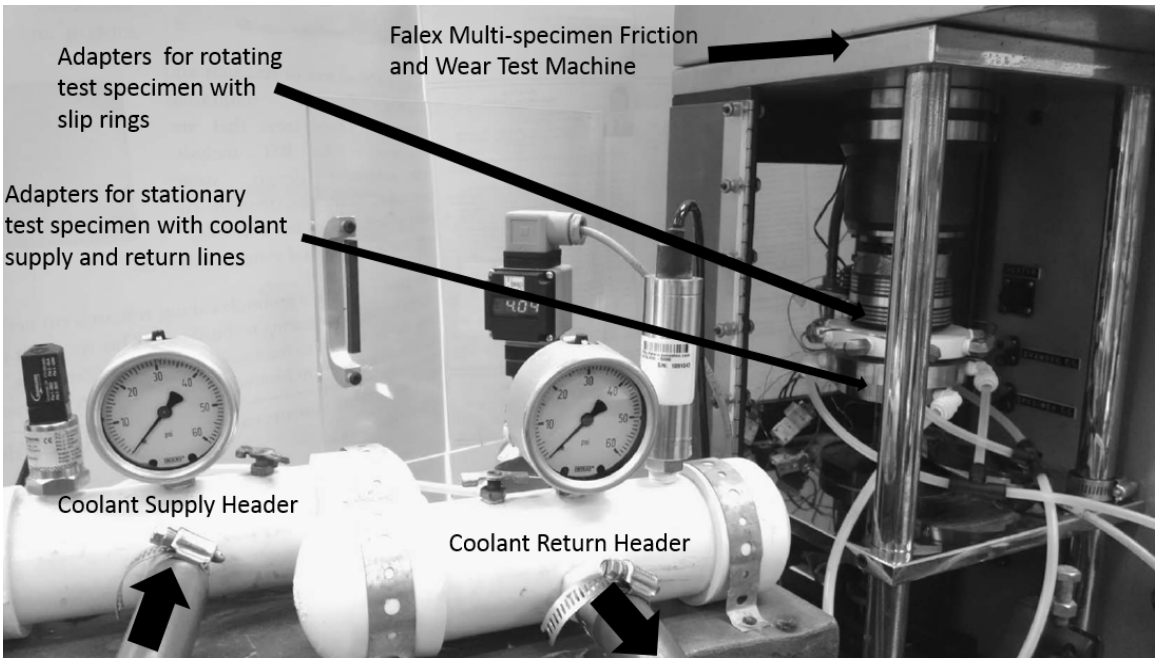

Figure 3.1: Modified Falex Multi-specimen Friction and Wear Test Machine

3.2.2 Test Fixtures and Adapters

The test fixture design involved a single component: a lower adapter. This component provided the supply lines from the coolant distribution (supply) header and return lines to the coolant collection (return) header. The lower adapter, along with inserts for the slots, provided anti-rotation for the stationary seal. Figure 3.2 shows a schematic of the test setup with the lower adapter. An image of the lower adapter with the slot inserts on the stage is provided in Figure 3.3 and Figure 3.4. An elastomer backing was used below the stationary seal to maintain coolant flow path through the lower adapter to the seal, preventing the coolant from escaping at the inner and outer diameters of the static seal, as well as preventing coolant from tunneling from one slot to another.

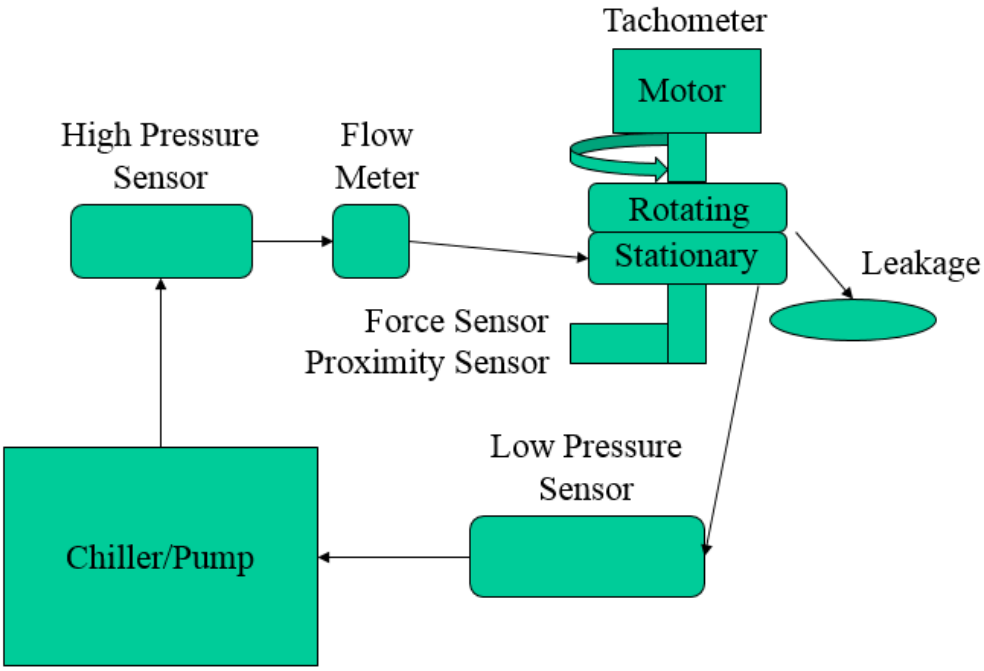

Figure 3.2: Schematic of experimental setup

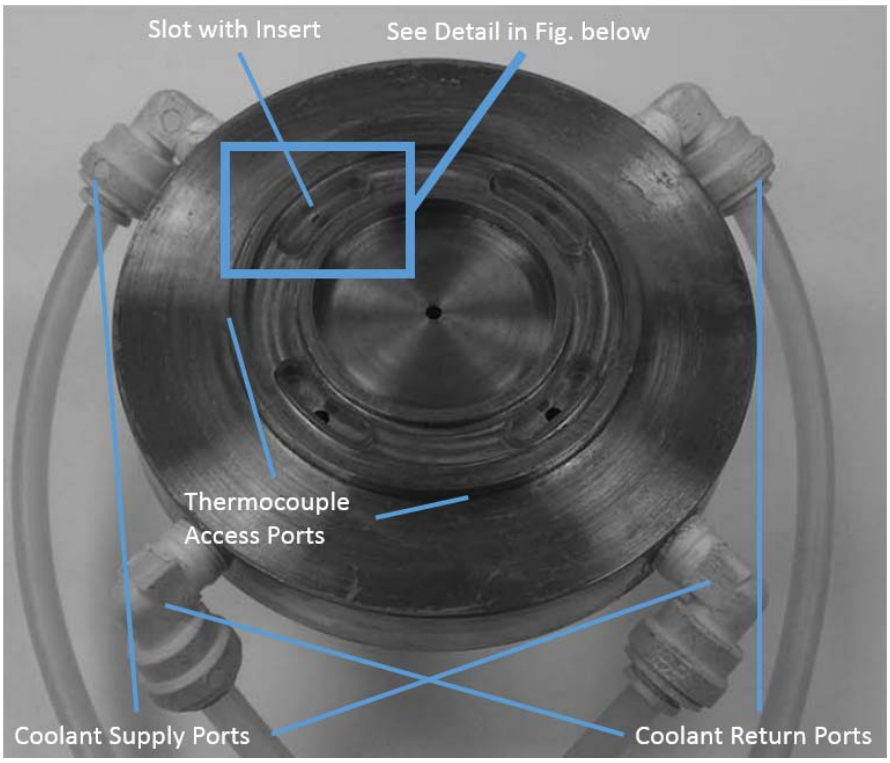

Figure 3.3: The lower adapter with the anti-rotation inserts

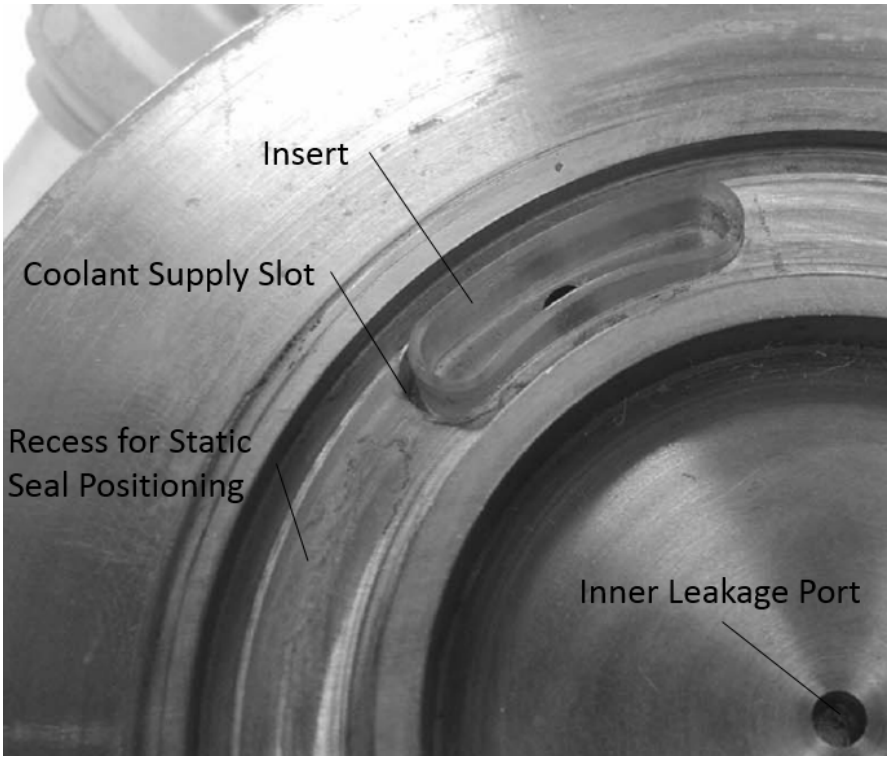

Figure 3.4: Close-up of an anti-rotation insert within a slot

Two chillers were utilized during the experimental testing. The first chiller (Figure 3.5) was used in the initial testing to supply water to the coolant distribution head while the second chiller (Figure 3.6) supplied a mixture of ethylene glycol and water. The header supplied the coolant to two port connectors in the lower adapter. These two port connectors supplied the fluid to the inlet slots. The fluid then passed into the rotating seal face via the timing valve and then passed through a stainless steel tube that lead to a timing valve aligned with an outlet slot. The fluid continued to flow into the lower adaptor where two port connectors channeled the coolant to the return header and then to the coolant reservoir (unit chiller).

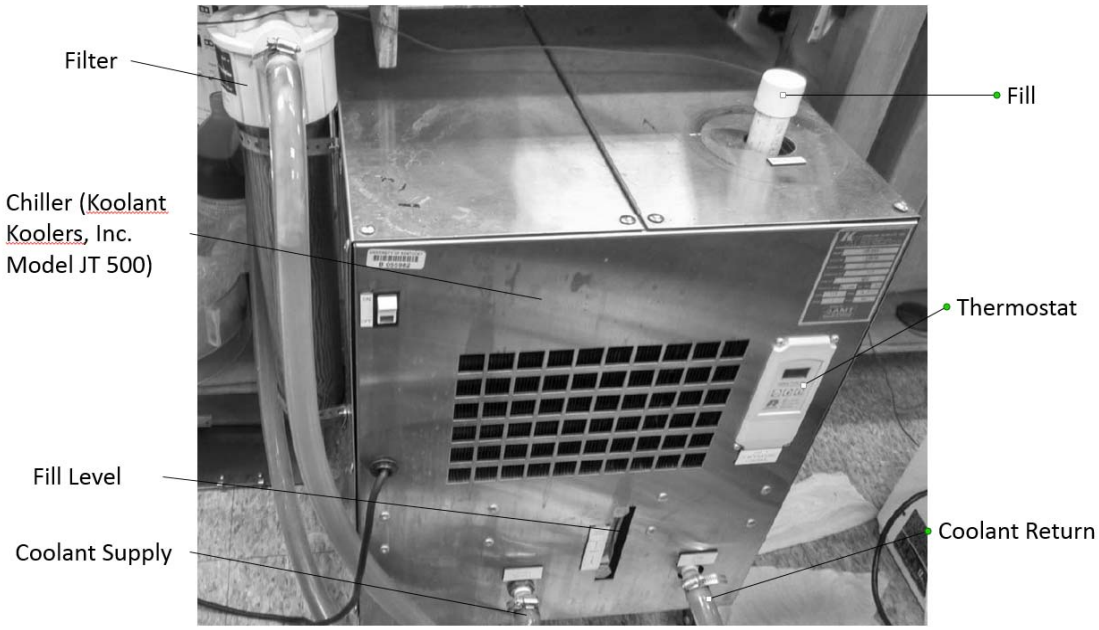

Figure 3.5: Chiller unit with water

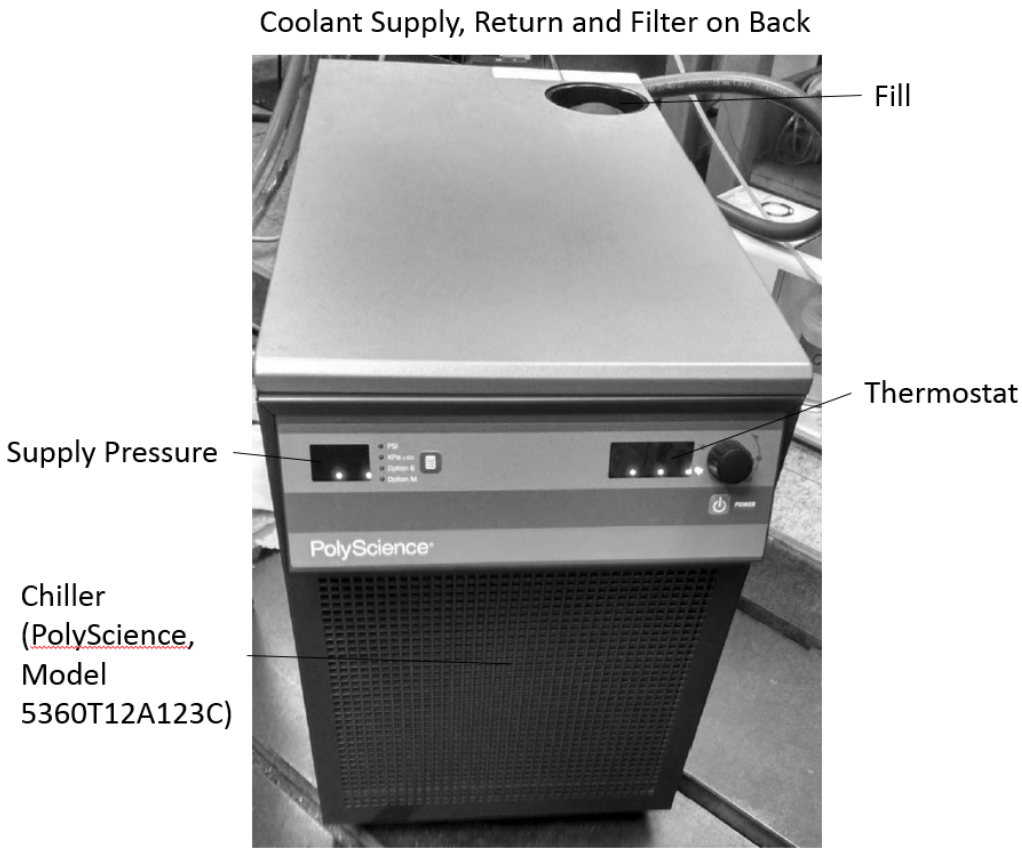

Figure 3.6: Chiller unit with mixture of ethylene glycol and water

3.2.3 Instrumentation and Data Acquisition

Rotational speed, applied load, frictional torque, coolant flow rate, and multiple temperature thermocouples were monitored during each experimental test. Figure 3.2 (schematic of experimental setup) outlines the measurements recorded during each experiment as well as the location of each thermocouple. A tachometer was utilized to monitor the rotational speed and verified with a handheld tachometer while the load was applied through a 2:1 lever system using dead weights. The friction torque was measured by the use of a torque arm attached to a lower section of the stage that contacts a load cell. The coolant was supplied via a chiller, as previously described, and the flowrate was measured using a Pelton wheel flow sensor. Both chillers maintained the coolant temperature within $\pm$1.0°C of the set point. In the water-based experiments, the coolant is passed through a 20 µm, low pressure drop filter to prevent large particles and debris from affecting the sealing surface. This water chiller unit was the same and the flow loop was similar to that described by Hayden in The Heat Sink Mechanical Seal: A Centrifugal Pump Application (Hayden, 2004). The second chiller has a 20 µm, low pressure drop filter after the rotary valve seal and therefore filters the large particles and debris from entering the reservoir. There is also a filter that is used when the reservoir is being filled. The second chiller utilizes a turbine pump rather than the positive displacement pump, but still has a similar flow loop to what was previously mentioned. To automate the system, pressure transducers were installed on the coolant supply and return headers. The temperatures of the rotating and stationary test specimens were recorded via embedded thermocouples located in or near the test seals. Through the use of slip rings, one type K thermocouples in the rotating ring is located 0.10 inches from the interface while two type T thermocouples, 90° apart, are located in the lower adaptor below the static seal and elastomer backing at 0.14-0.26 inches from the interface depending on the geometry of the static seal. An additional type T

thermocouple monitored the test chamber temperature. Table 3.1 summarizes the measurements acquired during each experiment, the method in which the measurement was made, and the accuracy of each measurement.

Table 3.1: Instrumentation, methods of measurements, and accuracy

Measurement	Instrument/Method	Accuracy
Rotational Speed	Tachometer	±9-18 RPM
Applied Load	Bale Rod with 2:1 Lever Arm	±0.1-0.3 lb.
Friction Torque	Load Cell	±0.008-0.05 in.lb.
Rotating Specimen Temperature	Type K Thermocouple	±1.1°C
Stationary Specimen Temperature	Type T Thermocouple (x2)	±0.4°C
Chamber Temperature	Type T Thermocouple	±0.5°C
Coolant Flow Rate	Pelton wheel flow sensor	±0.007 gpm
Wear	Eddy Current Probe System	±38 µm
Inlet Pressure	Pressure Transducer	±0.4%
Outlet Pressure	Pressure Transducer	±0.25%

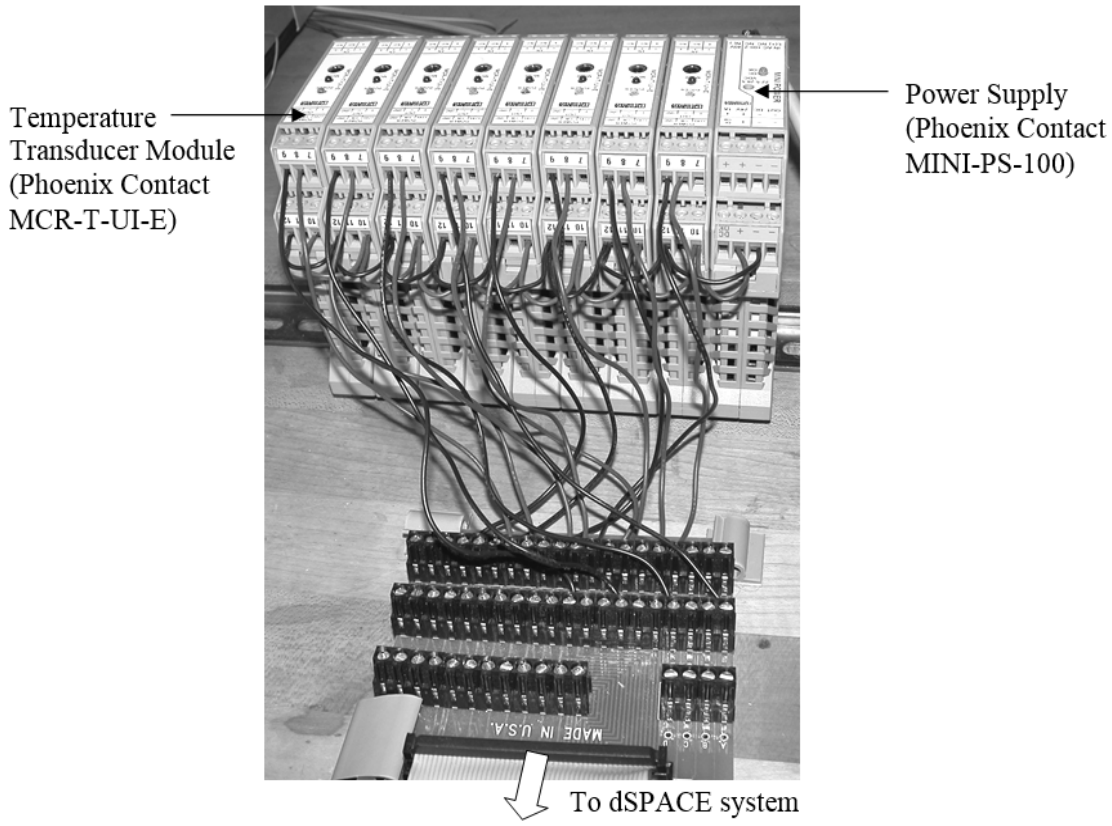

Figure 3.7: Temperature modules (Schneider, 2006)

Data was collected during the experiment through the use of a dSPACE modular system (DS1005 PPC Board, DS2003 Multi-Channel A/D Board, DS 2103 Fast D/A Board) at a rate of one sample per second. Three OMEGA thermocouples were used during each experiment (documented in Table 3.1) utilizing Phoenix Contact Temperature Transducer Modules (MCR-T/UI-E, shown in Figure 3.7). The thermocouples were previously calibrated through the use of the Phoenix Contact Configuration Software (MCR-PI-CONF-WIN). The temperature module outputs a voltage ($\pm$10V) corresponding to the temperature over the user specified temperature range. The sensitivity and offset values that resulted from the auto-calibration procedure were input by the user prior to testing in the data acquisition control center (see Figure 3.8). Similarly, calibration values were input for the tachometer and the friction torque measurements. Through the use of the dSPACE modular system, the friction torque, critical temperatures, fluid

pressures, and flow rate were monitored and test cut-offs established to terminate an experiment on the occasion of especially harsh operating conditions. Figure 3.8 shows the control center of the data acquisition system that was utilized during each experiment.

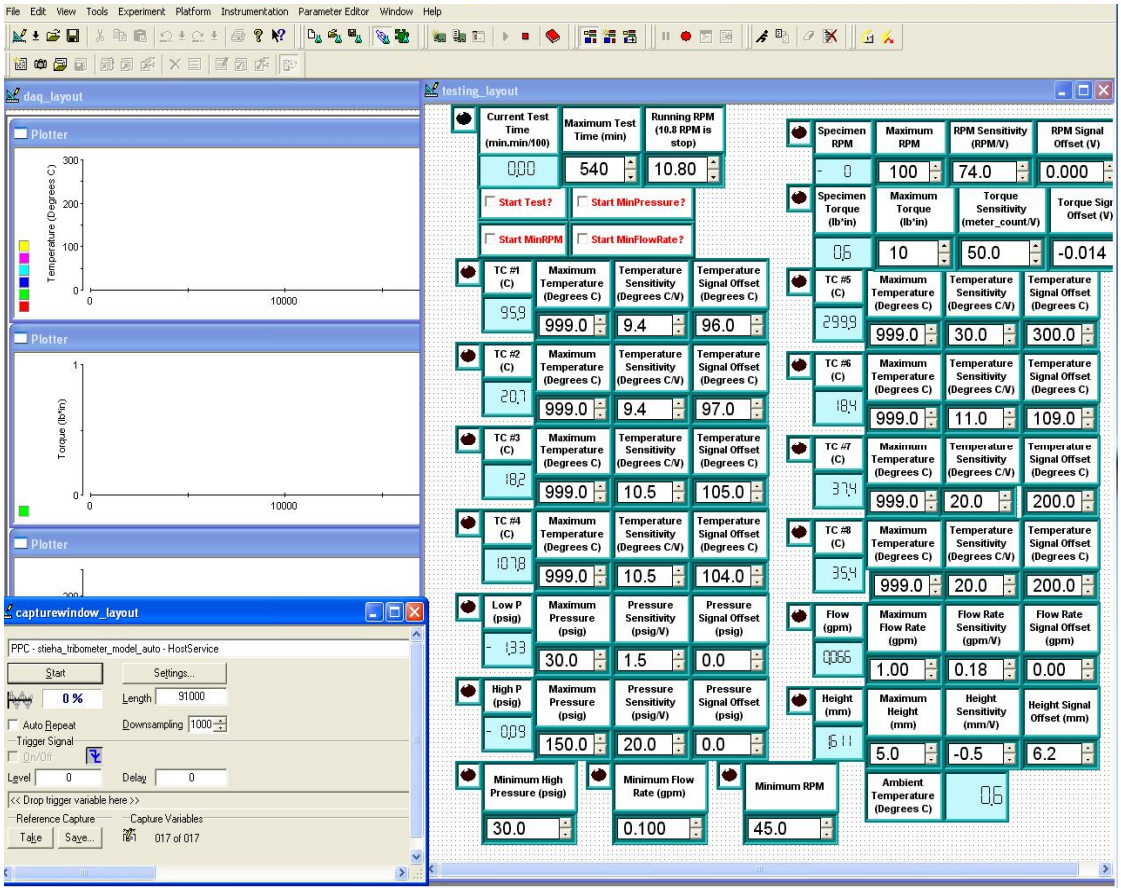

Figure 3.8: Data acquisition control center

An experiment was terminated if the following circumstances occurred:

- The friction torque spikes to large values
- The temperature range of the thermocouples is exceeded (provided by OMEGA and dependent on the thermocouple type)
- The flow rate increases or decreases to outside a given range due to blockage within the fluid path or if the seal excessively leaks

- The high pressure fluid increases or decreases outside a given range due to blockage within the fluid path or if the seal excessively leaks
- The rotational speed increases or decreases to outside a given range

Some of the set points for these critical parameters were established for each experiment in the control center prior to beginning each experiment while others were established after the experimental start-up period. These test cutoff parameters allow for the safe continuous testing of the material pairs.

3.3 Test Materials

In this study, multiple material pairs were examined. Table 3.2 shows the material properties of the materials investigated. To gather materials, consultation with companies for their recommendations were held and investigations of the coefficient of friction of materials were accomplished. For all tests, the softer of the two materials served as the stationary seal unless the test involves the same materials as both sealing surfaces (i.e. DLC vs. DLC). Some of the material pairs were examined because of its use in end face mechanical seal applications. Others were examined for the low frictional torque that would be generated.

Table 3.2: Material Properties of test specimens provided on material data sheets

Material	Description	Thermal Conductivity (W/mK)	Elastic Modulus (ksi)	Tensile Strength (ksi)	Yield Strength (ksi)
PTFE	virgin PTFE	0.25	58-81	4.5	2.86-3.15
PTFEmod	premium grade PTFE modified with a dye providing greater wear resistance	--	--	4.5	--
PTFEwMoly	premium grade PTFE including molydenum disulfide	--	--	4.5	--
PTFEwGlassMoly	PTFE containing 15% glass fiber and 5% molydenum disulfide	0.46	--	2.13-3.13	1.3-3.2
UHMW	UHMW Polyethylene	--	--	6	--
Acetal-Co	acetal copolymer containing a silicon structure on the chain	--	333	8.7	3.3
Delrin	Delrin 150, acetal homopolymer,	0.37	350	10	9
303SS	303 Stainless Steel	16.3	28000	75	30
Bronze	954 Bronze, Aluminum Bronze	58.7	15500	85	32
DLC	Diamond-Like Carbon (DLC) on 4140 steel	--	--	--	--
4140	carbon steel 4140	42.6	30000	95	62

The geometry dimensions of the static and rotary seals shown in Figure 2.1 are provided in Table 3.3 with each material corresponding to the geometry provided. The variation in geometries were related to how the material was manufactured and with respect to the material manufacturer's request. In the case of PTFE, the material was laser cut at GE Appliances from a large stock sheet. This material is flexible enough that a very small load can create a sealing surface. The Delrin is manufactured using a CNC milling machine at the University of Kentucky from a stock cylinder of material. Since this material has a higher stiffness than PTFE, a

larger soft face thickness was utilized for this material to decrease the chance of internal stresses causing the piece to deform and require higher loads to create a sealing surface.

Table 3.3: Geometries of the stationary and rotary test specimens

Stationary Seal Materials and Dimensions	PTFE	modPTFE, PTFEwMoly, UHMW	Delrin, Acetal-Co, DLC, PTFEwGlassMoly
Inner Radius (in)	0.838	0.839	0.843
Outer Radius (in)	1.163	1.160	1.158
Radius to Center of Slot (in)	1.000	1.000	1.000
Slot Angle (deg)	45.00	45.00	45.00
Slot Width (in)	0.200	0.200	0.200
Thickness (in)	0.061	0.059	0.180

Rotary Seal Materials And Dimensions	Delrin, Bronze, SS, DLC, Acetal-Co
Inner Radius (in)	0.750
Outer Radius (in)	1.250
Radius to Center of Ports (in)	1.000
Port Diameter (in)	0.100

Prior to testing, the rotary specimen was lapped using a successively smaller grit size to a polished finish. After polishing, the rotary specimen was then textured through the use of grit paper to get the prescribed surface texture. This procedure will be further discussed in Section 3.5. This procedure can also be used for the static seal, but was considered based on the potential of grit being impregnated into the surface which would then create third body particles that could cause excessive wear. Some static surfaces were tested using a processed surface while others were installed with a manufactured surface. The surface texture can have directionality, isotropic or circumferential, and can vary in R_a and RMS roughness values. Figure 3.9 and Figure 3.10 show a collection of rotary and static seals, respectively, and a sample of a

surface profile obtained from the three-dimensional surface texture analyzer (Zygo NewView 5000 series scanning white light interferometer). Surface profilometry results after the experiments will be presented and discussed in Chapter 4. The data is filtered using MetroPro™ version 8.1.0 software.

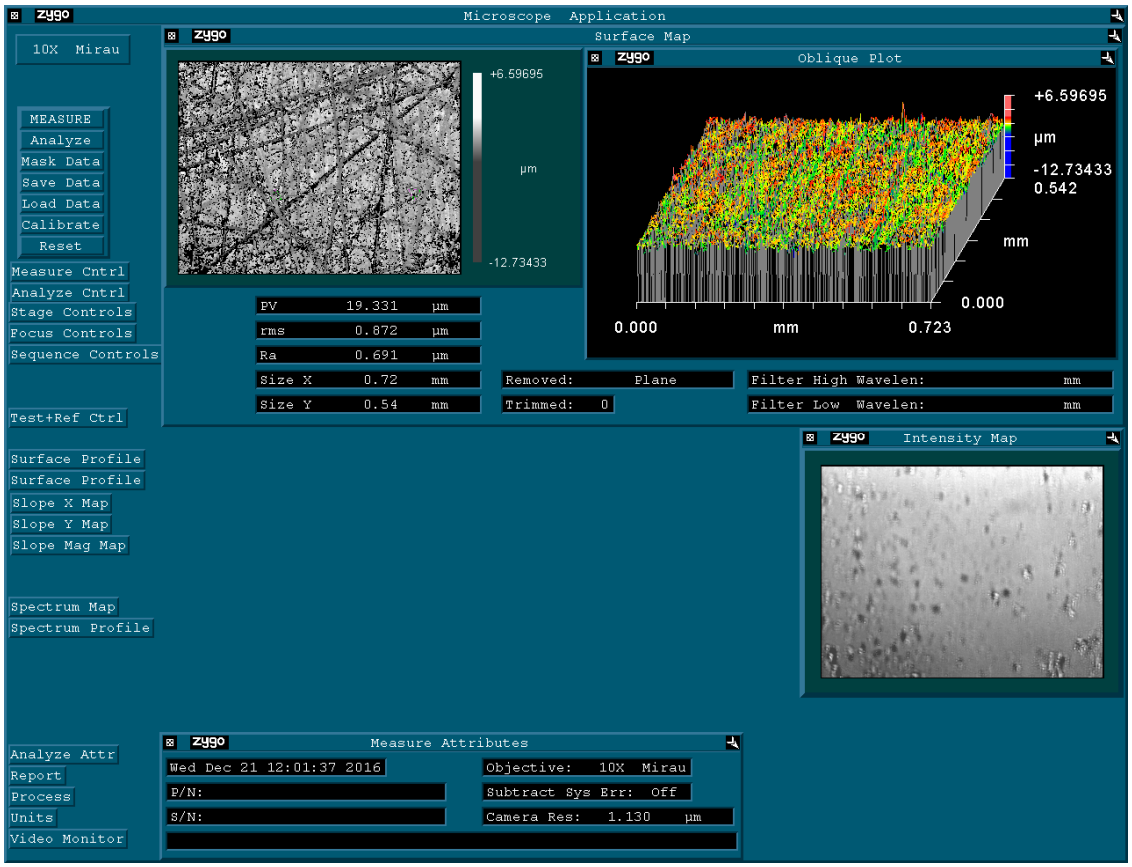

Figure 3.9: Rotary seals and sample starting surface profile

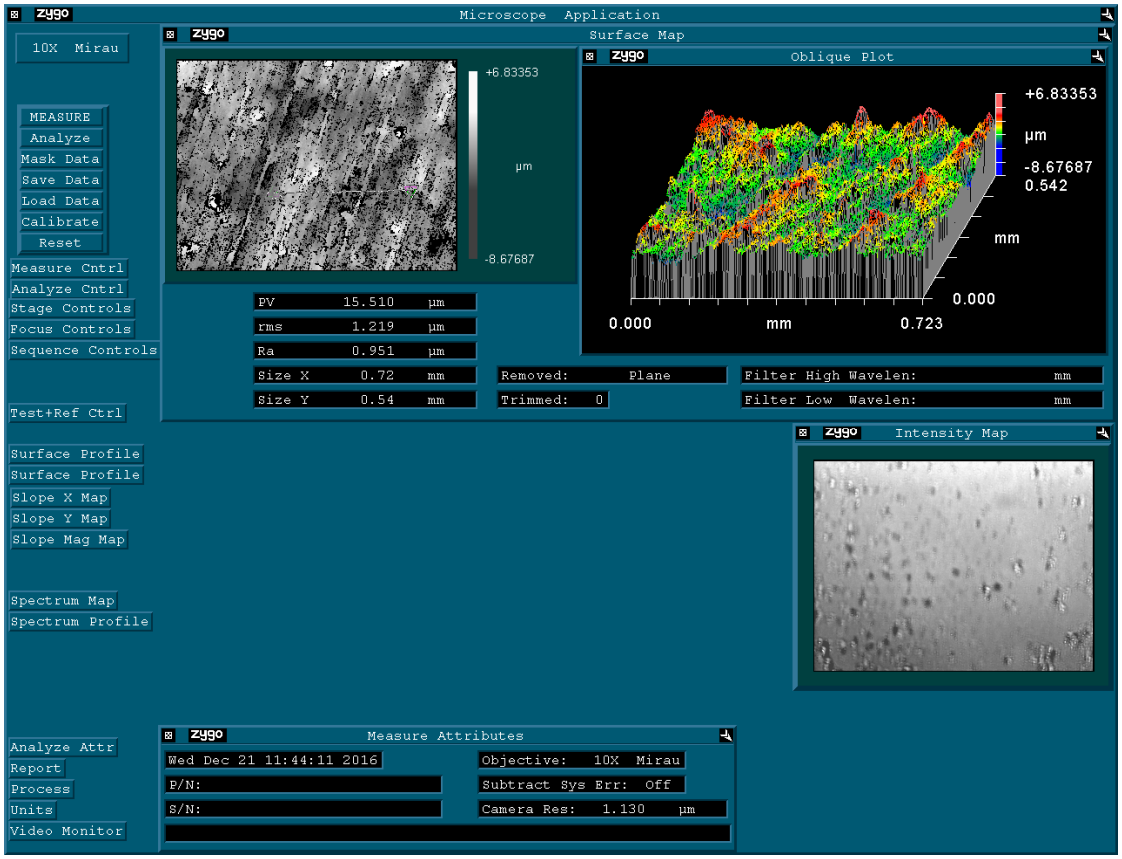

Figure 3.10: Stationary seals and sample starting surface profile

3.4 Experimental Design

In order to determine the impact of the material pairs on the power loss and leakage, a screening process utilizing comparative experimentation was implemented. The comparative objective design of experiment was chosen because the major factor for the experiment is if the material pair can meet the power loss and leakage requirements while considering the wear for a low power sealing application. A screening process was utilized to reduce the time spent on material pairings that did not meet the requirements. This allowed for more testing time for those material pairings that met the requirements or have the potential to meet the requirements.

3.4.1 Comparative Objective

In this study, a comparative objective was implemented in which the power loss, leakage rate, and wear rate were examined. The different material pairings were varied in combination. Within the experimental run, the load was varied to reduce the leakage to the required allowance and/or to within the power loss allowance. As the study continues, length of testing was increased to allow for more data collection and the coolant fluid was varied to examine the outcome of the leakage, power loss, and wear rates.

Table 3.4: Design of Experiment test conditions

Test	Length of Testing	Fluid (set point Temperature)
Phase 1	Approx. 24 Hours	Water (70 degF)
Phase 2	48 Hours or longer	Water (70 degF)
Phase 3	48 Hours or longer	45% Ethylene Glycol/55% Water (20 degF)

3.5 Procedure

Before performing the experiments, the sample must be prepared. Preparation includes attaching the transfer tubes to the rotary seal fixture to allow for fluid to flow through the rotary mount and pre-processing the surface as mentioned in Section 3.3. To remove any major scratches, a large grit dry sandpaper is used to remove the surface containing the scratches by sliding the seal surface across the sandpaper in a figure eight pattern and continuously rotated after multiple passes. This is continued until the scratches are no longer visible. The grit size is then reduced to remove more material from the sealing surface until a smoother surface finish is achieved. The reduction in grit size is continued until a polished surface is achieved. The polishing creates a near flat surface without any high peaks that could cause high leakage. Next, larger grit a new surface is created to meet the desired surface roughness. The surface directionality can be adjusted between isotropic (figure eight pattern) and circumferential

(rotational). The surface is cleaned throughout the process to monitor and prevent any major scratches which would then require the process to start over. If the static seal face requires processing, the same steps are followed as the rotary seal surface. A set number of optical surface profiles were collected from distinct locations shown in Figure 3.11 and Figure 3.12 for the rotary and stationary seal faces, respectively.

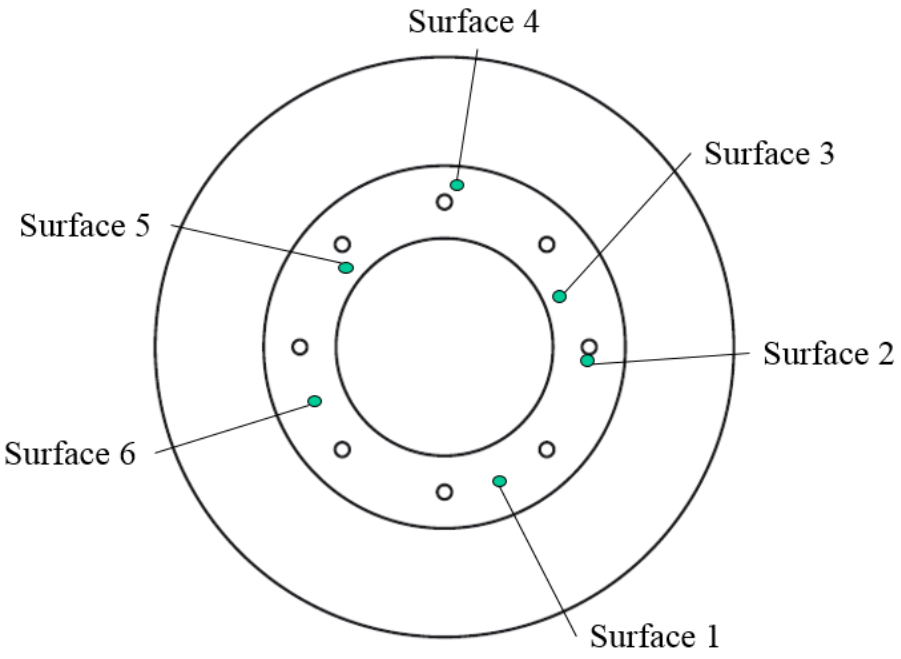

Figure 3.11: Locations of surface images on rotary seal face

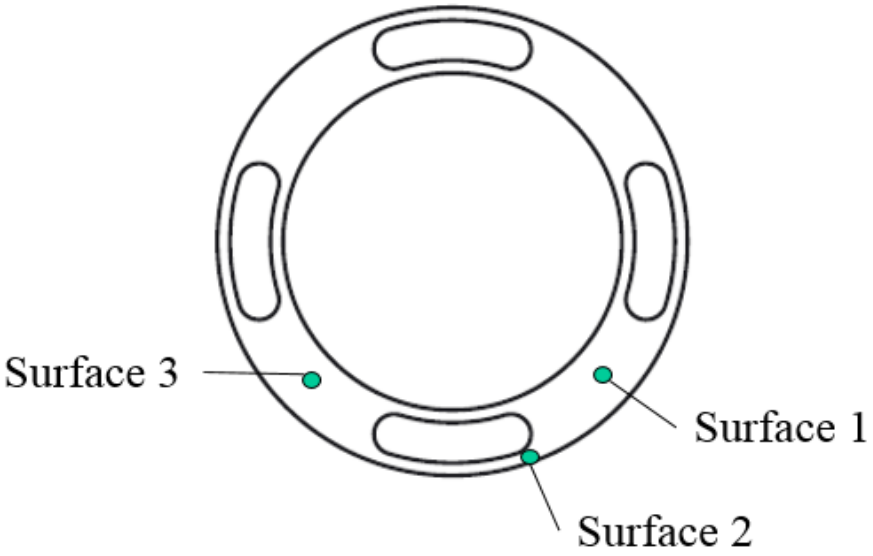

Figure 3.12: Locations of surface images on stationary seal face

3.5.1 Experimental Procedure

For each experiment, the fluid lines were checked to validate that no residual torque is on the system, which would cause incorrect values when calculating the power loss. The following sequence of events generally describes the process that was carried out for each experiment:

1. Prepare test specimens and perform surface characterization (obtain surface profilometry data and measure sample heights using calipers).
2. Install the elastomer backing and stationary seal into the lower adapter and the rotary seal on the upper spindle.
3. Apply starting load and circulate coolant through the flow path and increase the pressure using the bypass valve to achieve the desired inlet pressure.
4. Set the test cut-off parameters and begin acquiring data (see section 3.2.3).
5. Start the test at the desired rotational speed (60 rpm) and turn on the lower limit cut-off parameters.

6. Perform the experiment.
    a. As data is collected, increase or decrease load to help direct the test towards desired results for leakage and power loss.
    b. Save and restart data collection if testing for longer durations (every 24 hours).
7. Save final data, turn off the lower limit cut-off parameters and reduce the rotational speed to 0 to stop the experiment.
8. Reduce inlet pressure by opening the bypass valve and turn off chiller.
9. Remove the applied load and separate the test specimens.
10. Turn off or stop the rest of the equipment (tribometer and DAQ) and allow the system to return to room temperature.
11. Extract the test specimens from the test chamber.
12. Perform surface characterization and process measured data (torque, leakage, wear, temperatures, etc.).
13. Return to step one and perform the next experiment.

3.5.2 Calculations

When processing the data, the power loss, leakage rate, and wear rate are calculated. The power loss is calculated for each experiment using Equation 3.1.

$$P = \omega T \tag{3.1}$$

In this case T, ω, and P represent the average experimental friction torque at a specific load, the rotational speed in radians per second, and power loss, respectively. The leakage rate and wear rate are calculated using Equation 3.2 where the absolute value of the change in measurement is divided by the change in time between the measurements.

$$rate = abs\left(\frac{m_{final} - m_{initial}}{t_{final} - t_{initial}}\right) \quad (3.2)$$

Finally, after each test, both the rotating and stationary specimens are characterized using a three-dimensional surface texture analyzer to examine surface roughness. Next, scanning electron microscopy (SEM) and energy dispersive spectrometry (EDS) analyses are performed to investigate film transfer.

Having provided motivation, seal design and function, a description of the design of experiment, and experimental procedures, experimental results are discussed in Chapter 4.

4. Experimental Results

4.1 Introduction

Chapter 4 provides experimental results for the comparison design of experiment described in Chapter 3. These results have been split into 4 sections. Section 4.2 provides the initial screening results including observations during testing. Section 4.3 presents the second screening data, and Section 4.4 provides the data from the final testing, in which the seals were run under low temperature conditions using a mixture of ethylene glycol and water. Section 4.5 provides the pre- and post-run wear patterns of the seal faces. Finally, section 4.6 presents the results of the first-order model that was derived in Chapter 2.

4.2 Initial Screening Performance

For overall testing, target requirements were developed after a discussion with an industrial partner. For this process to be utilized within a consumer refrigeration system, the operating temperature required is -10 to 110 °F and the sealed fluid is a 45/55 mixture of ethylene glycol in water by weight. The leakage rate requirement was set to be one drop or less of fluid per minute (approx. 6 g/hr) as a puddle of fluid is not desired developing from the application. The power loss requirement was set to less than 4 watts, as this allows the technology to be cost efficient as a replacement to the previous refrigeration units. There was no specific value determined for the wear rate, but based on seals found within the sealing industry a 1-inch linear wear rate over a 10-year life at a continuous 60 rpm was selected, this calculates to be 0.29 microns per hour. During the initial screening performance test, material pairs were tested for approximately 24 hours. Water was used as the liquid coolant, reducing exposure to harmful ethylene glycol, and the temperature was set to 70°F. During the 24-hour testing, the leakage rate was monitored and load was changed if necessary.

A single-factor test was run to validate the use of a specific surface roughness for Dupont's Delrin 150 (further referred to as Delrin) against Dupont's virgin PTFE with respect to the leakage and power loss within the seal. In one test seal, the surface was polished and finished using a 3-micron particle size paper (from LapMaster). The other test seal was finished with the 320 grit sandpaper (average 36-micron particle size, from Norton's Blue-Bak Waterproof products). This single-factor test examined the behavior of the seal surface, examining if it functioned similarly to a hard surface, such as tungsten carbide paired with carbon graphite (Lebeck A. O., 1991) which works best with a smooth surface. Figure 4.1 shows the results of this test when the load was 80 pounds and the surface texture was isotropic for each seal run. For testing, 10000 g/hr denotes a value that was not calculable, such as leakage from spraying. High leakage was observed within 15 minutes of beginning the test on the polished seal face, while acceptable leakage was observed on the seal face that had been finished with the large particle grit paper. Based on the extracted data, the preferred surface was the surface finished with the 320 grit sandpaper. A higher surface roughness, created by using a larger particle size grit paper, would lead to higher leakage rates as evidenced in Chapter 2. The RMS surface roughness for Delrin was measured after using different grit papers and is displayed in Figure 4.2.

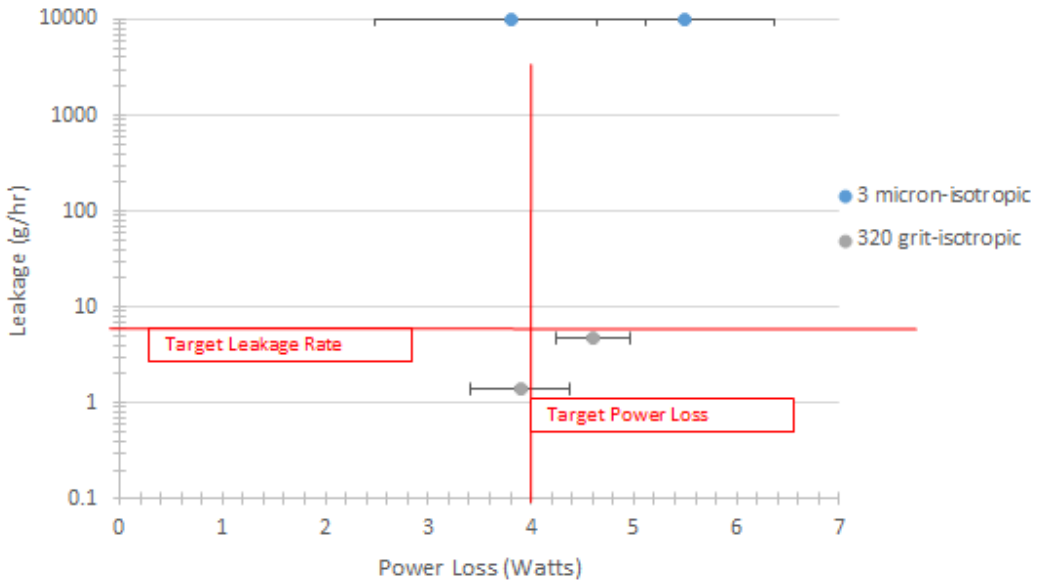

Figure 4.1: Data from surface roughness test for PTFE and Delrin pair

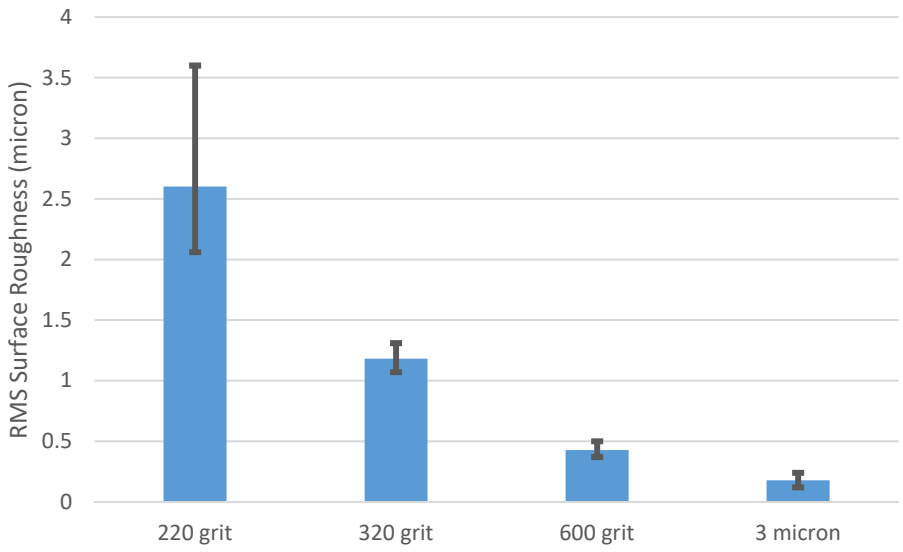

Figure 4.2: Collected raw data from Delrin of RMS surface roughness based on the grit size

Another test was conducted to assess the effectiveness of the two surface textures that can be created: isotropic and circumferential. This assessment used the Delrin and virgin PTFE as the material pairing. The isotropic surface was created by polishing the seal face with 320 grit sandpaper in a figure eight pattern. The circumferential surface was created by attaching the

rotary seal to the Falex system with the sandpaper applied to the surface and rotating the rotary seal face. The results are plotted in Figure 4.3 below.

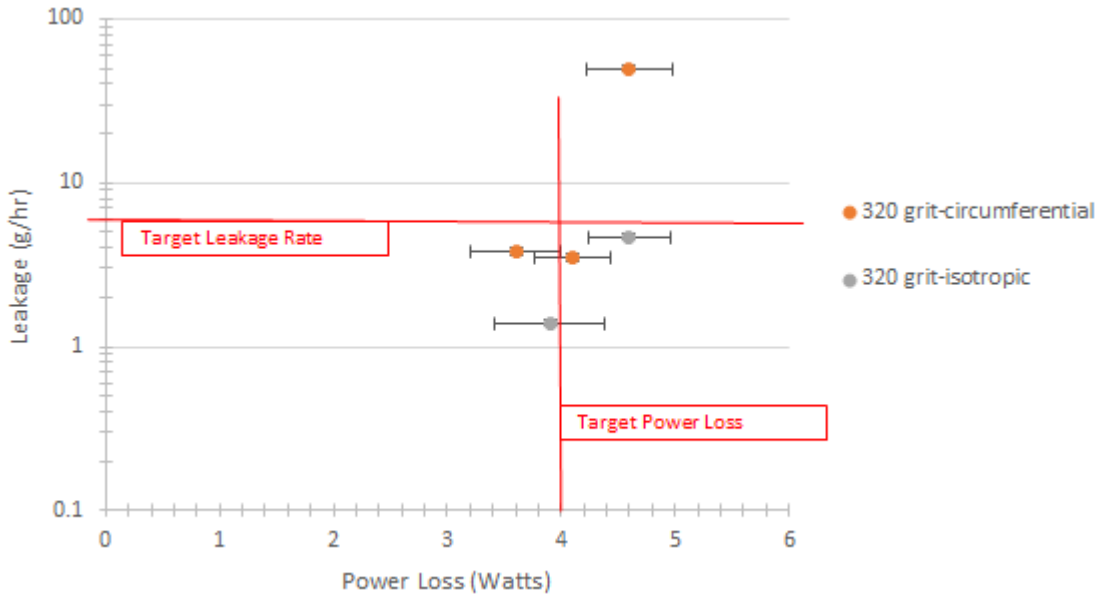

Figure 4.3: Data from surface texture tests for PTFE and Delrin pair

The data suggests the power loss to be approximately the same since the film thickness and actual contact area are within similar values. As for the leakage, outside of the higher leakage data point for the circumferential, the values are in the same magnitude. Since the isotropic seal face achieved a lower minimum value than the circumferential, the isotropic surface texture selected for further testing within this study. An additional reason for the selection of the isotropic surface is that it allows for the seal faces to wear into each other and create unique sealing zones, while the circumferential forces the wearing of specific zones based on the random locations of the peaks and valleys within the seal surface.

Different material pairs were examined during the initial screening. Table 4.1 provides the different material pairings. Each seal pairing was tested multiple times to examine the consistency of leakage rate, power loss, and load requirements. Figure 4.4 provides the data for

a modified PTFE with molybdenum disulfide (PTFEwMoly) and 954 Bronze. The data, combined with previous test data, suggests the requirements will vary from test to test. Figure 4.5 and Figure 4.6 show the material pairings with the best results from the initial screening test.

Table 4.1: Table of testing material pairs (Bolded pairs were not tested during initial screening due to when the materials were obtained)

Stationary Seal Material	Rotary Seal Material
PTFE	Delrin
PTFE	Bronze
PTFEmod	Delrin
PTFEmod	Bronze
PTFEmod	303SS
PTFEmod	**Acetal-Co**
PTFEwMoly	Delrin
PTFEwMoly	Bronze
PTFEwMoly	303SS
UHMW	Delrin
UHMW	Bronze
Delrin	Delrin
Delrin	Bronze
PTFEwGlassMoly	Delrin
PTFEwGlassMoly	Bronze
DLC	**DLC**
Acetal-Co	**Acetal-Co**

Figure 4.4: Testing results of PTFEwMoly and Bronze

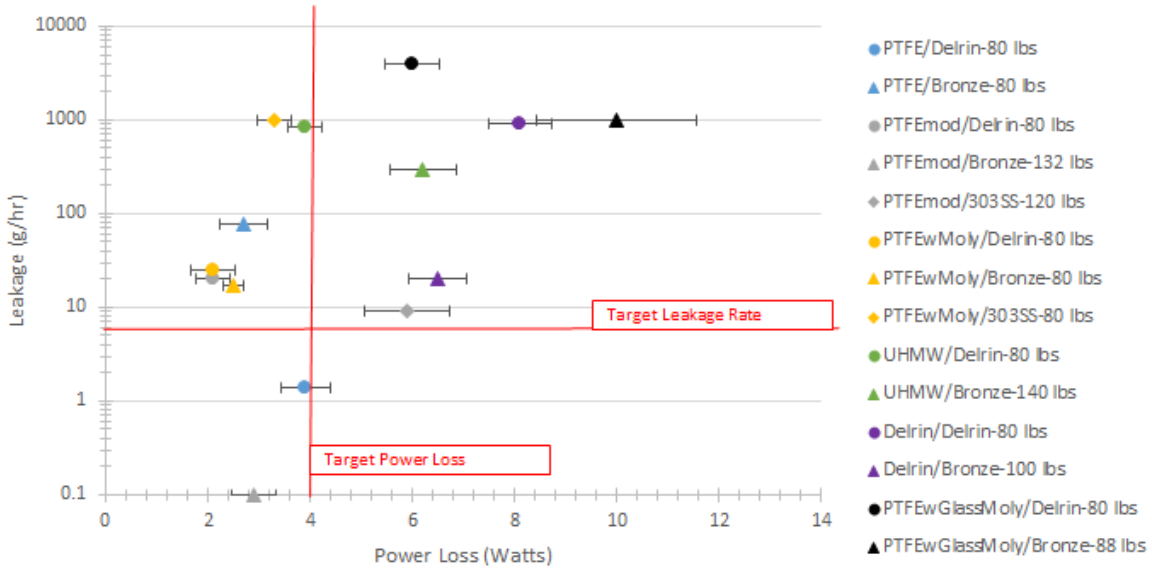

Figure 4.5: Leakage and power loss results of initial 24-hr testing with face load

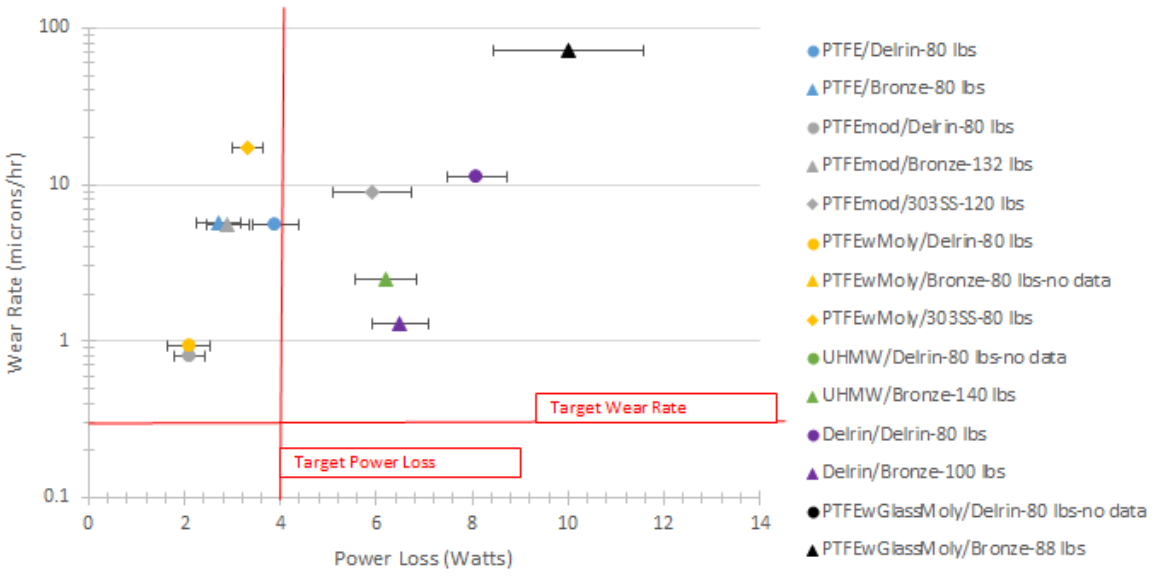

Figure 4.6: Wear rate and power loss results of initial 24-hr testing with face load

Prior to moving in to the extended testing phase, the power loss was initially considered. For the seals to be considered the seals needed to be less than the established power loss limit of 4 watts. Next, the leakage was considered. Technically, for those that did not meet the leakage requirements of 6 g/hr, load could have been increased to help reduce the leakage. But due to the negative impact on power loss, the seals that were well below the target power loss but had higher than the target leakage rate were considered. Another consideration to add with an increased load is the effect on wear rate. With the increase in load, the wear rate would increase. Seals selected for the next testing phase met both the leakage rate and power loss requirements or met the power loss requirement but were within a certain magnitude of the target leakage rate.

Several mathematical Performance Numbers were developed to eliminate the possibility for personal bias. Since a minimum of 4 Watt power loss and 6 g/hr of leakage are targeted, a minimum performance value is desired. The different performance numbers utilized different mathematical functions. One performance number was obtained by multiplying the

power loss by the leakage rate. The two other equations involved sum of the squares where one normalized the power loss and leakage rate based on the sum total of the two numbers and the other was purely the sum of the squares of those two variables. In these calculations, better performance is indicated by a lower value. The results of these calculations are shown in Table 4.2.

Table 4.2: Performance Numbers for each material pair

Materials		Performance Number		
Stationary	Rotary	Multiplier	SOS	Norm. SOS
PTFE	Delrin	5.46	17.17	0.61125
PTFE	Bronze	207.9	5936.29	0.934541
PTFEmod	Delrin	42	404.41	0.828013
PTFEmod	Bronze	0.29	8.42	0.935556
PTFEmod	303SS	53.1	115.81	0.521643
PTFEwMoly	Delrin	52.5	629.41	0.857028
PTFEwMoly	Bronze	42.5	295.25	0.776463
PTFEwMoly	303SS	3300	1000011	0.993443
UHMW	Delrin	3354	739615.2	0.991012
UHMW	Bronze	1860	90038.44	0.960324
Delrin	Delrin	7290	810065.6	0.98232
Delrin	Bronze	130	442.25	0.629761
PTFEwGlassMoly	Delrin	24000	16000036	0.997009
PTFEwGlassMoly	Bronze	10000	1000100	0.980394

Utilizing this data, 5 sealing pairs continued to the extended testing phase: PTFE and Delrin; modPTFE and Delrin; modPTFE and Bronze; PTFEwMoly and Delrin; and PTFEwMoly and Bronze. From the previous figures (Figure 4.5 and Figure 4.6), PTFE and Bronze did not continue because of the large wear values measured throughout testing. The variation in wear rate measured from a low of 5.7 microns per hour for one test to a high of 1169 microns per hour for another. ModPTFE and 303SS were eliminated from the extended testing phase due to power loss and

leakage rates that were higher than the requirements, although this pairing was comparable to other materials based on performance numbers.

The leakage rates and power loss varied widely as the load was increased or decreased, as shown in Figure 4.7. This response will come into contention during the next testing phase as these materials are given more time to run. In the next section, the 48-hour testing data from the extended testing phase will be presented.

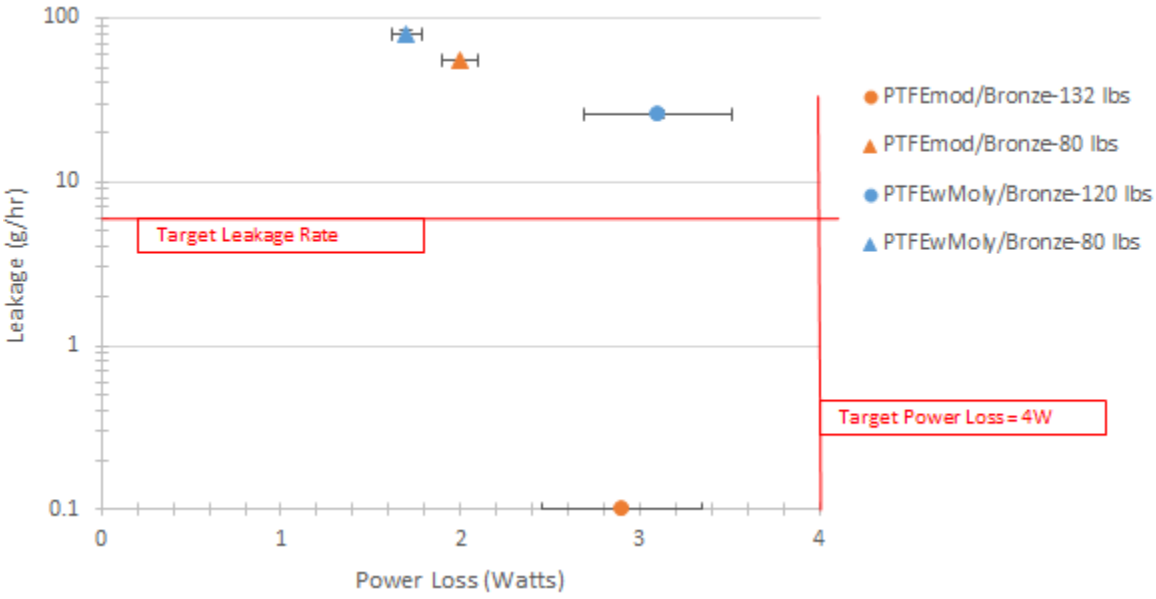

Figure 4.7: Leakage and power loss results for varied face load

4.3 Extended Testing Results

The extended test utilized the same setup as the initial screening, but allowed for the material pairs to be evaluated for a longer period. This testing involved the 5 material pairs that were discussed in the previous section. The test ran for 48-hours or longer if steady state was not reached after the initial 48 hours of testing in order to validate the results. The best results for each material pairing are shown in Figure 4.8 and Figure 4.9. As reported in Section 4.2, continued circumferential wear patterns developed in both the rotary and stationary seal faces.

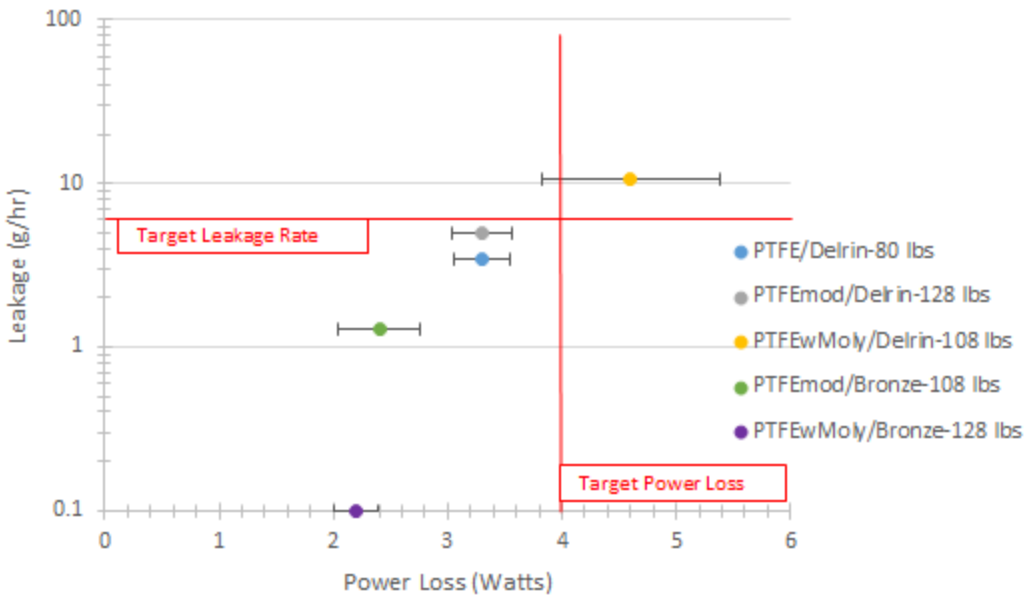

Figure 4.8: Leakage and power loss results of extended testing with face load

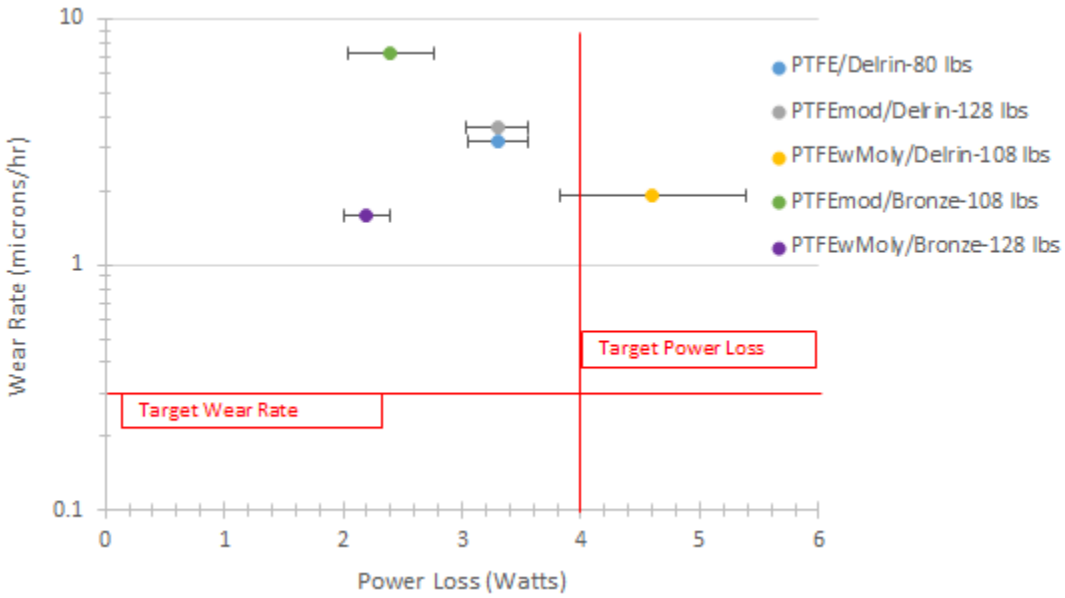

Figure 4.9: Wear rate and power loss results of extended testing with face load

For some of the materials, multiple data points were gathered at different face loads.

Two different sets of PTFE and Delrin paired seals were run at 80 pound face load but each had

different results for power loss and leakage rates. This was also noticed during the initial phase tests. It was observed that the seals shifted into different regions on those pairings that had not previously met the leakage rate requirements but had a low power loss. This shift was mentioned at the end of the previous section and caused the PTFEwMoly and Delrin material pair to be eliminated from the next test phase. The remain pairs moved into the third phase of testing, in which the ethylene glycol and water mixture was used to complete low temperature testing. Section 4.4 discusses these results.

4.4 Low Temperature Testing

In the third phase of testing, the seals were pre-processed as previously done in the other testing phases. The following pairs were examined in the third phase: PTFE and Delrin; modPTFE and Delrin; modPTFE and Bronze; and PTFEwMoly and Bronze. In this phase, the pairs were run for 48-hours, or until steady state was reached after 48 hours frame, under the ethylene glycol and water mixture at a set point of 20 degrees Fahrenheit. It is important to note that an additional variable was present during this phase of the experiment: The outlet slots on theis chiller were not at atmospheric pressure due to the manufacturer recommended filter placement. The slots were at a slightly higher pressure as compared to the water test phases which could cause variation within the results. This will be discussed in the next chapter. The best results for each material pairing are shown in Figure 4.10 and Figure 4.11. Continued circumferential wear patterns developed in both the rotary and stationary seal faces as was noticed in the previous test phase.

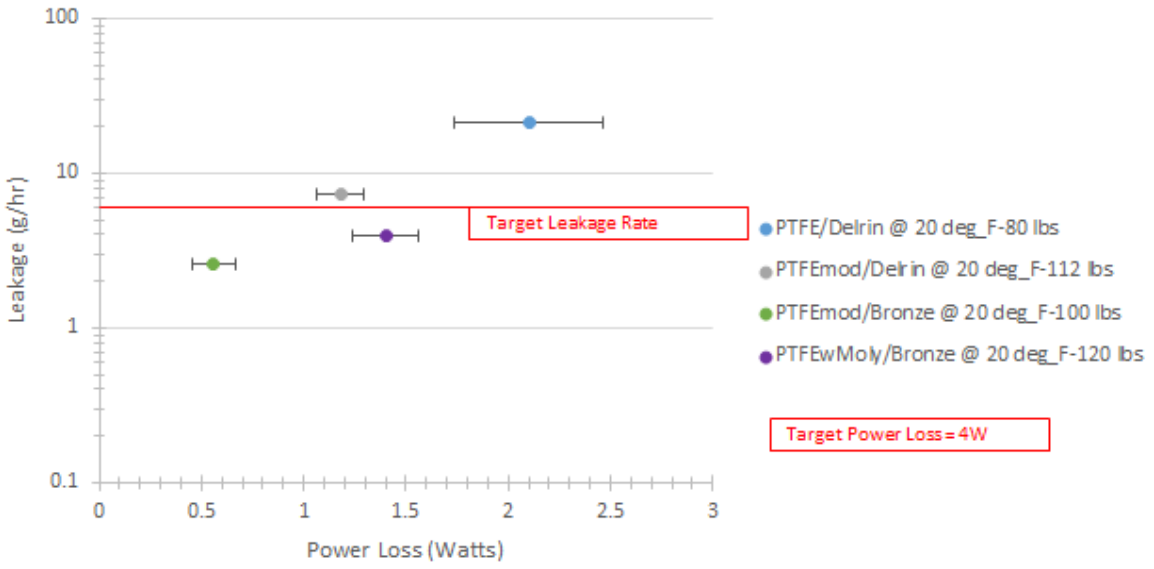

Figure 4.10: Leakage and power loss results of low temperature testing with face load

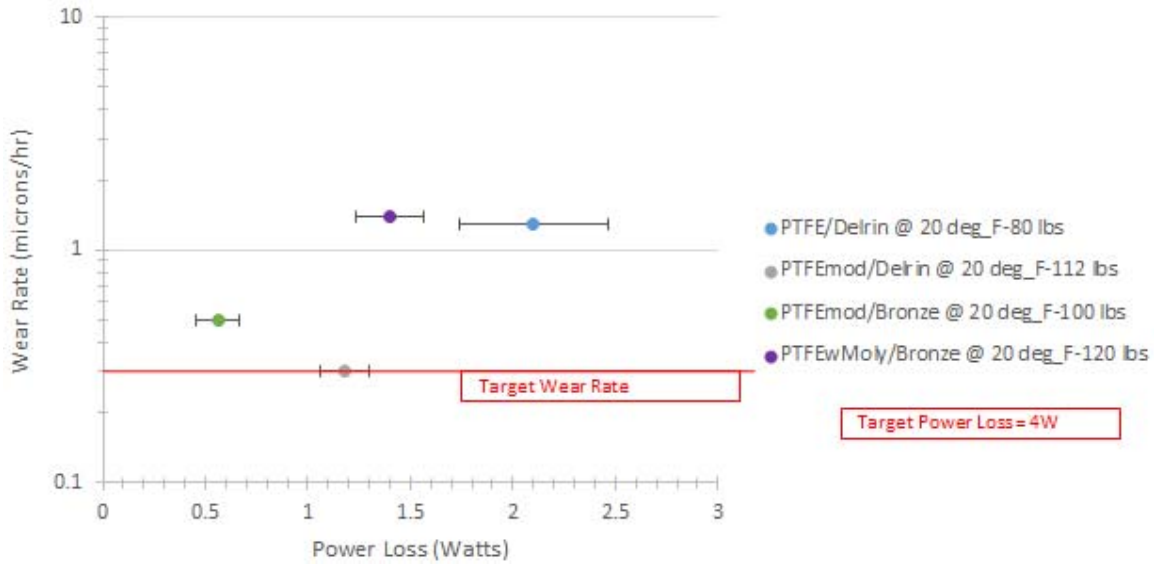

Figure 4.11: Wear rate and power loss results of low temperature testing with face load

During this phase, it was observed that the power loss was not a concern in this phase, the leakage rate became the focal point of the testing. Each seal was tested to get

approximately 6 g/hr leakage rate to reduce the wear rate of the seal faces. The PTFE and Delrin seal pairing was held at a constant load to allow for possible comparisons of previous and future materials. Additional tests were conducted at room temperature to determine the impact of temperature on the outcomes. Leakage rates, power losses, and wear rates are presented in Figure 4.12 and Figure 4.13 below.

Additional face pairings that were tested at room temperature were: DLC and DLC, Acetal-Co and Acetal-Co, and modPTFE and Acetal-Co. The best wear results were from the DLC and DLC pairing, however the power loss and leakage rate were too high when the rotational speed was 60 RPM.

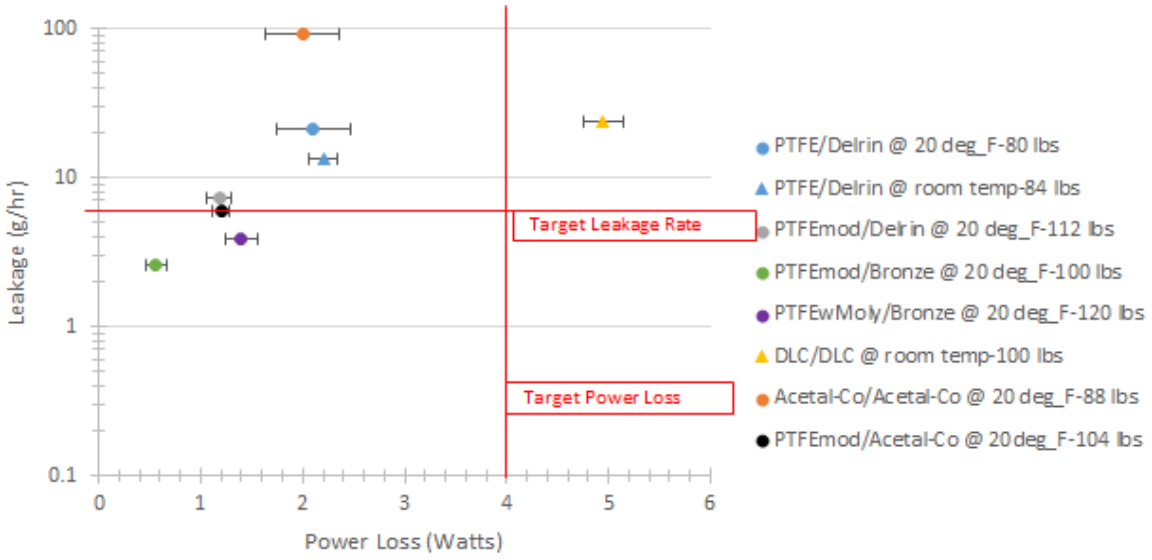

Figure 4.12: Leakage and power loss results of low temperature testing with face load

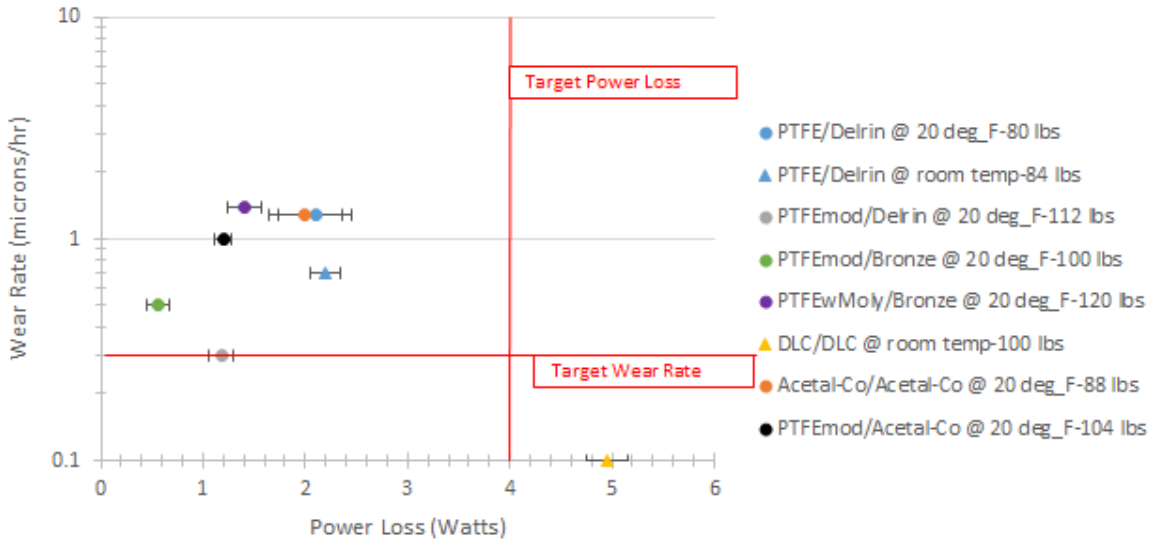

Figure 4.13: Wear rate and power loss results of low temperature testing with face load

The results from the third phase indicate that the pairing of modPTFE and Bronze is the best material pairing to provide a low power loss and low leakage rate. If wear rate was a determining factor, the modPTFE and Delrin would appear to be the best pair, however, upon deeper study, the leakage rate is higher than the required rate and the power loss is approximately twice the loss of the modPTFE and Bronze pairing. Wear of the seals is examined in section 4.5 with the presentation of surface analysis and results from the computational model that will be discussed in section 4.6.

4.5 Pre- and Post-Processing of Seal Faces

In this section, a sealing surface analysis will be presented for the PTFE and Delrin material pair. This seal experienced 24-hours of testing. The results were visibly similar for the other material pairs. Energy dispersive x-ray analysis (EDS) is used to validate a transfer film. Like materials (e.g. Delrin and Delrin) were not examined as the elements of each surface are the same.

Figure 4.14 shows an image of the Delrin rotary seal surface using white light interferometry, mentioned in Chapter 3, with the x- and y-direction signifying the radial and circumferential direction, respectively. This figure shows a pre-run surface with an RMS surface roughness of 1.004 microns. This image show the raw data collected from the scan without any applied filter. The pre-run PTFE is provided as manufactured and shown as Figure 4.15. The RMS surface roughness is 0.767 microns. There is texture directionality that is noticeable and is visible on the rest of the seal face. This texture depends on the x- and y- direction instead of the radial and circumferential, so as the seal is rotated to examine other locations, the texture also rotates.

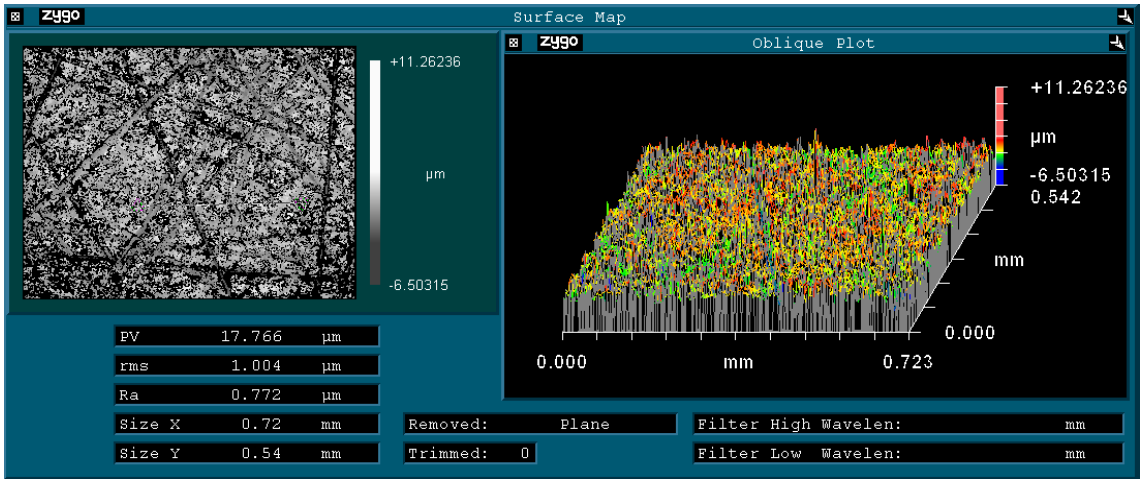

Figure 4.14: Pre-run Delrin rotary surface displayed in MetroPro 8.1.0 program

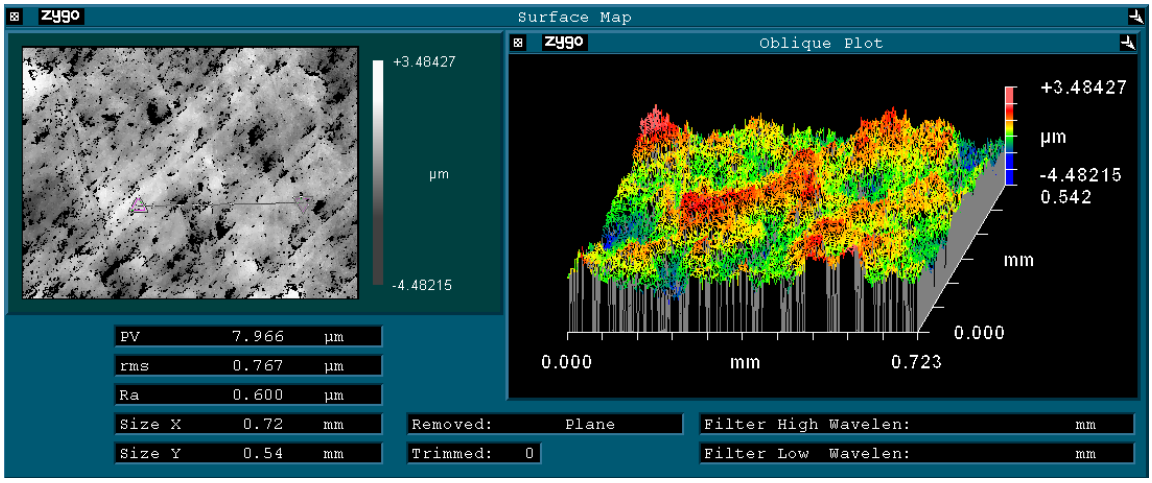

Figure 4.15: Pre-run PTFE stationary surface displayed in MetroPro 8.1.0 program

After the testing, the Delrin was measured in the same region as prior to the run. Thed images are presented in Figure 4.16 and Figure 4.17. The wear that occurred created a noticeable track in the surface in a circumferential direction and has also started to wear away the isotropic surface. When paired with the stationary PTFE seal face, a softer material, the Delrin created a circumferential pattern across the majority of the surface of the PTFE seal face within the 24-hour run time. This can be seen in Figure 4.17. When these surfaces are mated, the grooves will align. This sealing surface is critical in decreasing external leakage through the development of sealing zones near the inner and outer radius of the seal.

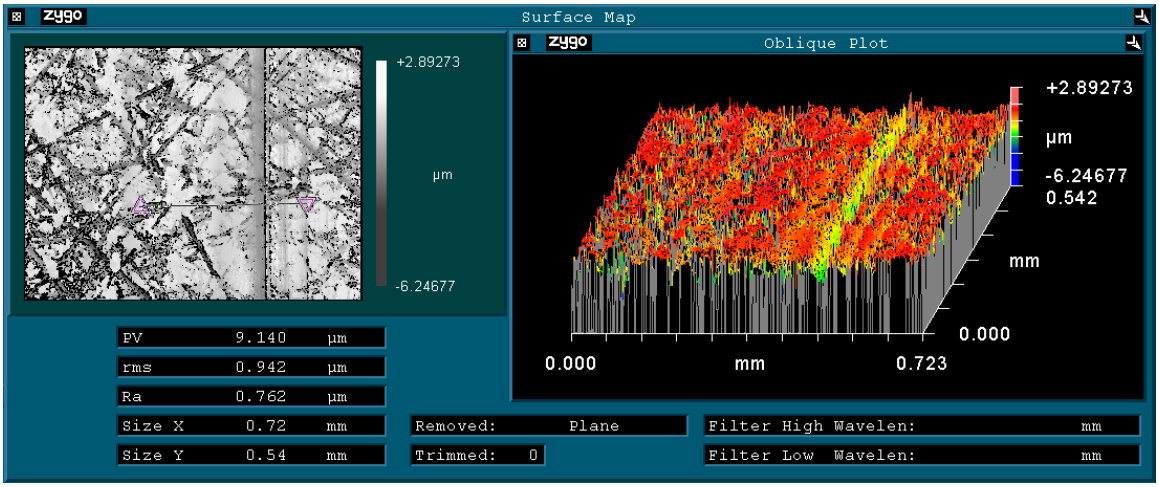

Figure 4.16: Post-run Delrin rotary surface displayed in MetroPro 8.1.0 program

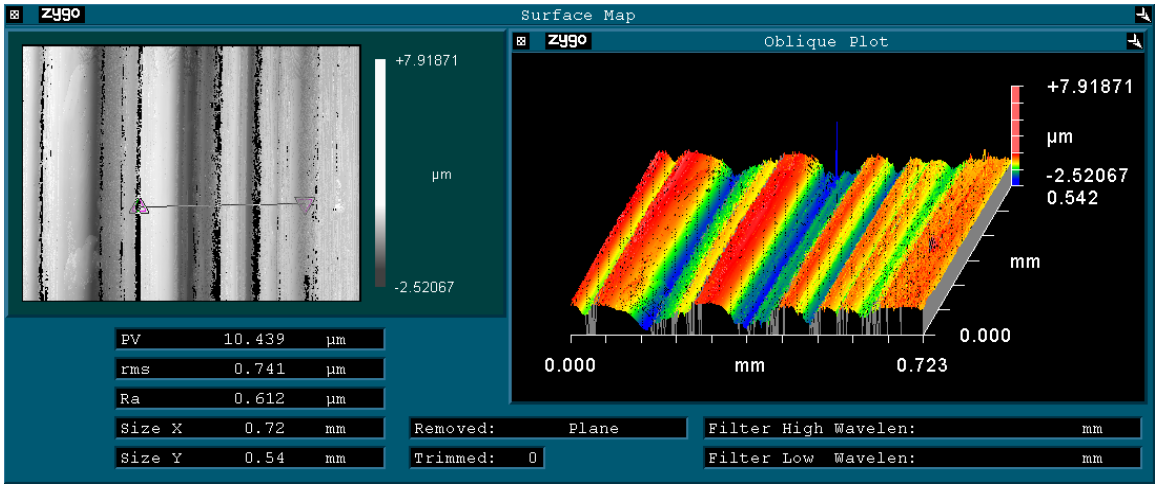

Figure 4.17: Post-run PTFE stationary surface displayed in MetroPro 8.1.0 program

To further examine the sealing surfaces, a scanning electron microscope (SEM) with EDS was utilized to look at the elements and see if there were any noticeable film or particle transfers. Samples were prepared with copper tape and gold-palladium sputtering on the surface. This prevents the surface from becoming charged from the high beam voltage, which would cause the SEM image to be of a low quality. It also allows for non-metallic surfaces to be visible within the SEM. Film transfer was not expected on the PTFE, as it was the softer of the two face materials. For the opposite reason, film transfer was expected to occur from the PTFE to the Delrin. To help distinguish the results it is important to know the composition of each material. The PTFE compound is C_2F_4 while Delrin is $(CH_2O)_n$. When examining the Delrin surface, evidence of Fluorine will indicate a transfer. When examining the surface of PTFE, presences of hydrogen and oxygen will indicate a transfer. Due to the limitations of the EDS, hydrogen is not visible on the spectrum, so oxygen must be used to evaluate the film transfer. The results for the PTFE surface are shown in Figure 4.18. The analysis suggests that there was no transfer film from the Delrin to the PTFE, as was expected.

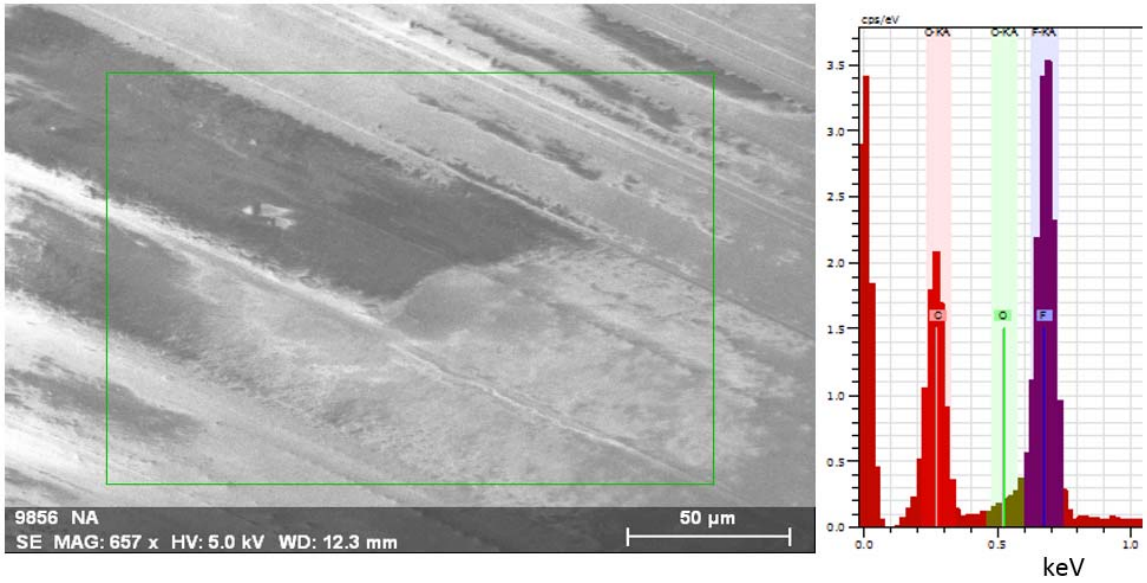

Figure 4.18: SEM image with EDS analysis of the stationary PTFE seal surface. (Seal 7)

The results of the Delrin surface are shown as a color map on the SEM image in Figure 4.19. When examining the figure, a noticeable piece of PTFE can be seen laying on the surface and others that appear to be embedded or attached to the surface. This data was taken near the edge of the inner radius of the seal since the rotary seal has a smaller inner radius than the stationary surface. In Figure 4.20, EDS is examined within the sealing zone where fluorine is visible within the image and on the inner edge (bottom right-hand corner) where the surfaces did not contact during the testing phase. The non-contact region did contain fluorine, but this is most likely contributed due to the wear particles of the PTFE being displaced from the sealing zone. Figure 4.21 and Figure 4.22 show the results and the elemental composition of each zone.

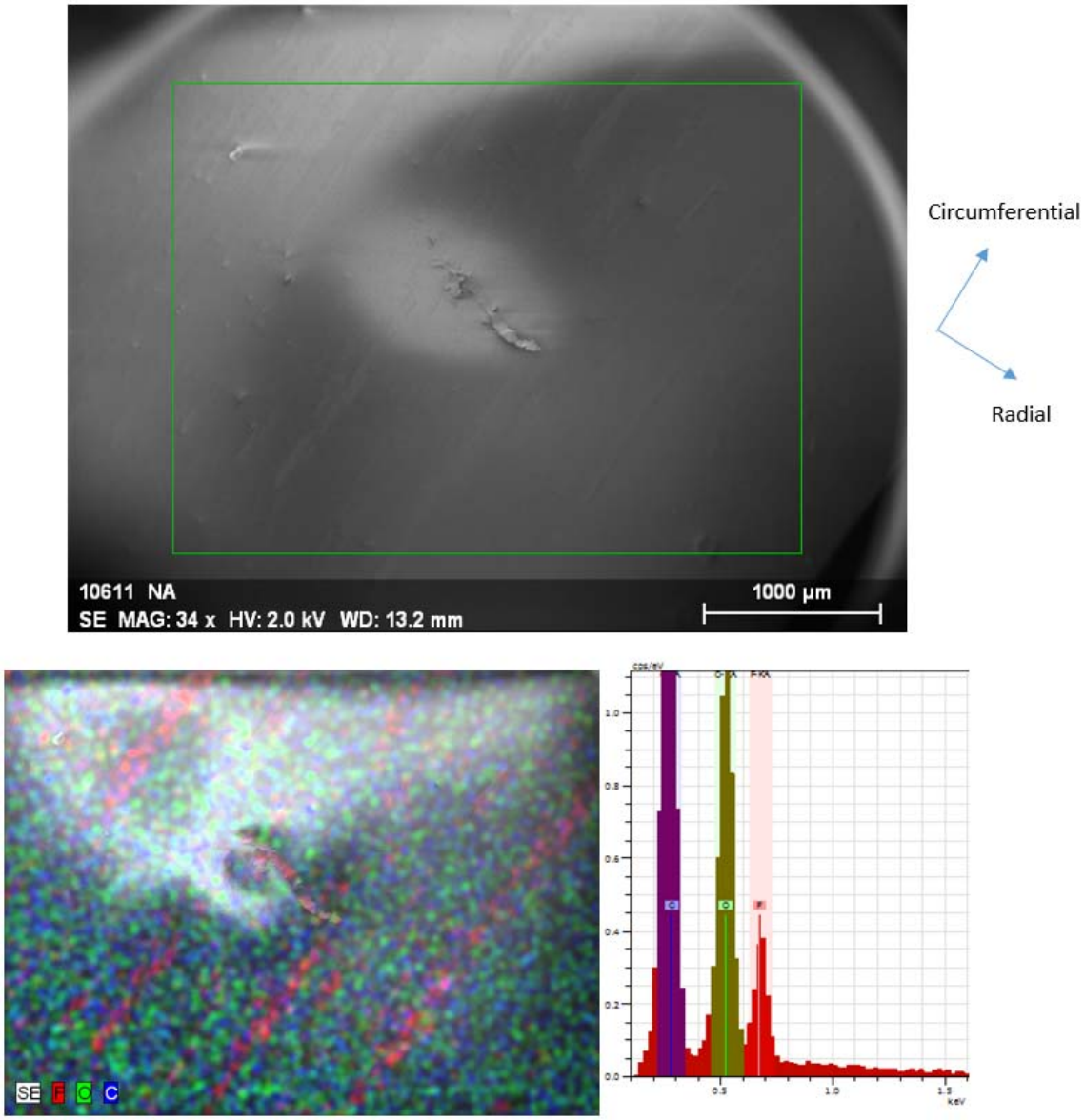

Figure 4.19: SEM image and SEM image with EDS analysis of the rotary Delrin surface.

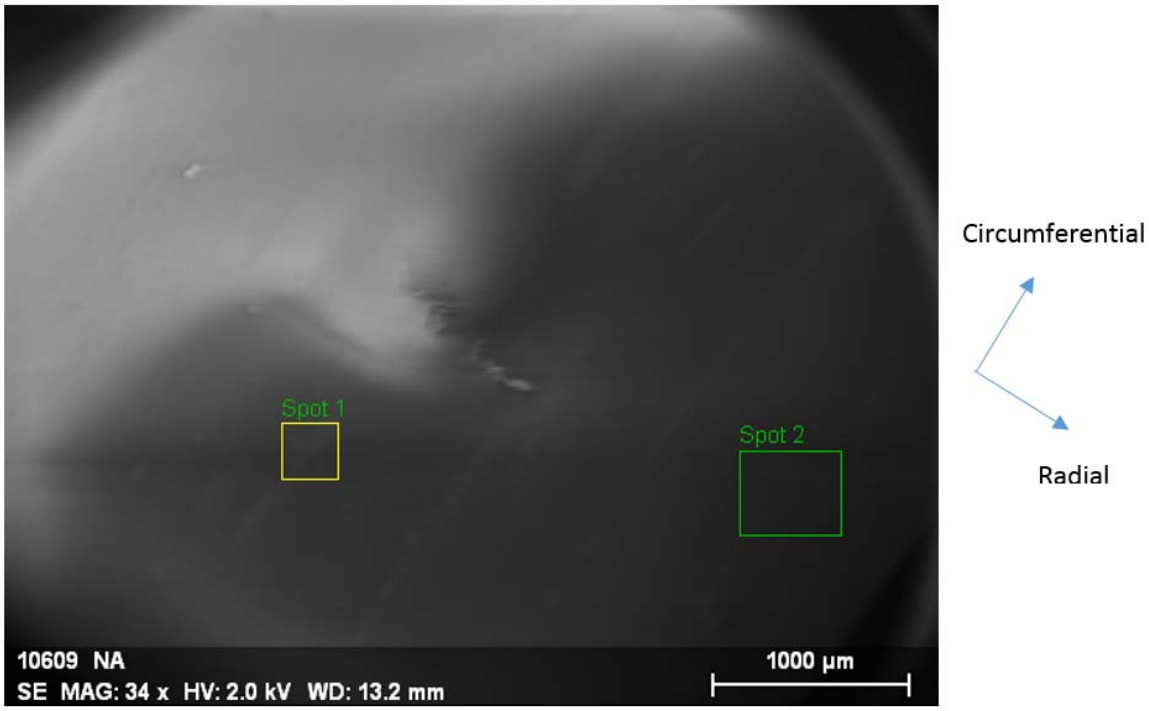

Figure 4.20: SEM image with locations of contact (Spot 1) and non-contact areas (Spot 2).

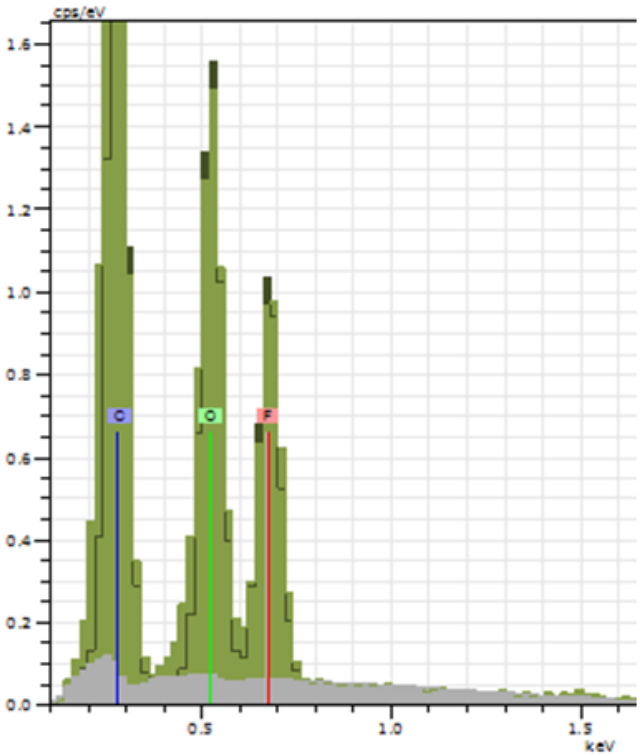

Spectrum: Spot 1

Element	Series	unn. C [wt.%]	norm. C [wt.%]	Atom. C [at.%]	Error (3 Sigma) [wt.%]
Fluorine	K-series	30.78	30.78	24.31	13.83
Oxygen	K-series	34.57	34.57	32.41	14.67
Carbon	K-series	34.65	34.65	43.28	13.88
	Total:	100.00	100.00	100.00	

Figure 4.21: EDS results for Spot 1 in Figure 4.20.

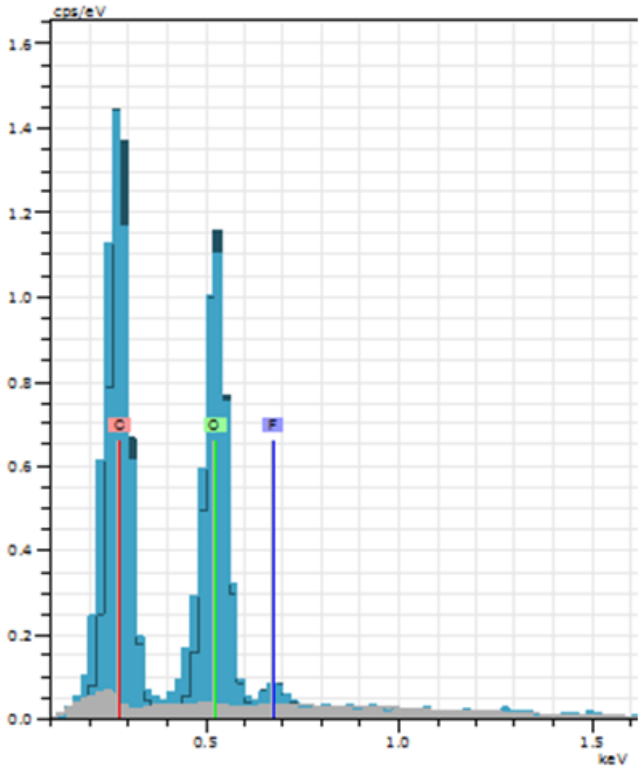

Spectrum: Spot 2

Element	Series	unn. C [wt.%]	norm. C [wt.%]	Atom. C [at.%]	Error (3 Sigma) [wt.%]
Carbon	K-series	41.83	41.83	49.17	17.07
Oxygen	K-series	54.56	54.56	48.15	22.79
Fluorine	K-series	3.60	3.60	2.68	3.03
	Total:	100.00	100.00	100.00	

Figure 4.22: EDS results for Spot 2 in Figure 4.20.

4.6 First-Order Model Results

Based on the mathematical model developed in Chapter 2, the predicted pressure profile is able to provide an insight into the load generated by the fluid. This predicted pressure profile, presented in Figure 4.23, uses an inlet pressure of 50 psi and an outlet pressure of 0 psi, the same as what was used in the first two phases of testing. Due to the increase in outlet pressure in the third phase of testing, Figure 4.24 was generated with the same 50 psi inlet pressure but 2 psi as the outlet pressure.

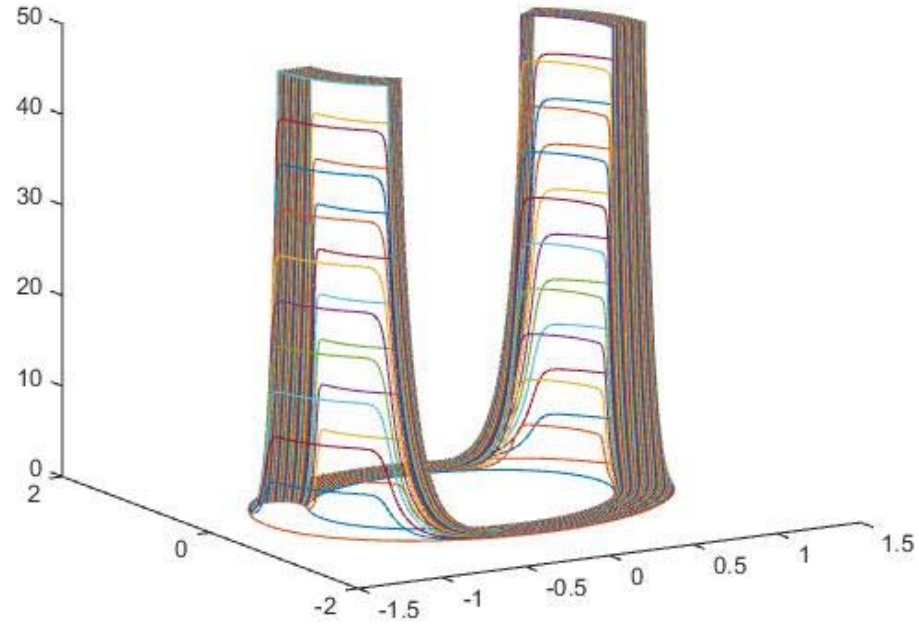

Figure 4.23: Predicted pressure profile for 50 psi inlet and 0 psi outlet

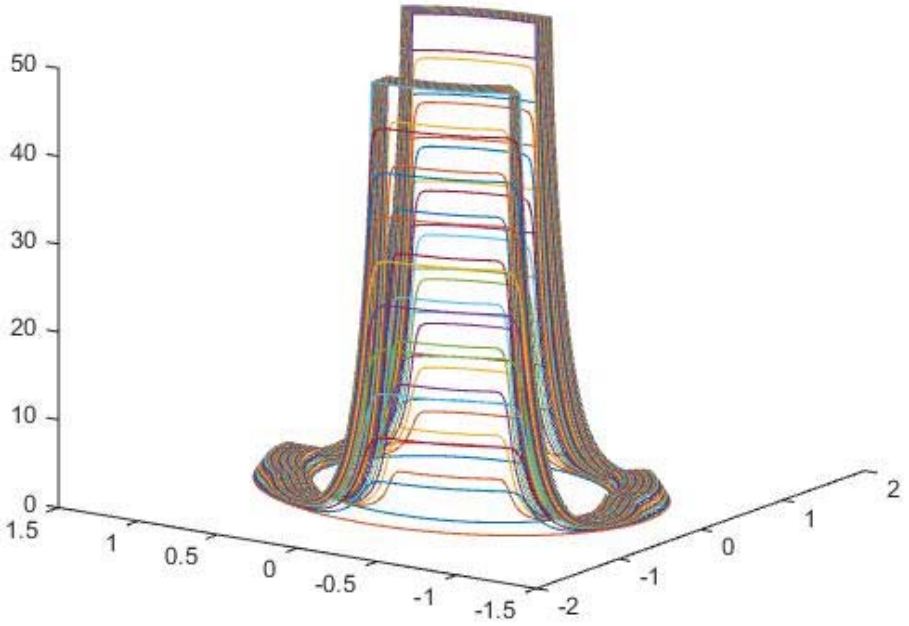

Figure 4.24: Predicted pressure profile for 50 psi inlet and 2 psi outlet

Table 4.3 shows the different number of data points in the radial and circumferential directions and the load results that were calculated for each based on 0 psi outlet pressure. The number of circumferential data points were dictated by the number of radial data points to create a grid that is of approximately equal lengths as the circumferential is considered to be an arc length. If the model that is based on two parallel flat surfaces is to have a leakage of 6 grams per hour, the film thickness is predicted to be 1.000 microns for water at 70 degrees Fahrenheit. For 45% ethylene glycol in water at 30 degrees Fahrenheit, the film thickness is predicted to be 1.870 microns.

Table 4.3: Computational Results with approximate run time using a Dell Optiplex 790 (Figure 4.23 and Figure 4.24 are 51x1001)

Radial	Circumferential	Predicted Load (lbs)	Run Time
11	201	24.50	Seconds
21	401	24.82	Minutes
51	1001	25.10	Days
101	2001	25.13	Over A Week

With this data, the lubrication regime can be predicted based on the sealing surface and the predicted film thickness. Chapter 5 will provide an in-depth discussion on the results of the sealing test along with the predicted lubrication regime.

5. Discussion and Analysis

Chapter 5 provides a discussion of the results that have been presented in Chapter 4 with regards to seal performance. The seal wear will be examined through the study of the predicted lubrication regime.

5.1 Seal Performance

From the initial screening test, there were material pairs that met the required leakage rate and power loss. These material pairs were modPTFE/Bronze and PTFE/Delrin. Using the performance numbers, those material pairings that did not meet the leakage ratebut had low power loss were considered for the extended phase of the testing. Using this data, modPTFE and Delrin, PTFEwMoly and Delrin, and PTFEwMoly and Bronze pairings were added to the second phase of testing, creating a work sample of 5 different pairings. During the second phase of testing, the seals were run for at least 48 hours.

After the 48-hour testing, it was determined that PTFE and Delrin, modPTFE and Delrin, modPTFE and Bronze, and PTFEwMoly and Bronze met both the power loss and leakage rate targets that were required to advance this research for product application. As the load was increased and leakage rate decreased, PTFEwMoly and Delrin experienced a high power loss, causing this material pair to be removed from further experimentation. This loss can be seen in the previous chapter in Figure 4.8.

A basic comparison of results can be made from the data gathered in the final phase of testing due to the close proximity of the leakage rate. The best performance related to power loss and leakage is the modPTFE and Bronze material pairing. This produced approximately 50% less power loss than the next competing seal. The wear rate of the modPTFE and Bronze material pairing is concerning but the value is within the magnitude of the desired wear rate. If

the results were based purely on wear rate and power loss, the final low temperature phase testing shows modPTFE and Delrin to be a considerable material. The leakage rate for modPTFE and Delrin was at 7.3 grams/hour with a wear rate of 0.3 microns/hour while the modPTFE and Bronze were at 2.6 grams/hour with a wear rate of 0.5 microns/hour. The best wear results were achieved with DLC and DLC, a material pairing already in use in the end face mechanical seal community. However, this material pair did not meet the power loss and leakage requirements.

5.2 Lubrication Regime

The lubrication regime is very important when considering the power loss of the system as the lubrication regime provides the type of torque that is being generated. There are three types of lubrication regimes: boundary lubrication (contact is the major factor), hydrodynamic lubrication (fluid shear is the major factor) and mixed lubrication (both contact and fluid shear are considered). Patir and Cheng (Patir, 1978) discussed the implications that $h/\sigma < 3$ is in the partial (mixed) lubrication regime where h is the film thickness and σ is defined by Equation 5.1 where σ_1 and σ_2 are the root mean square roughness of the two surfaces. With the advancement of technology, rather than finding the RMS of a line, it can now be solved for a surface which provides an even better approximation for the surface.

$$\sigma = \sqrt{\sigma_1^2 + \sigma_2^2} \tag{5.1}$$

This regime implies that the boundaries or surfaces are in contact and therefore power loss would take into account not only that generated by the fluid, but also the torque caused by the interaction of the asperities in contact.

The model provides a first order approximation of the fluid load capacity and leakage rate. The predicted film thickness 1.000 microns for water at 70 degrees Fahrenheit. For 45%

ethylene glycol in water at 30 degrees Fahrenheit, the film thickness is predicted to be 1.870 microns. Table 5.1 provides the h/σ for each of the best results previously discussed in each of the phases. Notably, all except one seal meets the mixed lubrication regime requirement mentioned by Patir and Cheng (Patir, 1978). The PTFEwMoly (PTFE with molybdenum disulfide) and Bronze pair run in the final study provided a 4.397 ratio which would imply a hydrodynamic lubrication regime where the surfaces do not contact, yet a circumferential wear pattern was still visible for this material pair test which suggests contact still occurred.

Table 5.1: Lubrication regime study (h is based on the film thickness to provide a leakage rate of 6 grams/hour)

Phase 1	Fluid Temp (°F)	σ (microns)	film thickness (microns)	h/σ	Max Sq
PTFE/Delrin	70	1.253	1.000	0.798	1.376
PTFE/Bronze	70	0.574	1.000	1.741	0.607
modPTFE/Delrin	70	0.651	1.000	1.536	1.052
modPTFE/Bronze	70	0.572	1.000	1.749	0.841
modPTFE/303SS	70	0.852	1.000	1.173	1.680
PTFEwMoly/Delrin	70	0.935	1.000	1.069	1.232
PTFEwMoly/Bronze	70	0.547	1.000	1.829	0.753
PTFEwMoly/303SS	70	0.626	1.000	1.599	1.162
UHMW/Delrin	70	1.741	1.000	0.574	1.869
UHMW/Bronze	70	1.893	1.000	0.528	2.577
Delrin/Delrin	70	2.730	1.000	0.366	7.406
Delrin/Bronze	70	0.620	1.000	1.613	0.723
PTFEwGlassMoly/Delrin	70	2.399	1.000	0.417	8.081
PTFEwGlassMoly/Bronze	70	1.158	1.000	0.864	2.975

Continuation of Table 5.1

Phase 2					
PTFE/Delrin	70	1.967	1.000	0.508	3.250
modPTFE/Delrin	70	0.683	1.000	1.465	1.042
PTFEwMoly/Delrin	70	0.551	1.000	1.816	0.900
modPTFE/Bronze	70	0.518	1.000	1.930	0.777
PTFEwMoly/Bronze	70	0.985	1.000	1.015	1.778
Ethylene Glycol Phase					
PTFE/Delrin	30	4.337	1.870	0.431	4.326
PTFE/Delrin	70	1.093	1.411	1.291	1.103
modPTFE/Delrin	30	0.949	1.870	1.971	1.189
modPTFE/Bronze	30	0.695	1.870	2.689	0.872
PTFEwMoly/Bronze	30	0.425	1.870	4.397	0.588
DLC/DLC	70	1.166	1.411	1.210	0.989
Acetal-Co/Acetal-Co	30	1.846	1.870	1.013	4.173
modPTFE/Acetal-Co	30	1.240	1.870	1.508	1.341

The model predicted the load generated by the fluid to be approximately 25 pounds and the minimal load that was used within the presented experimental data was 80 pounds, a 55-pound difference. In order to account for the 55 pounds, it can be inferred that the surfaces were in contact with each other and, therefore, created the surface wear.

5.3 Seal Life

After examining the predicted lubrication regime and the results from the experimentation, a prediction of expected lifetime of the seal can be predicted. In the case where a ½" thick ring is manufactured and a duty cycle of 50% is assumed (common duty cycle for a compressor-based refrigerator) the expected life of the different material pairs can be calculated. The results are shown below in Table 5.2.

Table 5.2 Life expectancy approximation of a 0.5" seal based on experimental wear rate data

Material Pair	Average Wear Rate (micron/hr)	Time to Failure (years)
PTFE/Delrin	1.3	1.1
PTFE/Delrin	0.7	2.1
modPTFE/Delrin	0.3	4.8
modPTFE/Bronze	0.5	2.9
PTFEwMoly/Bronze	1.4	1.0

If the duty cycle were to be doubled to 100%, the predicted time to failure would be about half that displayed in Table 5.2 but if the thickness were doubled to 1", the predicted time to failure would be twice as long. On these results, at ½" thickness, the seal pairs would predictably fail before the desired 10 year life. For applications that are less than 5 year life expectancy or even less than 2 years, some of these pairings could be utilized to reduce the power loss experienced from the seal.

5.4 Geometric Analysis

A geometry study using the code developed to predict film thickness was conducted to consider the slot angle, slot width, and the seal radius. To conduct an experimental study testing various geometry differences was cost prohibitive and would be time intensive.

To examine the potential effects of these geometric changes, the generation of the power loss must be used. The energy loss of the seal is due to the torque that is generated between the friction force of the surfaces in contact and the shearing of the fluid between the surfaces. The power loss can be written as Equation 5.2 where F_n is the normal force, f is the coefficient of friction, R_{avg} is the average radius of the seal, and ω is the rotational speed in radians/sec (Lebeck A. O., 1999).

$$P = F_n f R_{avg} \omega \tag{5.2}$$

The coefficient of friction is a combination of the hydrodynamic and contact effects. Therefore the power loss can be rewritten as Equation 5.3.

$$P = \left(f_{fluid} + f_{contact}\right)F_n R_{avg}\omega = P_{fluid} + P_{contact} \tag{5.3}$$

From Newton's Postulate and the assumptions made in Chapter 2, the power loss due to fluid can be rewritten and calculated as Equation 5.4, where A is the surface area of the seal face.

$$P_{fluid} = \frac{\mu}{h}\left({R_{avg}}^2\omega^2 A\right) \tag{5.4}$$

For this study, the geometry layout of the PTFE and Delrin pairing contained four slots and sealing width distance from the inner seal radius to the outer seal radius was held constant. The selected fluid was 45% ethylene glycol in water at 30 °F, the fluid film thickness was based on a leakage rate of 6 g/hr, a rotational speed of 60 RPM, a face pressure of 38.8 psi to create sealing between the seal faces, and the fluid pressure was 50 psi and 0 psi for the supply and return slots, respectively. From this data, Equation 5.4 was calculated for each data point. From the experimental results and the calculation based on the PTFE paired with Delrin, a contact friction coefficient was calculated using Equation 5.5.

$$f_{contact} = \frac{\left(P_{experiment} - P_{fluid}\right)}{F_n R_{avg}\omega} \tag{5.5}$$

This contact coefficient of friction was calculated to be 0.052. One consideration or limitation of this calculation is that this coefficient of friction is not an independent variable but a function of the rotational speed, contact area, film thickness, and many other factors and could change for each geometry within this study. For simplicity, this coefficient of friction value was used for each of the data points in this analysis.

For the first geometry analysis, the slot angle was examined. In this study, the slot angle was varied from 15° to 75° with 45° being used in the experiment. The results are shown in Figure 5.1: Analysis of various slot angles.

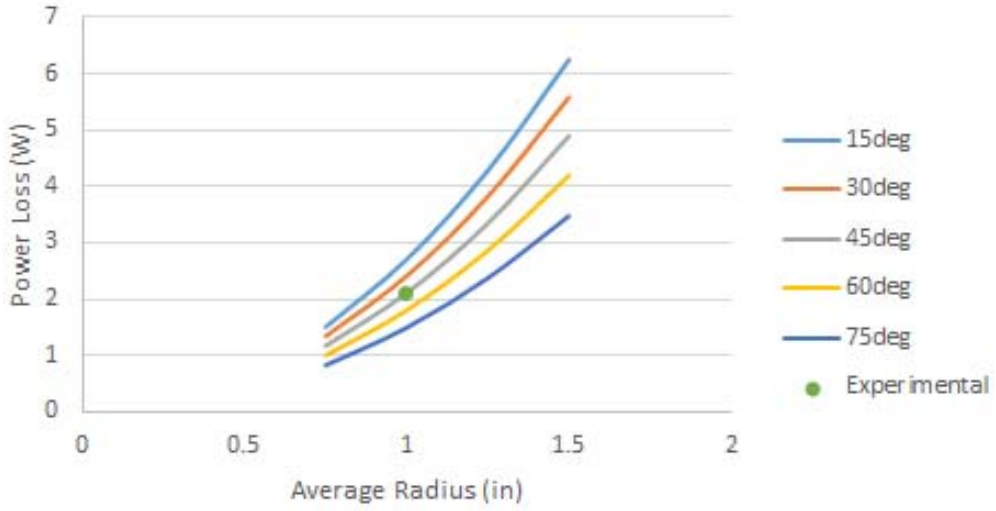

Figure 5.1: Analysis of various slot angles

As the radius increased, the power loss increased. One reason for this was that the surface area of the seal increased, causing the normal force that was required for sealing. This caused an increase causing an increase in the friction force which was exacerbated by the torque arm being longer compared to the smaller radii. The results show the larger slot angle to have less power loss. This is due to the decrease in contact surface area of the seal. This reduces the normal force thereby reducing the torque and power loss of the seal. This could suggest that if the slot angle was not to extend past the experimental testing of 45°, cutouts could be made to reduce the contact surface area of the stationary seal face. In order to test this theory, a seal was run using cutouts between the slots so that the area would be equal to that of a 72° slotted seal. The preliminary results from this test suggested an average power loss of 1.7±0.3 Watts with a leakage rate of 60 g/hr compared to the experimental data of 2.1±0.3 Watts with a

leakage rate of 21 g/hr. It was also found that the fluid film thickness increased with the reduction in the average radius.

As the film thickness increases, less contact friction is generated. This implies that both the power loss and wear rate could be reduced, as seen in the comparison of the second and third phases of testing. The results of the film thickness for the various slot angles is shown in Figure 5.2.

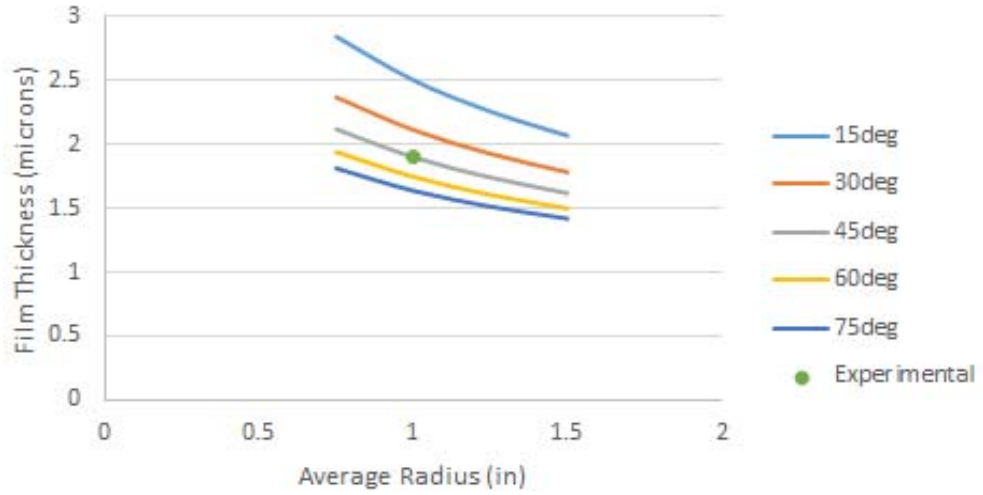

Figure 5.2: Film thickness results of various radii and slot angles

In the other geometrical analysis, the slot width based on a 45° slot angle was examined. The width was varied from 0.100” (31%) to 0.240” (74%) with 0.200” (62%) being used for the previously mentioned experimental results with the seal width at 0.325” from inner radius to the outer radius. The results of this study are shown in Figure 5.3.

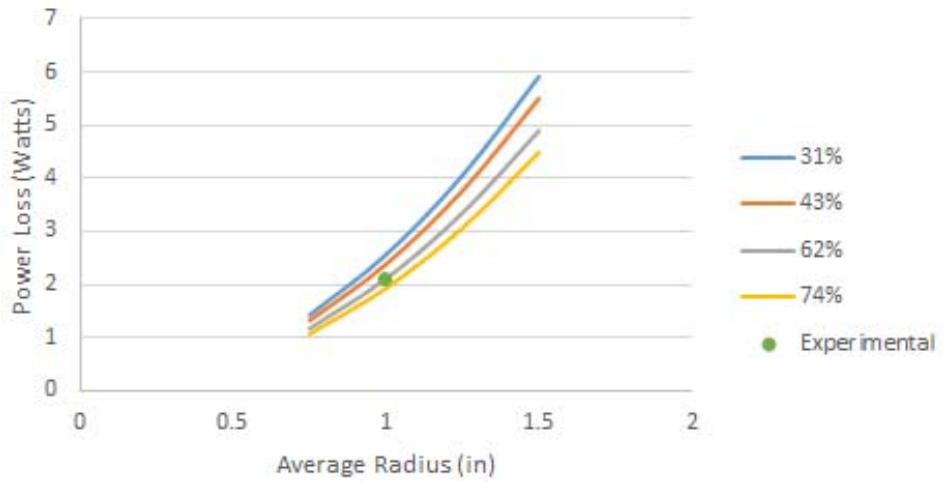

Figure 5.3: Analysis of various slot widths

The increase in radius causes a large increase in the power loss of the seal. When the slot width increased, there was a decrease in power loss. Similar to the increase in slot angle, this increase in slot width reduced the contact surface area of the seal, which reduced the power loss because of the face pressure required to have a low value of leakage. Experimentally, a 43% slot width ratio was tested and was found to have a higher leakage rate of 150 g/hr at the same load as the 62% experiments which was able to be within the 6 g/hr requirement. At this high leakage rate of the 43% slot width seal, the power loss was measured to be 4.1±0.4 Watts while the 62% was 3.9±0.5 Watts. The power loss increased as the face load increased to reduce the leakage rate of the 43% slot width seal. This suggests the model trends are correct.

Chapter 6 will provide the conclusions from the experiment and modeling and future work recommendations to further advance the understanding of the seal.

6. Conclusions and Recommendations

6.1 Conclusions

The following conclusions follow from the work presented in this thesis:

1. Under short run studies, modPTFE and Aluminum Bronze 954 provided the best results with regards to power loss and leakage rate at 0.56W and 2.6 g/hr, respectively, while the modPTFE and Dupont's Delrin 150 provided the lowest wear rate at 0.3 microns/hr. This wear rate would require a seal thickness of approximately 1" to last the full 10 years with a 50% duty cycle.
2. The initial isotropic surface applied to hard face allows for run-in to create the sealing surface, allowing the creation of a circumferential surface with a preferred sealing zone. This is in contrast to the initial circumferential surface, which did not experience the low leakage rate because it already had the circumferential grooving in the seal face.
3. Ethylene glycol and water mix reduced the wear rates compared to the experiments run with water.
4. Based on the required load to seal and the first order model, contact between the surfaces exists and the seal is operating in a partial lubricated regime.
5. Surface characterization studies show surface transfer of the softer stationary surface to the harder rotary surface. Also, the studies show circumferential wearing on both the rotary and stationary surfaces.
6. Geometry studies and experimental analysis suggest reducing the surface area by a combination of reducing the average radius of the seal, increasing the slot angle, increasing the slot width, and/or adding cutout would decrease the power loss of the rotary seal. From the study, reducing the average radius suggests the film thickness will

increase, which would predict a decrease in the wear rate. Increasing the slot angle and slot width had the opposite effect related to film thickness and would predictably increase the wear rate.

6.2 Future Work

The following recommendations are made for future work in this area:

1. An examination of longer testing duration that would allow for long term wear rates to be measured and to examine the effects of the initial isotropic surface over time.
2. Testing of other material pairs that may provide lower wear rates.
3. The impact of the rotational speed on the wear, power loss, and leakage.
4. Perform dry run conditions to examine the effects of the fluid flow on the surface temperature similar to that seen by Schneider (Schneider, 2006).
5. Perform repeat experiments for the conditions tested in this study to determine the repeatability of the results as various results were observed when run under the same conditions which could be caused by unseen defects in materials, material manufacturer's process, seal manufacturing differences, and other variables not controlled by the experiment.
6. Perform various factorial experiments to study the impact of input parameters on the output values and create empirical equations to predict these output results.
7. Create a more robust predictive model to solve for leakage rate, wear rate, and torque by applying surface roughness, material properties, and contact to the model with Patir and Cheng (Patir, 1978) and FEM. There are so many initial conditions to consider that would cause the modeling to grow rapidly.

Appendix A: Pressure Field and Load, Torque, COF, and Leakage Calculator Codes

Matlab Code for Pressure Field for a seal in cylindrical coordinates

```
clear
clc

go=input('****Will overwrite saved data in folder name "task" if the
folder already exists.****\nDo you want to continue? (y=1/n=0): ');
if go==1;
    %%%define the variables/boundary conditions
    P_in=0; %gage pressure of inner seal fluid
    P_out=0; %gage pressure of outer seal fluid
    P_cav=0; %cavitation pressure
    R_in=.8375; %inner radius of seal
    R_out=1.1625; %outer radius of seal
    num_r=21; %number of data points in the radial-direction
    num_theta=401; %number of points in the theta-direction
    max_iter=1000000; %number of iterations
    eps_max=1e-12; %convergence criterion
    omega=.3;%SOR multiplier (**most accurate solution when omega<<1**)
    type=1; %1 if geometry is for a 4 slot low power fluid timing
rotary valve, that of GE project
    R_inslot=.9; %radius to inner slot wall, must be within R_in and
R_out
    R_outslot=1.1; %radius to outer slot wall, must be within R_in and
R_out
    slot_angle=45; %angle in degrees that slot covers
    P_1=50; %pressure of slot 1
    P_2=0; %pressure of slot 2
    P_3=P_1; %pressure of slot 3
    P_4=P_2; %pressure of slot 4

    %%%create a domain map
    r_step=(R_out-R_in)/(num_r-1); %step size in r-direction
    theta_step=2*pi()/(num_theta-1); %step size in theta-direction
    if type==1;
        slot_rad=slot_angle*(pi()/180); %slot in radians
    end

    %%%from R_in to R_out
    r(num_r)=zeros;
    for i=1:num_r;
        r(i)=R_in+r_step*(i-1); %radial location from center
    end
    %%%from 0 to 2pi (2pi included)
    theta(num_theta)=zeros;
    for j=1:num_theta;
        theta(j)=0+theta_step*(j-1); %theta location
    end
```

```
    %%%x and y coordinates
    x(num_theta,num_r)=zeros;
    y(num_theta,num_r)=zeros;
    for i=1:num_theta;
        for j=1:num_r;
            x(i,j)=r(j)*cos(theta(i)); %x-coordinate of each node
            y(i,j)=r(j)*sin(theta(i)); %y-coordinate of each node
        end
    end

    %%%create pressure profile
    P(num_theta,num_r)=zeros;
    P(:,1)=P_in;
    P(:,num_r)=P_out;

    for iter=1:max_iter;
        P_old=P;
        %Using Successive-Over-Relaxation (SOR)
        for i=1:(num_theta-1);
            for j=2:(num_r-1);
                a_22=(2*r(j))/((r_step)^2)+2/(r(j)*(theta_step^2));
                a_32=(r(j)+0.5*r_step)/(r_step^2);
                a_12=(r(j)-0.5*r_step)/(r_step^2);
                a_21or3=1/(r(j)*(theta_step^2));
                if type==1;
                   if r(j)>=R_inslot && r(j)<=R_outslot &&
((theta(i)>=0 && theta(i)<=slot_rad)||(theta(i)>=pi()/2 &&
theta(i)<=(slot_rad+pi()/2))||(theta(i)>=2*pi()/2 &&
theta(i)<=(slot_rad+2*pi()/2))||(theta(i)>=3*pi()/2 &&
theta(i)<=(slot_rad+3*pi()/2)));
                       if theta(i)>=0 && theta(i)<=slot_rad;
                           P(i,j)=P_1;
                       elseif theta(i)>=pi()/2 &&
theta(i)<=(slot_rad+pi()/2);
                           P(i,j)=P_2;
                       elseif theta(i)>=2*pi()/2 &&
theta(i)<=(slot_rad+2*pi()/2);
                           P(i,j)=P_3;
                       else theta(i)>=2*pi()/2 &&
theta(i)<=(slot_rad+2*pi()/2);
                           P(i,j)=P_4;
                       end
                   elseif i==1;
                       P(i,j)=(1-
omega)*P_old(i,j)+(omega/a_22)*(a_32*P_old(i+1,j)+a_12*P(num_theta-
1,j)+a_21or3*(P_old(i,j+1)+P(i,j-1)));
                       P(num_theta,j)=P(i,j);
                   else i>1;
                       P(i,j)=(1-
omega)*P_old(i,j)+(omega/a_22)*(a_32*P_old(i+1,j)+a_12*P(i-
1,j)+a_21or3*(P_old(i,j+1)+P(i,j-1)));
                   end
               else
                    if i==1;
```

```
                        P(i,j)=(1-
omega)*P_old(i,j)+(omega/a_22)*(a_32*P_old(i+1,j)+a_12*P(num_theta-
1,j)+a_21or3*(P_old(i,j+1)+P(i,j-1)));
                        P(num_theta,j)=P(i,j);
                    else i>1;
                        P(i,j)=(1-
omega)*P_old(i,j)+(omega/a_22)*(a_32*P_old(i+1,j)+a_12*P(i-
1,j)+a_21or3*(P_old(i,j+1)+P(i,j-1)));
                    end
                end
                %if cavitation occurs
                if (P(i,j)<P_cav);
                    P(i,j)=P_cav;
                end
            end
        end
        %Convergence check
        d1=0;
        for ii=1:num_theta;
            for jj=1:num_r;
                d1=d1+((P(ii,jj)-P_old(ii,jj))/max(max(P_old)))^2;
            end
        end
        eps(iter)=(1/(num_theta*num_r))*sqrt(d1);
        if eps(iter)<=eps_max
            break
        end
        P(num_theta,:)=P(1,:);
    end

    %%%plot diagram
    figure(1)
    plot3(x,y,P)

    %%%save data
    mkdir('task')
    saveas(figure(1),[pwd '/task/task.fig'])
    save([pwd '/task/task.mat'])
    fprintf('\nAll data is saved in the folder named task!!!!\n')
end
```

Matlab code for Load, Torque, COF, and Leakage Calculator

```
%Calculation of load, torque, friction coefficient, and leakage related
to
%a seal in cylindrical coordinates, such as the 4 slot low power fluid
%timing rotary valve

go=input('****Must have data you want to analyze already open.****\nDo
you want to continue? (y=1/n=0/Torque and Leakage=2): ');
while go==1||go==2;
    %%%can this run? (Simpson's rule requires odd number of num_theta
and num_r)
    if mod(num_theta,2)==0;
        fprintf('\nnum_theta is REQUIRED to be ODD to run, check num_r
also!\n')
        break
    end
    if mod(num_r,2)==0;
        fprintf('\nnum_r is REQUIRED to be ODD to run!\n')
        break
    end

    %%%define the variables
    height=0.00005553; %height in units used by previous code
    dim=1; %1 for dimensions in english (inches), 0 for metric (m)
    viscosity=0.03; %dynamic viscosity at fluid temp in Poise (metric)
    %(water=0.01 @ room temp, 45%EG in H2O=0.07 @ 30 deg_F, 45%EG in
H2O=0.03 @ 70 deg_F)
    density=1041; %density of water=1000 kg/m^3, density of 45% EG in
water=1041 kg/m^3, density of 100% EG=1097 kg/m^3
    area=1.422;%seal surface area
    rot_speed=60; %rotational speed (rpm)
    applied_load=80; %externally applied load to seal faces

    %%%calculated variables
    rot_omega=rot_speed*2*pi()/60; %rotation speed (rad/sec)
    if dim==1;
        viscosity=viscosity*(14.5)/1000000; %1 cP=.145 microReyns and 1
Reyns=1 lb*s/in^2
    end

    %%%Torque and friction coeff
    Torque=(viscosity/height)*((R_out+R_in)/2^2)*rot_omega*area;
    friction_coeff=(Torque/((R_in+R_out)/2))/applied_load;
    if go==2
        display(Torque); %display Torque value
        display(friction_coeff); %display friction coeff value
    end

    %%%Inner Leakage using forward differencing and Simpson's Rule
    Q_inner=0;
    for i=1;
        a_inner=(1/r_step)*(theta_step/3)*(-
(height^3)*r(i))/(12*viscosity);
        for j=1:num_theta;
```

```
            if j==1||j==num_theta;
                Q_inner=Q_inner+a_inner*(P(j,i+1)-P(j,i));
%length^3/sec
            elseif mod(j,2)==0;
                Q_inner=Q_inner+a_inner*4*(P(j,i+1)-P(j,i));
%length^3/sec
            else
                Q_inner=Q_inner+a_inner*2*(P(j,i+1)-P(j,i));
%length^3/sec
            end
        end
    end
    Q_inner=Q_inner*3600; %length^3/hr

    %%%Outer Leakage using backward differencing and Simpson's Rule
    Q_outer=0;
    for i=num_r;
        a_outer=(1/r_step)*(theta_step/3)*(-
(height^3)*r(i))/(12*viscosity);
        for j=1:num_theta;
            if j==1||j==num_theta;
                Q_outer=Q_outer+a_outer*(P(j,i)-P(j,i-1));
%length^3/sec
            elseif mod(j,2)==0;
                Q_outer=Q_outer+a_outer*4*(P(j,i)-P(j,i-1));
%length^3/sec
            else
                Q_outer=Q_outer+a_outer*2*(P(j,i)-P(j,i-1));
%length^3/sec
            end
        end
    end
    Q_outer=Q_outer*3600;  %length^3/hr

    %%%Environmental Leakage
    if dim==1;
        density=density*(1000/61023.7); %g/in^3
    else
        density=density*1000; %g/m^3
    end
    Q_inner_mass=-Q_inner*density; %g/hr
    Q_outer_mass=Q_outer*density; %g/hr
    Q_envir_mass=Q_inner_mass+Q_outer_mass; %g/hr
    if go==2;
        display(Q_envir_mass) %g/hr
        break
    end

    if go==1
        %%%Load using 2-D Simpson's Rule
        Load=0;
        for i=1:(num_theta);
                for j=1:(num_r);
                    if i==1||i==num_theta;
                        if j==1||j==num_r;
```

```
Load=Load+((r_step*theta_step)/9)*1*P(i,j)*r(j);
                        elseif mod(j,2)==0;

Load=Load+((r_step*theta_step)/9)*4*P(i,j)*r(j);
                        else

Load=Load+((r_step*theta_step)/9)*2*P(i,j)*r(j);
                        end
                    elseif mod(i,2)==0;
                        if j==1||j==num_r;

Load=Load+((r_step*theta_step)/9)*4*P(i,j)*r(j);
                        elseif mod(j,2)==0;

Load=Load+((r_step*theta_step)/9)*16*P(i,j)*r(j);
                        else

Load=Load+((r_step*theta_step)/9)*8*P(i,j)*r(j);
                        end
                    else
                        if j==1||j==num_r;

Load=Load+((r_step*theta_step)/9)*2*P(i,j)*r(j);
                        elseif mod(j,2)==0;

Load=Load+((r_step*theta_step)/9)*8*P(i,j)*r(j);
                        else

Load=Load+((r_step*theta_step)/9)*4*P(i,j)*r(j);
                        end
                    end
                end
        end

        %%%Leakage at SLOT 1
        %%%Leakage at slot 1, at inner slot edge
        Q_innerslot1=0;
        %find inner slot edge
        for i=1:num_r;
            if r(i)>=R_inslot;
                i=i-1; %data point location before slot edge
                a_innerslot1=(1/r_step)*(theta_step)*(-
(height^3)*R_inslot)/(12*viscosity);
                %find data points of slot
                for jj=1:num_theta;
                    if theta(jj)>slot_rad;
                        jj=jj-1; %point before end of slot
                        break
                    end
                end
                for j=1:jj;
                    if mod(jj,2)==1; %Simpson's Rule
                        if j==1 || j==jj;

Q_innerslot1=Q_innerslot1+(a_innerslot1/3)*(P(j,i+1)-P(j,i));
%length^3/sec
```

```
                        elseif mod(j,2)==0

Q_innerslot1=Q_innerslot1+(a_innerslot1/3)*4*(P(j,i+1)-P(j,i));
%length^3/sec
                        else

Q_innerslot1=Q_innerslot1+(a_innerslot1/3)*2*(P(j,i+1)-P(j,i));
%length^3/sec
                        end
                    else %Trapezoidal Rule
                        if j==1 || j==jj;

Q_innerslot1=Q_innerslot1+(a_innerslot1/2)*(P(j,i+1)-P(j,i));
%length^3/sec
                        else

Q_innerslot1=Q_innerslot1+(a_innerslot1/2)*2*(P(j,i+1)-P(j,i));
%length^3/sec
                        end
                    end
                end
                break
            end
        end
        Q_innerslot1=-Q_innerslot1*3600; %Leakage out of the slot in
length^3/hr
        Q_innerslot1_mass=Q_innerslot1*density; %g/hr
        %%%Leakage at slot 1, at outer slot edge
        Q_outerslot1=0;
        %find outer slot edge
        for ii=1:num_r;
            if r(ii)>=R_outslot;
                ii=ii-1; %data point location before slot edge
                a_outerslot1=(1/r_step)*(theta_step)*(-
(height^3)*R_outslot)/(12*viscosity);
                for j=1:jj; %use previous found jj, point before end of
slot
                    if mod(jj,2)==1;%Simpson's Rule
                        if j==1 || j==jj;

Q_outerslot1=Q_outerslot1+(a_outerslot1/3)*(P(j,ii+1)-P(j,ii));
%length^3/sec
                        elseif mod(j,2)==0

Q_outerslot1=Q_outerslot1+(a_outerslot1/3)*4*(P(j,ii+1)-P(j,ii));
%length^3/sec
                        else

Q_outerslot1=Q_outerslot1+(a_outerslot1/3)*2*(P(j,ii+1)-P(j,ii));
%length^3/sec
                        end
                    else %Trapezoidal Rule
                        if j==1 || j==jj;

Q_outerslot1=Q_outerslot1+(a_outerslot1/2)*(P(j,ii+1)-P(j,ii));
%length^3/sec
                        else
```

```
Q_outerslot1=Q_outerslot1+(a_outerslot1/2)*2*(P(j,ii+1)-P(j,ii));
%length^3/sec
                        end
                    end
                end
                break
            end
        end
        Q_outerslot1=Q_outerslot1*3600; %Leakage out of the slot in
length^3/hr
        Q_outerslot1_mass=Q_outerslot1*density; %g/hr
        %%%Leakage at slot 1, at theta=0
        Q_lowerslot1=(height*rot_omega/2)*(R_outslot^2-R_inslot^2);
%length^3/sec
        a_lowerslot1=(-
(height^3)/(12*viscosity))*(r_step/(theta_step));
        for iii=(i+1):1:ii;
            if mod((ii-i),2)==1; %Simpson's Rule
                if iii==(i+1) || iii==ii;

Q_lowerslot1=Q_lowerslot1+(a_lowerslot1/(3*r(iii)))*(P(1,iii)-
P(num_theta-1,iii)); %length^3/sec
                elseif mod((iii-i),2)==0

Q_lowerslot1=Q_lowerslot1+(a_lowerslot1/(3*r(iii)))*4*(P(1,iii)-
P(num_theta-1,iii)); %length^3/sec
                else

Q_lowerslot1=Q_lowerslot1+(a_lowerslot1/(3*r(iii)))*2*(P(1,iii)-
P(num_theta-1,iii)); %length^3/sec
                end
            else %Trapezoidal Rule
                if iii==(i+1) || iii==ii;

Q_lowerslot1=Q_lowerslot1+(a_lowerslot1/(2*r(iii)))*(P(1,iii)-
P(num_theta-1,iii)); %length^3/sec
                else

Q_lowerslot1=Q_lowerslot1+(a_lowerslot1/(2*r(iii)))*2*(P(1,iii)-
P(num_theta-1,iii)); %length^3/sec
                end
            end
        end
        Q_lowerslot1=-Q_lowerslot1*3600; %Leakage out of the slot in
length^3/hr
        Q_lowerslot1_mass=Q_lowerslot1*density; %g/hr
        %%%Leakage at slot 1, at theta=slot_rad
        Q_upperslot1=(height*rot_omega/2)*(R_outslot^2-R_inslot^2);
%length^3/sec
        a_upperslot1=(-
(height^3)/(12*viscosity))*(r_step/(theta_step));
        for iii=(i+1):1:ii; %jj, point before end of slot
            if mod((ii-i),2)==1; %Simpson's Rule
                if iii==(i+1) || iii==ii;
```

```
Q_upperslot1=Q_upperslot1+(a_upperslot1/(3*r(iii)))*(P(jj+1,iii)-
P(jj,iii)); %length^3/sec
                elseif mod((iii-i),2)==0

Q_upperslot1=Q_upperslot1+(a_upperslot1/(3*r(iii)))*4*(P(jj+1,iii)-
P(jj,iii)); %length^3/sec
                else

Q_upperslot1=Q_upperslot1+(a_upperslot1/(3*r(iii)))*2*(P(jj+1,iii)-
P(jj,iii)); %length^3/sec
                end
            else %Trapezoidal Rule
                if iii==(i+1) || iii==ii;

Q_upperslot1=Q_upperslot1+(a_upperslot1/(2*r(iii)))*(P(jj+1,iii)-
P(jj,iii)); %length^3/sec
                else

Q_upperslot1=Q_upperslot1+(a_upperslot1/(2*r(iii)))*2*(P(jj+1,iii)-
P(jj,iii)); %length^3/sec
                end
            end
        end
        Q_upperslot1=Q_upperslot1*3600; %Leakage out of the slot in
length^3/hr
        Q_upperslot1_mass=Q_upperslot1*density; %g/hr
        %%%Total Leakage of Slot 1

Q_totalslot1_mass=Q_innerslot1_mass+Q_outerslot1_mass+Q_lowerslot1_mass
+Q_upperslot1_mass; %g/hr

        %%%Leakage at SLOT 2
        %%%Leakage at slot 2, at inner slot edge
        Q_innerslot2=0;
        %r(i) is point before inner slot edge, r(ii) is point before
outer slot edge
        a_innerslot2=(1/r_step)*(theta_step)*(-
(height^3)*R_inslot)/(12*viscosity);
        %find data point of first theta point of slot
        for jj=1:num_theta;
            if theta(jj)>=(pi()/2); %theta(jj) is first line in slot
                break
            end
        end
        %find data point of last theta point of slot
        for jjj=1:num_theta;
            if theta(jjj)>(pi()/2+slot_rad);
                jjj=jjj-1; %theta(jjj) is line before end of slot
                break
            end
        end
        for j=jj:jjj;
            if mod((jjj+1-jj),2)==1; %Simpson's Rule
                if j==jj || j==jjj;
```

```
Q_innerslot2=Q_innerslot2+(a_innerslot2/3)*(P(j,i+1)-P(j,i));
%length^3/sec
                elseif mod((j+1-jj),2)==0

Q_innerslot2=Q_innerslot2+(a_innerslot2/3)*4*(P(j,i+1)-P(j,i));
%length^3/sec
                else

Q_innerslot2=Q_innerslot2+(a_innerslot2/3)*2*(P(j,i+1)-P(j,i));
%length^3/sec
                end
            else %Trapezoidal Rule
                if j==jj || j==jjj;

Q_innerslot2=Q_innerslot2+(a_innerslot2/2)*(P(j,i+1)-P(j,i));
%length^3/sec
                else

Q_innerslot2=Q_innerslot2+(a_innerslot2/2)*2*(P(j,i+1)-P(j,i));
%length^3/sec
                end
            end
        end
        Q_innerslot2=-Q_innerslot2*3600; %Leakage out of the slot in
length^3/hr
        Q_innerslot2_mass=Q_innerslot2*density; %g/hr
        %%%Leakage at slot 2, at outer slot edge
        Q_outerslot2=0;
        a_outerslot2=(1/r_step)*(theta_step)*(-
(height^3)*R_outslot)/(12*viscosity);
        for j=jj:jjj; %use previous found jj(first line of slot) and
jjj(line before end of slot)
            if mod((jjj+1-jj),2)==1;%Simpson's Rule
                if j==jj || j==jjj;

Q_outerslot2=Q_outerslot2+(a_outerslot2/3)*(P(j,ii+1)-P(j,ii));
%length^3/sec
                elseif mod((j+1-jj),2)==0

Q_outerslot2=Q_outerslot2+(a_outerslot2/3)*4*(P(j,ii+1)-P(j,ii));
%length^3/sec
                else

Q_outerslot2=Q_outerslot2+(a_outerslot2/3)*2*(P(j,ii+1)-P(j,ii));
%length^3/sec
                end
            else %Trapezoidal Rule
                if j==jj || j==jjj;

Q_outerslot2=Q_outerslot2+(a_outerslot2/2)*(P(j,ii+1)-P(j,ii));
%length^3/sec
                else

Q_outerslot2=Q_outerslot2+(a_outerslot2/2)*2*(P(j,ii+1)-P(j,ii));
%length^3/sec
                end
```

```
            end
        end
        Q_outerslot2=Q_outerslot2*3600; %Leakage out of the slot in
length^3/hr
        Q_outerslot2_mass=Q_outerslot2*density; %g/hr
        %%%Leakage at slot 2, at theta=pi/2
        Q_lowerslot2=(height*rot_omega/2)*(R_outslot^2-R_inslot^2);
%length^3/sec
        a_lowerslot2=(-
(height^3)/(12*viscosity))*(r_step/(theta_step));
        %use jj(first line of slot) and jjj(line before end of slot)
used for slot2
        for iii=(i+1):1:ii;
            if mod((ii-i),2)==1; %Simpson's Rule
                if iii==(i+1) || iii==ii;

Q_lowerslot2=Q_lowerslot2+(a_lowerslot2/(3*r(iii)))*(P(jj,iii)-P(jj-
1,iii)); %length^3/sec
                elseif mod((iii-i),2)==0

Q_lowerslot2=Q_lowerslot2+(a_lowerslot2/(3*r(iii)))*4*(P(jj,iii)-P(jj-
1,iii)); %length^3/sec
                else

Q_lowerslot2=Q_lowerslot2+(a_lowerslot2/(3*r(iii)))*2*(P(jj,iii)-P(jj-
1,iii)); %length^3/sec
                end
            else %Trapezoidal Rule
                if iii==(i+1) || iii==ii;

Q_lowerslot2=Q_lowerslot2+(a_lowerslot2/(2*r(iii)))*(P(jj,iii)-P(jj-
1,iii)); %length^3/sec
                else

Q_lowerslot2=Q_lowerslot2+(a_lowerslot2/(2*r(iii)))*2*(P(jj,iii)-P(jj-
1,iii)); %length^3/sec
                end
            end
        end
        Q_lowerslot2=-Q_lowerslot2*3600; %Leakage out of the slot in
length^3/hr
        Q_lowerslot2_mass=Q_lowerslot2*density; %g/hr
        %%%Leakage at slot 2, at theta=slot_rad
        Q_upperslot2=(height*rot_omega/2)*(R_outslot^2-R_inslot^2);
%length^3/sec
        a_upperslot2=(-
(height^3)/(12*viscosity))*(r_step/(theta_step));
        for iii=(i+1):1:ii; %jjj, point before end of slot
            if mod((ii-i),2)==1; %Simpson's Rule
                if iii==(i+1) || iii==ii;

Q_upperslot2=Q_upperslot2+(a_upperslot2/(3*r(iii)))*(P(jjj+1,iii)-
P(jjj,iii)); %length^3/sec
                elseif mod((iii-i),2)==0

Q_upperslot2=Q_upperslot2+(a_upperslot2/(3*r(iii)))*4*(P(jjj+1,iii)-
P(jjj,iii)); %length^3/sec
```

```
                else

Q_upperslot2=Q_upperslot2+(a_upperslot2/(3*r(iii)))*2*(P(jjj+1,iii)-
P(jjj,iii)); %length^3/sec
                end
            else %Trapezoidal Rule
                if iii==(i+1) || iii==ii;

Q_upperslot2=Q_upperslot2+(a_upperslot2/(2*r(iii)))*(P(jjj+1,iii)-
P(jjj,iii)); %length^3/sec
                else

Q_upperslot2=Q_upperslot2+(a_upperslot2/(2*r(iii)))*2*(P(jjj+1,iii)-
P(jjj,iii)); %length^3/sec
                end
            end
        end
        Q_upperslot2=Q_upperslot2*3600; %Leakage out of the slot in
length^3/hr
        Q_upperslot2_mass=Q_upperslot2*density; %g/hr
        %%%Total Leakage of Slot 2

Q_totalslot2_mass=Q_innerslot2_mass+Q_outerslot2_mass+Q_lowerslot2_mass
+Q_upperslot2_mass; %g/hr

        %%%Leakage at SLOT 3
        %%%Leakage at slot 3, at inner slot edge
        Q_innerslot3=0;
        %r(i) is point before inner slot edge, r(ii) is point before
outer slot edge
        a_innerslot3=(1/r_step)*(theta_step)*(-
(height^3)*R_inslot)/(12*viscosity);
        %find data point of first theta point of slot
        for jj=1:num_theta;
            if theta(jj)>=(2*pi()/2); %theta(jj) is first line in slot
                break
            end
        end
        %find data point of last theta point of slot
        for jjj=1:num_theta;
            if theta(jjj)>(2*pi()/2+slot_rad);
                jjj=jjj-1; %theta(jjj) is line before end of slot
                break
            end
        end
        for j=jj:jjj;
            if mod((jjj+1-jj),2)==1; %Simpson's Rule
                if j==jj || j==jjj;

Q_innerslot3=Q_innerslot3+(a_innerslot3/3)*(P(j,i+1)-P(j,i));
%length^3/sec
                elseif mod((j+1-jj),2)==0

Q_innerslot3=Q_innerslot3+(a_innerslot3/3)*4*(P(j,i+1)-P(j,i));
%length^3/sec
                else
```

```
Q_innerslot3=Q_innerslot3+(a_innerslot3/3)*2*(P(j,i+1)-P(j,i));
%length^3/sec
                end
            else %Trapezoidal Rule
                if j==jj || j==jjj;

Q_innerslot3=Q_innerslot3+(a_innerslot3/2)*(P(j,i+1)-P(j,i));
%length^3/sec
                else

Q_innerslot3=Q_innerslot3+(a_innerslot3/2)*2*(P(j,i+1)-P(j,i));
%length^3/sec
                end
            end
        end
        Q_innerslot3=-Q_innerslot3*3600; %Leakage out of the slot in
length^3/hr
        Q_innerslot3_mass=Q_innerslot3*density; %g/hr
        %%%Leakage at slot 3, at outer slot edge
        Q_outerslot3=0;
        a_outerslot3=(1/r_step)*(theta_step)*(-
(height^3)*R_outslot)/(12*viscosity);
        for j=jj:jjj; %use previous found jj(first line of slot) and
jjj(line before end of slot)
            if mod((jjj+1-jj),2)==1;%Simpson's Rule
                if j==jj || j==jjj;

Q_outerslot3=Q_outerslot3+(a_outerslot3/3)*(P(j,ii+1)-P(j,ii));
%length^3/sec
                elseif mod((j+1-jj),2)==0

Q_outerslot3=Q_outerslot3+(a_outerslot3/3)*4*(P(j,ii+1)-P(j,ii));
%length^3/sec
                else

Q_outerslot3=Q_outerslot3+(a_outerslot3/3)*2*(P(j,ii+1)-P(j,ii));
%length^3/sec
                end
            else %Trapezoidal Rule
                if j==jj || j==jjj;

Q_outerslot3=Q_outerslot3+(a_outerslot3/2)*(P(j,ii+1)-P(j,ii));
%length^3/sec
                else

Q_outerslot3=Q_outerslot3+(a_outerslot3/2)*2*(P(j,ii+1)-P(j,ii));
%length^3/sec
                end
            end
        end
        Q_outerslot3=Q_outerslot3*3600; %Leakage out of the slot in
length^3/hr
        Q_outerslot3_mass=Q_outerslot3*density; %g/hr
        %%%Leakage at slot 3, at theta=2pi/2
        Q_lowerslot3=(height*rot_omega/2)*(R_outslot^2-R_inslot^2);
%length^3/sec
```

```
        a_lowerslot3=(-
(height^3)/(12*viscosity))*(r_step/(theta_step));
        %use jj(first line of slot) and jjj(line before end of slot)
used for slot2
        for iii=(i+1):1:ii;
            if mod((ii-i),2)==1; %Simpson's Rule
                if iii==(i+1) || iii==ii;

Q_lowerslot3=Q_lowerslot3+(a_lowerslot3/(3*r(iii)))*(P(jj,iii)-P(jj-
1,iii)); %length^3/sec
                elseif mod((iii-i),2)==0

Q_lowerslot3=Q_lowerslot3+(a_lowerslot3/(3*r(iii)))*4*(P(jj,iii)-P(jj-
1,iii)); %length^3/sec
                else

Q_lowerslot3=Q_lowerslot3+(a_lowerslot3/(3*r(iii)))*2*(P(jj,iii)-P(jj-
1,iii)); %length^3/sec
                end
            else %Trapezoidal Rule
                if iii==(i+1) || iii==ii;

Q_lowerslot3=Q_lowerslot3+(a_lowerslot3/(2*r(iii)))*(P(jj,iii)-P(jj-
1,iii)); %length^3/sec
                else

Q_lowerslot3=Q_lowerslot3+(a_lowerslot3/(2*r(iii)))*2*(P(jj,iii)-P(jj-
1,iii)); %length^3/sec
                end
            end
        end
        Q_lowerslot3=-Q_lowerslot3*3600; %Leakage out of the slot in
length^3/hr
        Q_lowerslot3_mass=Q_lowerslot3*density; %g/hr
        %%%Leakage at slot 3, at theta=slot_rad+2pi/2
        Q_upperslot3=(height*rot_omega/2)*(R_outslot^2-R_inslot^2);
%length^3/sec
        a_upperslot3=(-
(height^3)/(12*viscosity))*(r_step/(theta_step));
        for iii=(i+1):1:ii; %jjj, point before end of slot
            if mod((ii-i),2)==1; %Simpson's Rule
                if iii==(i+1) || iii==ii;

Q_upperslot3=Q_upperslot3+(a_upperslot3/(3*r(iii)))*(P(jjj+1,iii)-
P(jjj,iii)); %length^3/sec
                elseif mod((iii-i),2)==0

Q_upperslot3=Q_upperslot3+(a_upperslot3/(3*r(iii)))*4*(P(jjj+1,iii)-
P(jjj,iii)); %length^3/sec
                else

Q_upperslot3=Q_upperslot3+(a_upperslot3/(3*r(iii)))*2*(P(jjj+1,iii)-
P(jjj,iii)); %length^3/sec
                end
            else %Trapezoidal Rule
                if iii==(i+1) || iii==ii;
```

```
Q_upperslot3=Q_upperslot3+(a_upperslot3/(2*r(iii)))*(P(jjj+1,iii)-
P(jjj,iii)); %length^3/sec
                else

Q_upperslot3=Q_upperslot3+(a_upperslot3/(2*r(iii)))*2*(P(jjj+1,iii)-
P(jjj,iii)); %length^3/sec
                end
            end
        end
        Q_upperslot3=Q_upperslot3*3600; %Leakage out of the slot in
length^3/hr
        Q_upperslot3_mass=Q_upperslot3*density; %g/hr
        %%%Total Leakage of Slot 3

Q_totalslot3_mass=Q_innerslot3_mass+Q_outerslot3_mass+Q_lowerslot3_mass
+Q_upperslot3_mass; %g/hr

        %%%Leakage at SLOT 4
        %%%Leakage at slot 4, at inner slot edge
        Q_innerslot4=0;
        %r(i) is point before inner slot edge, r(ii) is point before
outer slot edge
        a_innerslot4=(1/r_step)*(theta_step)*(-
(height^3)*R_inslot)/(12*viscosity);
        %find data point of first theta point of slot
        for jj=1:num_theta;
            if theta(jj)>=(3*pi()/2); %theta(jj) is first line in slot
                break
            end
        end
        %find data point of last theta point of slot
        for jjj=1:num_theta;
            if theta(jjj)>(3*pi()/2+slot_rad);
                jjj=jjj-1; %theta(jjj) is line before end of slot
                break
            end
        end
        for j=jj:jjj;
            if mod((jjj+1-jj),2)==1; %Simpson's Rule
                if j==jj || j==jjj;

Q_innerslot4=Q_innerslot4+(a_innerslot4/3)*(P(j,i+1)-P(j,i));
%length^3/sec
                elseif mod((j+1-jj),2)==0

Q_innerslot4=Q_innerslot4+(a_innerslot4/3)*4*(P(j,i+1)-P(j,i));
%length^3/sec
                else

Q_innerslot4=Q_innerslot4+(a_innerslot4/3)*2*(P(j,i+1)-P(j,i));
%length^3/sec
                end
            else %Trapezoidal Rule
                if j==jj || j==jjj;
```

```
Q_innerslot4=Q_innerslot4+(a_innerslot4/2)*(P(j,i+1)-P(j,i));
%length^3/sec
                else

Q_innerslot4=Q_innerslot4+(a_innerslot4/2)*2*(P(j,i+1)-P(j,i));
%length^3/sec
                end
            end
        end
        Q_innerslot4=-Q_innerslot4*3600; %Leakage out of the slot in
length^3/hr
        Q_innerslot4_mass=Q_innerslot4*density; %g/hr
        %%%Leakage at slot 4, at outer slot edge
        Q_outerslot4=0;
        a_outerslot4=(1/r_step)*(theta_step)*(-
(height^3)*R_outslot)/(12*viscosity);
        for j=jj:jjj; %use previous found jj(first line of slot) and
jjj(line before end of slot)
            if mod((jjj+1-jj),2)==1;%Simpson's Rule
                if j==jj || j==jjj;

Q_outerslot4=Q_outerslot4+(a_outerslot4/3)*(P(j,ii+1)-P(j,ii));
%length^3/sec
                elseif mod((j+1-jj),2)==0

Q_outerslot4=Q_outerslot4+(a_outerslot4/3)*4*(P(j,ii+1)-P(j,ii));
%length^3/sec
                else

Q_outerslot4=Q_outerslot4+(a_outerslot4/3)*2*(P(j,ii+1)-P(j,ii));
%length^3/sec
                end
            else %Trapezoidal Rule
                if j==jj || j==jjj;

Q_outerslot4=Q_outerslot4+(a_outerslot4/2)*(P(j,ii+1)-P(j,ii));
%length^3/sec
                else

Q_outerslot4=Q_outerslot4+(a_outerslot4/2)*2*(P(j,ii+1)-P(j,ii));
%length^3/sec
                end
            end
        end
        Q_outerslot4=Q_outerslot4*3600; %Leakage out of the slot in
length^3/hr
        Q_outerslot4_mass=Q_outerslot4*density; %g/hr
        %%%Leakage at slot 4, at theta=3pi/2
        Q_lowerslot4=(height*rot_omega/2)*(R_outslot^2-R_inslot^2);
%length^3/sec
        a_lowerslot4=(-
(height^3)/(12*viscosity))*(r_step/(theta_step));
        %use jj(first line of slot) and jjj(line before end of slot)
used for slot2
        for iii=(i+1):1:ii;
            if mod((ii-i),2)==1; %Simpson's Rule
```

```
                if iii==(i+1) || iii==ii;

Q_lowerslot4=Q_lowerslot4+(a_lowerslot4/(3*r(iii)))*(P(jj,iii)-P(jj-
1,iii)); %length^3/sec
                elseif mod((iii-i),2)==0

Q_lowerslot4=Q_lowerslot4+(a_lowerslot4/(3*r(iii)))*4*(P(jj,iii)-P(jj-
1,iii)); %length^3/sec
                else

Q_lowerslot4=Q_lowerslot4+(a_lowerslot4/(3*r(iii)))*2*(P(jj,iii)-P(jj-
1,iii)); %length^3/sec
                end
            else %Trapezoidal Rule
                if iii==(i+1) || iii==ii;

Q_lowerslot4=Q_lowerslot4+(a_lowerslot4/(2*r(iii)))*(P(jj,iii)-P(jj-
1,iii)); %length^3/sec
                else

Q_lowerslot4=Q_lowerslot4+(a_lowerslot4/(2*r(iii)))*2*(P(jj,iii)-P(jj-
1,iii)); %length^3/sec
                end
            end
        end
        Q_lowerslot4=-Q_lowerslot4*3600; %Leakage out of the slot in
length^3/hr
        Q_lowerslot4_mass=Q_lowerslot4*density; %g/hr
        %%%Leakage at slot 4, at theta=slot_rad+3pi/2
        Q_upperslot4=(height*rot_omega/2)*(R_outslot^2-R_inslot^2);
%length^3/sec
        a_upperslot4=(-
(height^3)/(12*viscosity))*(r_step/(3*theta_step));
        for iii=(i+1):1:ii; %jjj, point before end of slot
            if mod((ii-i),2)==1; %Simpson's Rule
                if iii==(i+1) || iii==ii;

Q_upperslot4=Q_upperslot4+(a_upperslot4/(3*r(iii)))*(P(jjj+1,iii)-
P(jjj,iii)); %length^3/sec
                elseif mod((iii-i),2)==0

Q_upperslot4=Q_upperslot4+(a_upperslot4/(3*r(iii)))*4*(P(jjj+1,iii)-
P(jjj,iii)); %length^3/sec
                else

Q_upperslot4=Q_upperslot4+(a_upperslot4/(3*r(iii)))*2*(P(jjj+1,iii)-
P(jjj,iii)); %length^3/sec
                end
            else %Trapezoidal Rule
                if iii==(i+1) || iii==ii;

Q_upperslot4=Q_upperslot4+(a_upperslot4/(2*r(iii)))*(P(jjj+1,iii)-
P(jjj,iii)); %length^3/sec
                else

Q_upperslot4=Q_upperslot4+(a_upperslot4/(2*r(iii)))*2*(P(jjj+1,iii)-
P(jjj,iii)); %length^3/sec
```

```
                end
            end
        end
        Q_upperslot4=Q_upperslot4*3600; %Leakage out of the slot in
length^3/hr
        Q_upperslot4_mass=Q_upperslot4*density; %g/hr
        %%%Total Leakage of Slot 4

Q_totalslot4_mass=Q_innerslot4_mass+Q_outerslot4_mass+Q_lowerslot4_mass
+Q_upperslot4_mass; %g/hr

        %%%Display all values
        if dim==1;
            height=height*(25.4)*1000; %height initially in inches to
microns
        else
            height=height*1000000; %height initially in meters to
microns
        end
        display(height); %in microns
        display(Torque); %display Torque value
        display(friction_coeff); %display friction coeff value
        display(Load); %lbs or Newtons
        display(Q_inner_mass); %g/hr
        display(Q_outer_mass); %g/hr
        display(Q_envir_mass); %g/hr
        display(Q_totalslot1_mass); %g/hr
        display(Q_totalslot2_mass); %g/hr
        display(Q_totalslot3_mass); %g/hr
        display(Q_totalslot4_mass); %g/hr

Q_allslot_mass=Q_totalslot1_mass+Q_totalslot2_mass+Q_totalslot3_mass+Q_
totalslot4_mass; %g/hr
        display(Q_allslot_mass); %g/hr
        Q_mass=Q_allslot_mass-Q_envir_mass; %g/hr
        display(Q_mass); %g/hr
        Q_mass_over_envir=Q_mass/Q_envir_mass*100; %percentage
        display(Q_mass_over_envir); %percentage
        break
    end
end
```

References

Benedict, M. A. (2012). *United States of America Patent No. 20140165594.*

Benedict, M. A. (2016). Design and performance of a novel magnetocaloric heat pump. *Science and Technology for the Built Environment*, 1-7.

Booser, E. R. (1997). *Tribology Data handbook:An Excellent Friction, Lubrication and Wear Resource.* New York: CRC Press.

Brück, E. (2005). Developments in magnetocaloric refrigeration. *Journal of Physics D: Applied Physics*, R381-R391.

Carson, D. B. (1959). *United States of America Patent No. 3,040,777.*

Hayden, M. A. (2004). *The heat sink mechanical seal: A centrifugal pump application.* Lexington, Ky: University of Kentucky.

Lebeck, A. O. (1991). *Principles and Design of Mechanical Face Seals.* New York: John Wiley and Sons.

Lebeck, A. O. (1999). Mixed lubrication in mechanical face seals with plain faces. *Proceedings of the Institution of Mechanical Engineers, Part J: Journal of Engineering Tribology*, 163-175.

Moeller, M. W. (2012). *United States of America Patent No. 20140007660.*

Müller, H. K. (1998). *Fluid Sealing Technology: Principles and Applications.* New York: Marcel Dekker.

Nichols, J. A. (1998). *United States of America Patent No. 6,012,488.*

Nichols, J. A. (2001). *United States of America Patent No. 6,453,946.*

Nichols, J. A. (2001). *United States of America Patent No. 6,672,336.*

Patir, N. C. (1978). An average flow model for determining effects of three-dimensional roughness on partial hydrodynamic lubrication. *Journal of Lubrication Technology*, 12-17.

Schneider, D. (2006). *The micro heat sink ring: A tribological study.* Lexington, KY: University of Kentucky.

Stich, B. (1991). *United States of America Patent No. 5,080,401.*

Stieha, J. K. (2016). Analysis of an end face mechanical seal with internal valving for low power applications. *71st STLE Annual Meeting.* Las Vegas.

Wan, H. (2012). *United States of America Patent No. 8,813,785.*

Warring, R. H. (1981). *Seals and Sealing Handbook.* Houston: Gulf Publishing Company.

Zimm, C. J. (1998). Description and performance of a near-room temperature magnetic refrigerator. *Advances in Cryogenic Engineering*, 1759-1766.

Vita

Joseph Kelly Stieha received both a Bachelor of Science in Physics and a Bachelor of Arts in Liberal Arts (Trombone) from the University of Kentucky in May of 2011. During his undergraduate studies, he joined the University of Kentucky Strachan Group as an undergraduate research assistant in January 2009. He collaborated on several publications: *Crystallographically-ordered Carbon Nanotubes Grown on Few-layer Graphene Films* (ACS Nano, Co-author), *The dispersal process of asexual propagules and the contribution to population persistence in Marchantia (Marchantiaceae)* (American Journal of Botany, Co-author), *Growth and Evolution of Catalysts on Graphene* (Kaleidoscope, Lead Author). After graduation, he was hired at nGimat LLC in Lexington, KY where he lead the production of nanopowders for various SBIR/STTR grants as a Process Scientist. He provided research samples for technical presentations and a PhD dissertation.

In 2013, Joseph returned to the University of Kentucky to pursue a Bachelor of Science in Mechanical Engineering, graduating with the degree in December of 2015. In March of 2015, he joined the University of Kentucky Bearings and Seals Laboratory as a graduate research assistant while also participating in the University Scholars program. He continued collaborating on publications including: *The Kentucky Re-entry Universal Payload System: Trajectory Analysis and Preliminary Subsystems* (54th AIAA Aerospace Sciences Meeting, Co-author), *Analysis of an End Face Mechanical Seal with Internal Valving for Low Power Applications* (71st STLE Annual Meeting and Exhibition, Lead Author)

His research interests include end-face mechanical seals, tribology, and design.